MODELING ATMOSPHERIC ^{14}C INFLUENCES AND ^{14}C AGES OF MARINE SAMPLES TO 10,000 BC

MINZE STUIVER and THOMAS F. BRAZIUNAS

Department of Geological Sciences, Quaternary Research Center, and Joint Institute for the Study of the Atmosphere and Ocean (JISAO), University of Washington, Seattle, Washington 98195 USA

INTRODUCTION

The detailed radiocarbon age *vs.* calibrated (cal) age studies of tree rings reported in this Calibration Issue provide a unique data set for precise ^{14}C age calibration of materials formed in isotopic equilibrium with atmospheric CO_2. The situation is more complex for organisms formed in other reservoirs, such as lakes and oceans. Here the initial specific ^{14}C activity may differ from that of the contemporaneous atmosphere. The measured remaining ^{14}C activity of samples formed in such reservoirs not only reflects ^{14}C decay (related to sample age) but also the reservoir ^{14}C activity. As the measured sample ^{14}C activity figures into the calculation of a conventional ^{14}C age (Stuiver & Polach 1977), apparent ^{14}C age differences occur when contemporaneously grown samples of different reservoirs are dated.

A correction for the apparent age anomaly is possible when the reservoir-atmosphere offset in specific ^{14}C activity is known. The offset (*e.g.*, ^{14}C age of marine sample – ^{14}C age of atmospheric sample) is expressed as a reservoir ^{14}C age, R(t), which need not be constant with time. When constant, however, the reservoir sample ^{14}C age, A, can be reconciled with the atmospheric one by deducting R(t) from A. Similar reservoir age corrections would be possible for a variable R(t), but complications arise because information on R time dependency usually is lacking. However, R(t) can be accounted for in the world oceans by using a marine calibration curve derived from carbon reservoir modeling (Stuiver, Pearson & Braziunas 1986). In these calculations, atmospheric ^{14}C change is attributed to solar- and geomagnetic-induced ^{14}C production change. Climate-induced changes in global carbon reservoirs, which may repartition ^{14}C among reservoirs, are not accounted for in these calculations.

Measuring a marine calibration curve is complicated because most marine samples lack the continuity and fine structure of tree rings. The ^{234}U/^{230}Th dating of corals (Bard *et al.* 1993) provides a good cal age equivalent, but measuring errors in the ^{234}U/^{230}Th ratio and ^{14}C accelerator mass spectrometry (AMS) determinations are such that the (bi)decadal chronological detail achieved for tree rings is not possible. Such detail, however, can be realized by calculating the response of the world oceans to tree-ring derived atmospheric ^{14}C changes.

The long-term trend of the ^{14}C age *vs.* cal age curve for the world oceans parallels that of the atmosphere. Short-term (century) variations, however, are smoothed in the oceans. Thus, whereas a constant, R, could be used for long-term variations, the shorter-term variations cannot be accounted for in this manner. Use of constant, R, and the atmospheric calibration curve assumes that the features of the marine and atmospheric curves are identical. The consequences of the constant R approach are obvious when the cal ages of a marine and atmospheric sample with identical (reservoir-corrected) ^{14}C age + standard deviation are evaluated. Calibration of both *vs.* the atmospheric curve yields identical results, whereas, in fact, the cal age range (and average number of intercepts) should be less for most marine samples because of the smoothed nature of the marine curve.
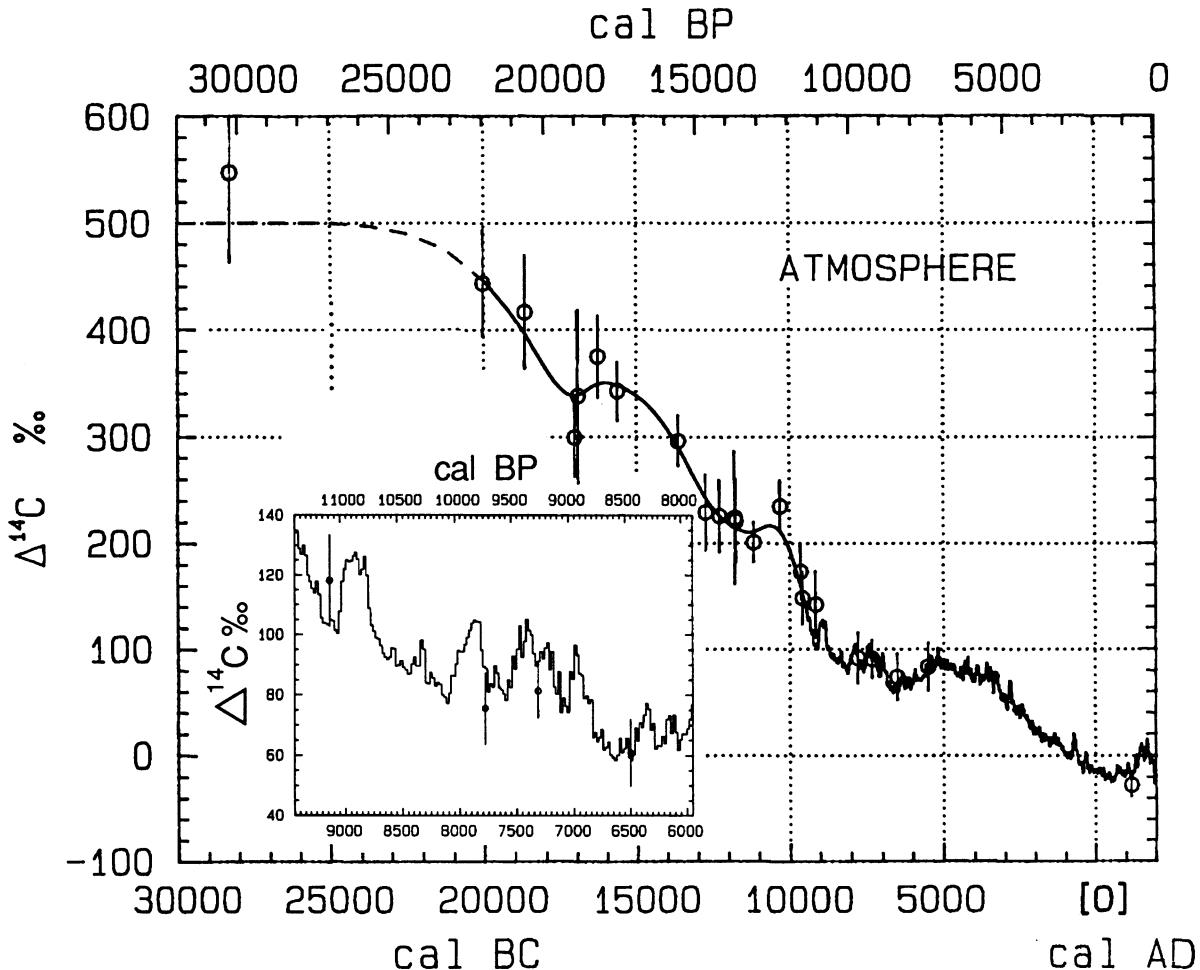
Fig. 1. The atmospheric $\Delta^{14}C$ record as derived from: dendrochronologically calibrated bidecadal tree-ring ^{14}C measurements (—— from 9440 BC to AD 1950), a cubic spline through the $^{234}U/^{230}Th$-calibrated coral ^{14}C averages corrected by 400 ^{14}C yr (—— from 20,000 to 9440 BC), and a smooth transition from an assigned pre-25,000 BC steady-state value of 500‰ (– –). The coral measurements (Bard *et al.* 1993) are shown as circles with 2 σ error bars. For the detailed coral/tree-ring comparison in the inset, the coral ages (1 σ error bars) were converted to cal ages using the marine calibration curve (Fig. 17) with $\Delta R = 0$.

Secular ^{14}C variations in the marine environment are represented by the modeled world ocean marine curve, but a world average curve does not account for the regional oceanic differences in specific ^{14}C activity; this is caused in part by regional variations in upwelling of ^{14}C-deficient waters. Here we define a region-specific ΔR term that represents the ^{14}C activity differences (in ^{14}C yr) of regional and world ocean surface layers. To a first order, the regional difference, ΔR, reflects oceanic mixing processes that contribute to the offset between regional and world ocean ^{14}C ages. Exchange with the atmosphere influences ΔR as well when regional atmospheric ^{14}C activity differs from the observed "global" ^{14}C activity. The ΔR term thus comprises two components: the portion of the shift in regional marine ^{14}C age attributable to a regional atmospheric ^{14}C age difference, and an additional shift in regional marine ^{14}C age, which reflects regional oceanic processes that differ from the parameters in the simulated global ocean.
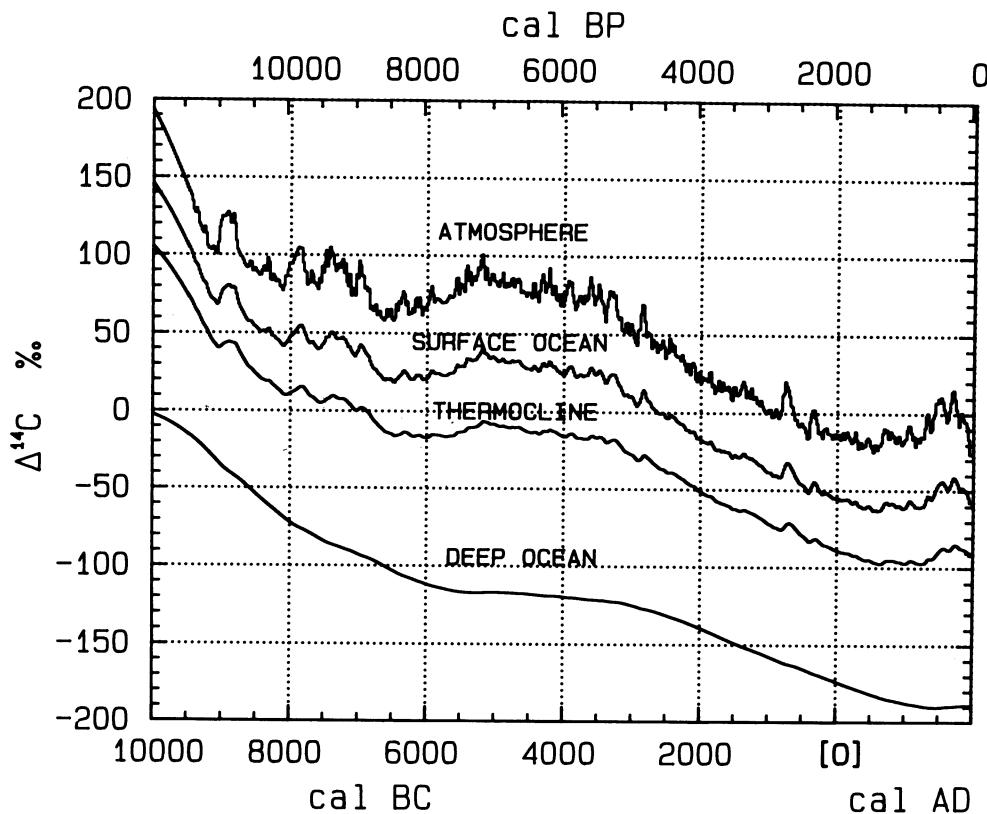
Fig. 2. Atmospheric $\Delta^{14}C$ (bidecadal values) as used for the model calculations and calculated surface ocean (0–75 m), thermocline (75–1000 m), and deep ocean (1000–3800 m) $\Delta^{14}C$ values

The R(t) term (incorporated in the global marine curve) accounts for secular changes, whereas ΔR represents the time-independent (as a first approximation) regional offsets from the world ocean ^{14}C age. The ΔR term corrects for regional activity differences in the calibration process, and can be determined from ^{14}C ages of marine samples of known historical age (Stuiver, Pearson & Braziunas 1986). A regional reservoir age, R′(t), on the other hand, represents a difference in ^{14}C age between the regional atmosphere and regional surface ocean. Thus, R′(t) = global R(t) + ΔR – ΔRa, in which ΔRa is the ^{14}C age difference between the regional atmosphere and our "global" (northern hemisphere tree-ring-based) atmospheric data base.

Previously, we did not consider regional variations in atmospheric ^{14}C activity. Then, ΔRa is zero, and the region-specific shift in marine ^{14}C age, ΔR, is equivalent to the regional reservoir age offset. For southern hemisphere samples, $\Delta Ra = 40$ ^{14}C yr (Vogel *et al.* 1993); in the northern hemisphere, $\Delta Ra = 0$. The atmospheric ^{14}C variations within each hemisphere representing decade-scale age differences have been neglected. These relations do not affect the calibration process, but the calculation of regional reservoir ages of the southern hemisphere entails the 40-^{14}C-yr adjustment.

The history of ^{14}C variations in the surface layer of the world ocean was previously modeled to about 7000 BC (Stuiver, Pearson & Braziunas 1986). We now use the extended and improved atmospheric record (Stuiver & Reimer 1993; summary of data from Bard *et al.* 1993; Kromer & Becker 1993; Pearson & Stuiver 1993; Pearson, Becker & Qua 1993; Stuiver & Pearson 1993) to
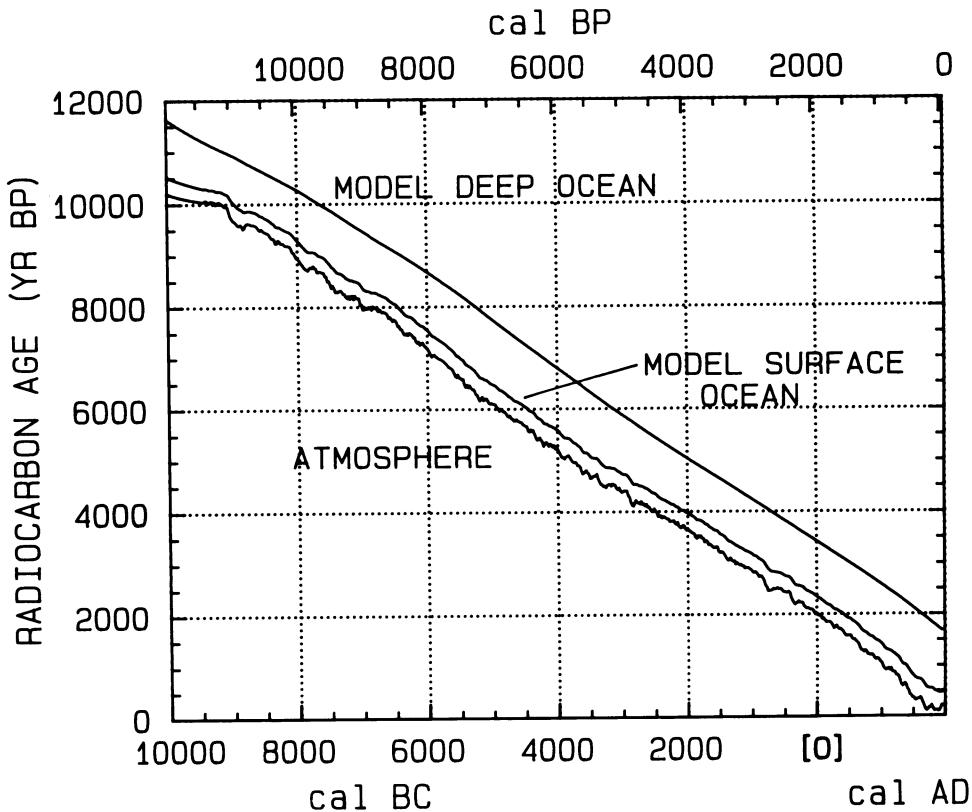
Fig. 3. ^{14}C ages of atmospheric samples (bidecadal values) and calculated conventional ^{14}C ages of the surface (0–75 m) and deep ocean (1000–3800 m)

generate the world ocean marine variations to 10,000 BC (≈10,200 ^{14}C yr BP). Because minor corrections had to be applied to the previously used tree-ring record, the model results are given for the entire AD 1950–10,000 BC interval.

THE GLOBAL CARBON MODEL

The global box-diffusion model, described originally in Oeschger *et al.* (1975), produces globally integrated depth-dependent marine ^{14}C variations in response to changes in atmospheric ^{14}C activity, as represented by the tree-ring (and coral) record. As previously indicated (Stuiver, Pearson & Braziunas 1986), we treat as constant the climate-influenced mixing parameters of the model (F, the air-sea CO_2 gas exchange rate; K_z, the oceanic vertical diffusion coefficient; and B_F, the air-land biospheric carbon uptake and release). We attribute the observed atmospheric Δ^{14}C (defined in Stuiver & Polach 1977) variability of at least the last 11,650 cal yr to solar (heliomagnetic) and geomagnetic modulation of the ^{14}C production rate, Q, induced by the cosmic-ray flux.

The parameter values and all reservoir CO_2 values remain as described for the earlier model version (Stuiver, Pearson & Braziunas 1986). Ocean exchanges (F = 19 moles m^{-2} yr^{-1} and K_z = 1.26 cm^2 sec^{-1}) are again calibrated to produce a surface ocean Δ^{14}C close to –50‰ (R ≈ 400 yr) and deep ocean (below 1 km) Δ^{14}C of –190‰ (R ≈ 1700 yr) for the bidecade centered at AD 1830. We arbitrarily chose the AD 1830 bidecade to use for model calibration; however, the model surface ocean Δ^{14}C of –46‰ for AD 1700 to AD 1900, which may better represent recent average
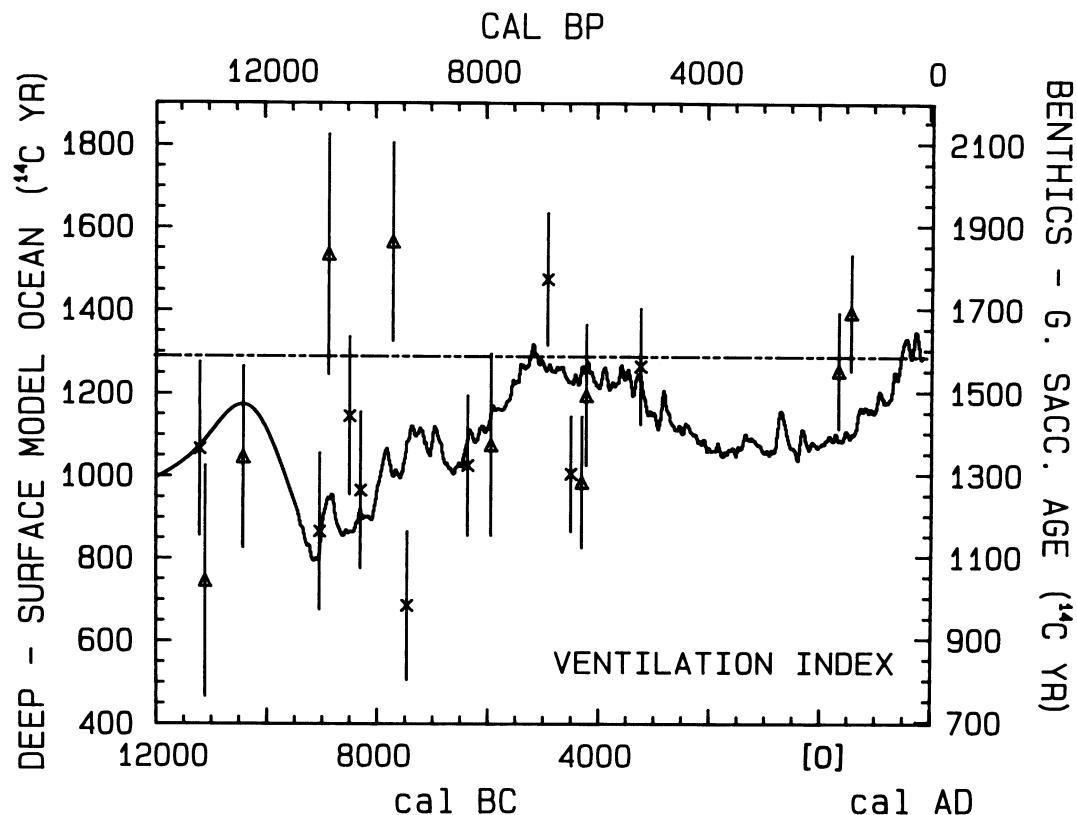
Fig. 4. The calculated deep ocean-surface ocean ^{14}C age differences (——) compared to benthic-planktonic foraminifera differences measured by Andrée *et al.* (1986) for the South China Sea ($\times$ = Core V35-6, Δ = Core V35-5). The deep water in the South China Sea is more ^{14}C deficient than our model ocean, causing a shift between the ventilation scales of 1585 (latest pre-anthropogenic age difference in Andrée *et al.* 1986) minus 1290 ^{14}C yr (model AD 1830 value), both indicated by (– – –). Ventilation calculations end in AD 1830, as fossil fuel CO_2 influences the latter part of the Δ^{14}C record. The planktonic foram age determinations were calibrated by using our marine calibration curve with $\Delta R = 0$.

natural conditions, also coincides with the observed "pre-industrial" estimate of $-45 \pm 15‰$ (Broecker *et al.* 1979; Lassey, Manning & O'Brien 1990).

Emphasis here is on the Holocene time interval, *i.e.*, the last 10,000 ^{14}C yr. The beginning of this interval corresponds to an uncertain cal age, because the atmospheric calibration curve flattens near 10,000 ^{14}C yr BP. Prior to 9440 BC, our model ocean responds to a 10,560-yr history of atmospheric Δ^{14}C derived from the ^{234}U/^{230}Th-calibrated coral ^{14}C activities (Bard *et al.* 1993; Stuiver & Reimer 1993). The spline through the coral-based atmospheric Δ^{14}C determinations (coral dates are corrected by 400 ^{14}C yr) is extrapolated to a pre-25,000 BC steady-state value of 500‰ (Fig. 1). The global model starts at 30,000 BC with this initial atmospheric Δ^{14}C condition, and calculates both a ^{14}C-production-rate history and an oceanic Δ^{14}C response curve compatible with the coral and tree-ring ^{14}C time series.

The reliability of the coral *vs.* tree-ring derived atmospheric Δ^{14}C values was verified by Bard *et al.* (1990) using a constant 400-yr reservoir age correction. More detailed reservoir age corrections are incorporated in the calibration curves of Figure 17. Although application of these curves minimizes coral/tree-ring differences (see Fig. 1 inset), a crucial offset near 11,100 cal BP remains.
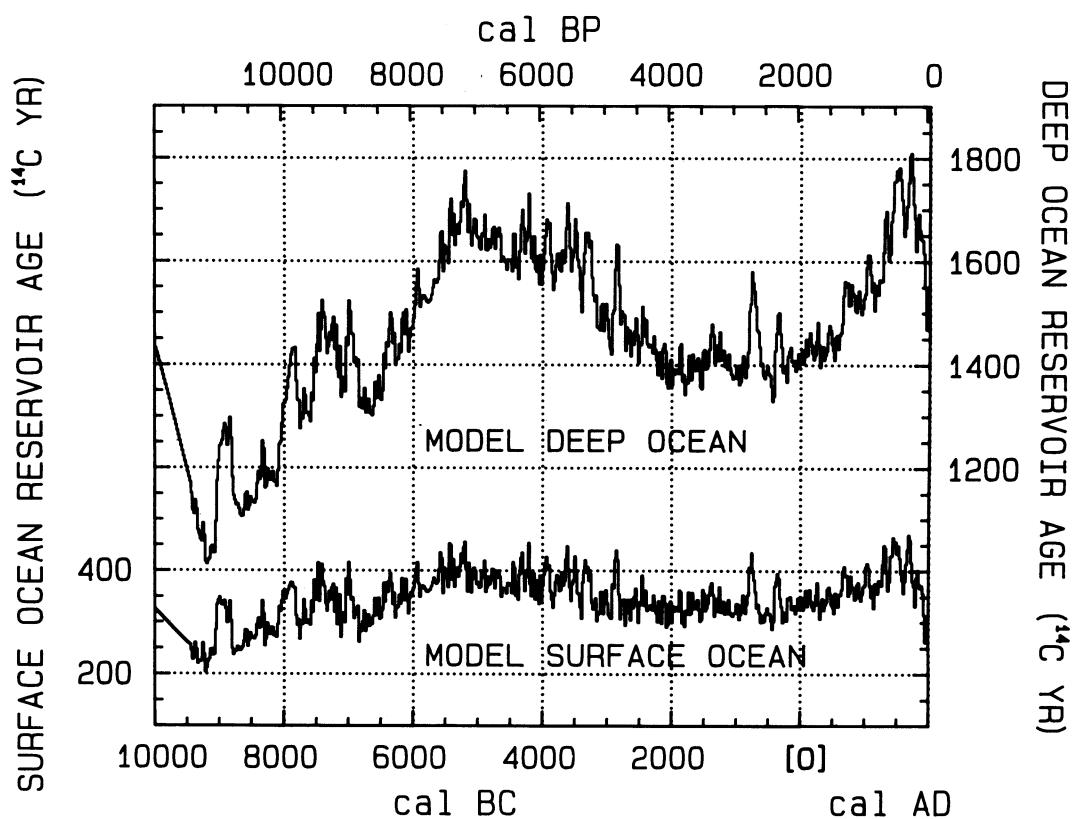
Fig. 5A. Variations in model-calculated reservoir ages R(t) of the surface ocean (bottom curve and left axis) and deep ocean (top curve and right axis) plotted by cal yr.
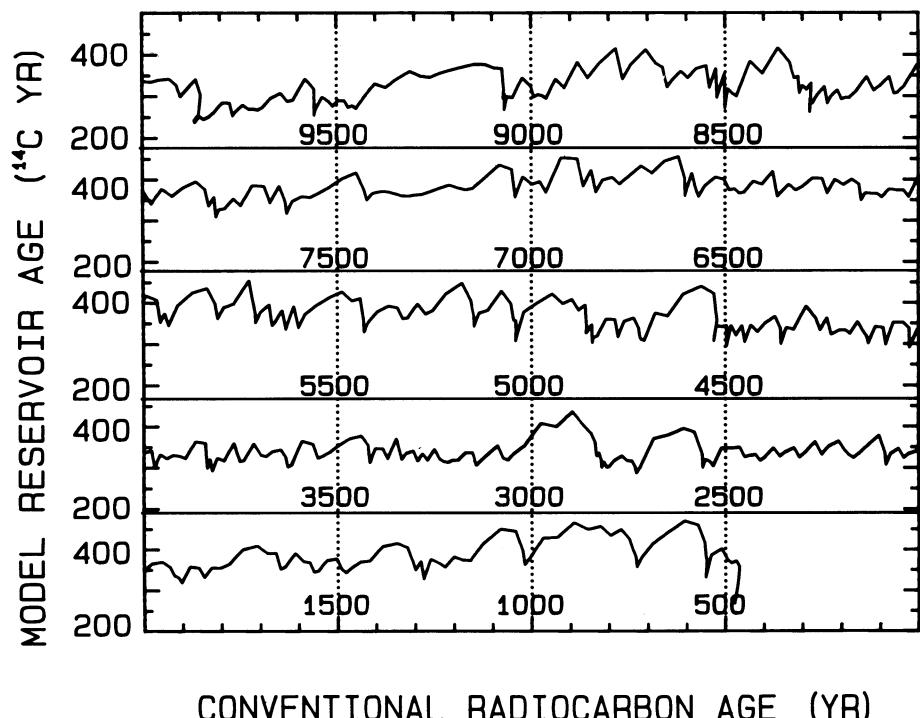

Fig. 5B. Variations in model-calculated surface ocean reservoir age, R(t), plotted vs. model-defined conventional ^{14}C age of surface-ocean waters. Each segment covers 2000 ^{14}C yr. Multiple intercepts occasionally occur for individual ^{14}C ages.
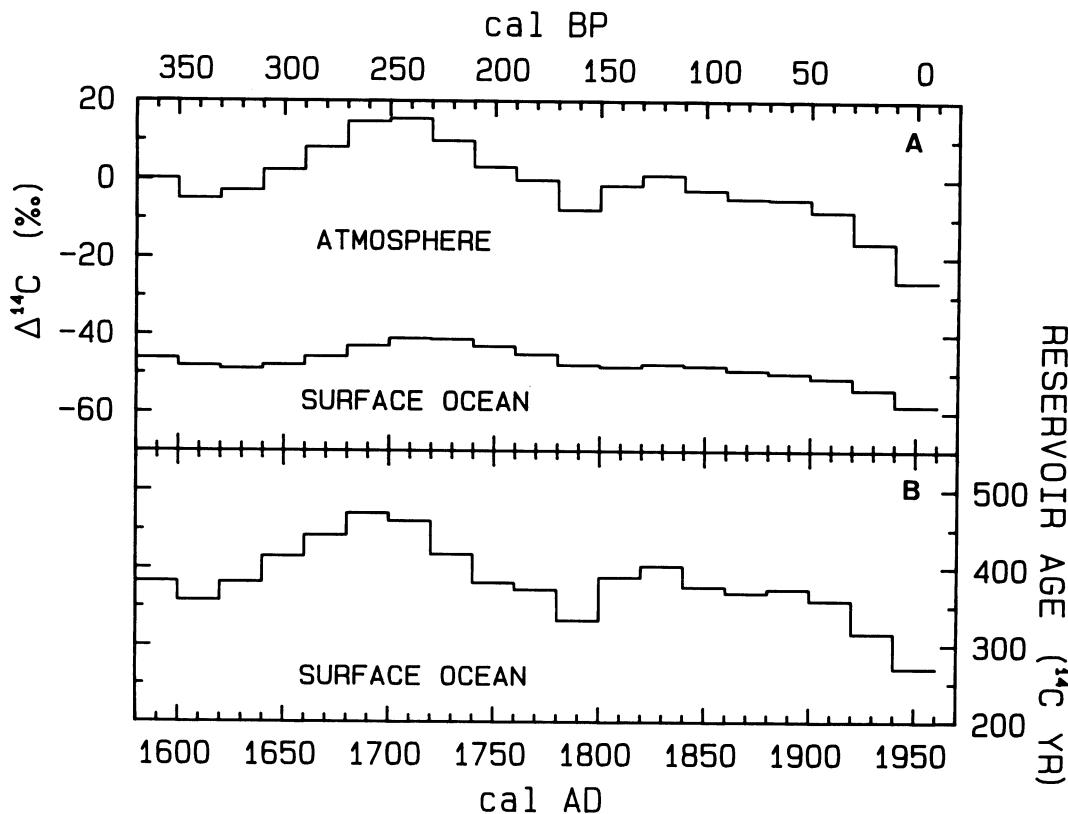
Fig. 6. A. Δ14C of the atmosphere and surface ocean. B. Surface ocean reservoir ages from AD 1600 to 1950.

As a first approximation, the model exchange parameters are constant during our 32,000-yr simulation, despite significant changes in atmosphere, ocean and terrestrial biosphere dynamics that occurred before 10,000 ^{14}C yr BP; these changes were associated with the glacial-interglacial climate transition (Adams *et al.* 1990; Broecker & Denton 1989). Three lines of evidence suggest that the differences among glacial, deglaciation and interglacial conditions had secondary effects on atmospheric (and oceanic) Δ^{14}C after 10,000 BC.

First, the model-derived ^{14}C production history agrees with the Q trend expected from documented changes in the geomagnetic dipole over the past 30,000 cal yr, such that no major climatic (oceanic) explanation for millennium-scale atmospheric Δ^{14}C variations is required (Bard *et al.* 1990; Stuiver *et al.* 1991; Mazaud *et al.* 1991).

Second, carbon model sensitivity tests show that the global-scale ^{14}C reservoirs respond relatively quickly to changes in ocean mixing processes, such that Holocene atmospheric and oceanic Δ^{14}C levels will have recovered substantially after 2000 cal yr (ocean turnover time) from any pre-Holocene climatic divergences (Braziunas 1990). Such model studies also show that surface ocean ^{14}C closely tracks changes in atmospheric ^{14}C, and that variations in reservoir age for much of the ocean surface generally will not exceed ± 100 ^{14}C yr (Bard 1988). Greater surface-ocean reservoir age variations, up to 200 ^{14}C yr, may also occur in response to sharp Q-induced shifts in atmospheric ^{14}C activity.
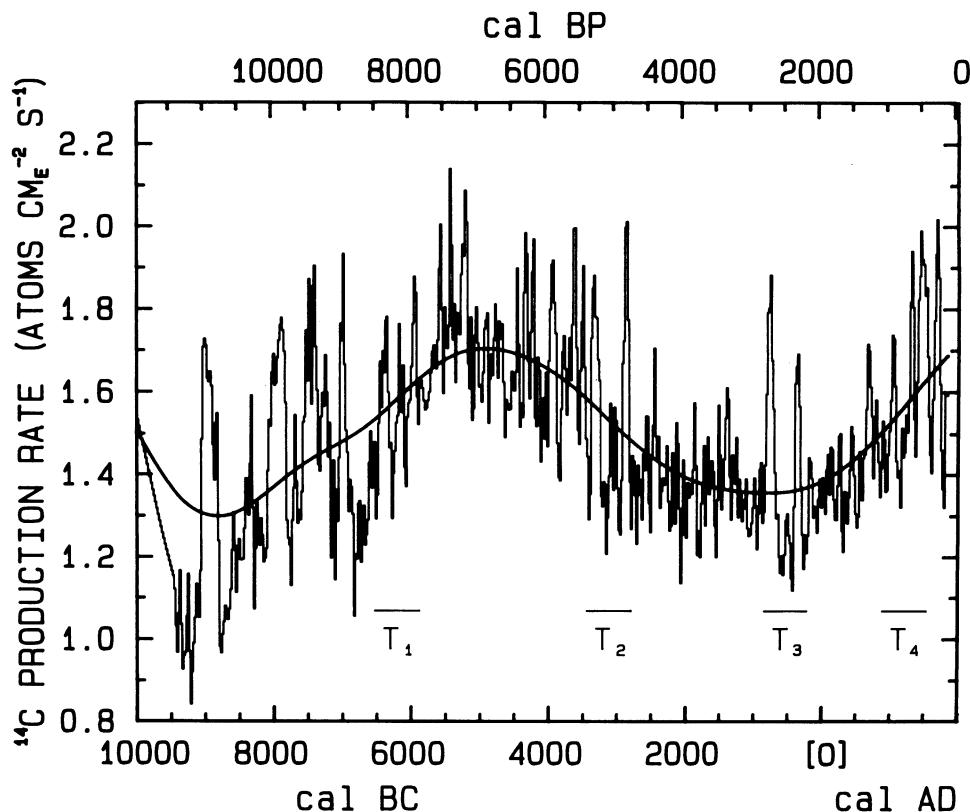
Fig. 7. ^{14}C production rate variations Q back to 10,000 BC. Q was calculated by using atmospheric Δ^{14}C variations (Fig. 1) as carbon reservoir model input. Triplet episodes (Stuiver & Braziunas 1989) are identified as T1–T4. The long-term spline approximates a 2000-yr moving average. The input for the first 500 yr is based on the coral spline, the remaining portion on the tree-ring record.

Finally, the available ^{14}C age differences between contemporaneous deep- and surface-dwelling foraminifera, as measured by AMS, suggest a relatively constant oceanic mixing rate over the past 12,500 ^{14}C yr (see below).

Several factors complicate the simple calculation of global oceanic ^{14}C responses. Distinctions in oceanic mixing between high- and low-latitude ocean regions may lead to dissimilar trends in surface-ocean Δ^{14}C (Toggweiler & Sarmiento 1985; Bard 1988), contrary to our notion of parallel oceanic calibration curves. Also, although the model-derived Q record fits with first-order geomagnetic forcing, uncertainties in the geomagnetic dipole record allow for significant climatic contributions to the atmospheric Δ^{14}C record. We do consider these to be of second-order importance for the Holocene, and note that measurements of pre-Holocene coral (Bard *et al.* 1993) establish a directly measured marine calibration curve for the 10,000–20,000 BC interval.

Despite an identical calibration procedure, our current marine simulation yields Δ^{14}C = –47.7‰ (R = 402 ^{14}C yr) for AD 1830, instead of –49.7‰ (R = 409 ^{14}C yr) reported in Stuiver, Braziunas and Pearson (1986). This difference is related to: 1) slight changes to the atmospheric ^{14}C data base; and 2) an explicit incorporation into the model of reservoir ^{13}C/^{12}C distinctions, rather than simple application of fractionation-corrected ^{14}C activities. Our choices for air-sea and terrestrial fractionation factors (Siegenthaler & Münnich 1981; Keeling 1973) fix δ^{13}C of the atmosphere at
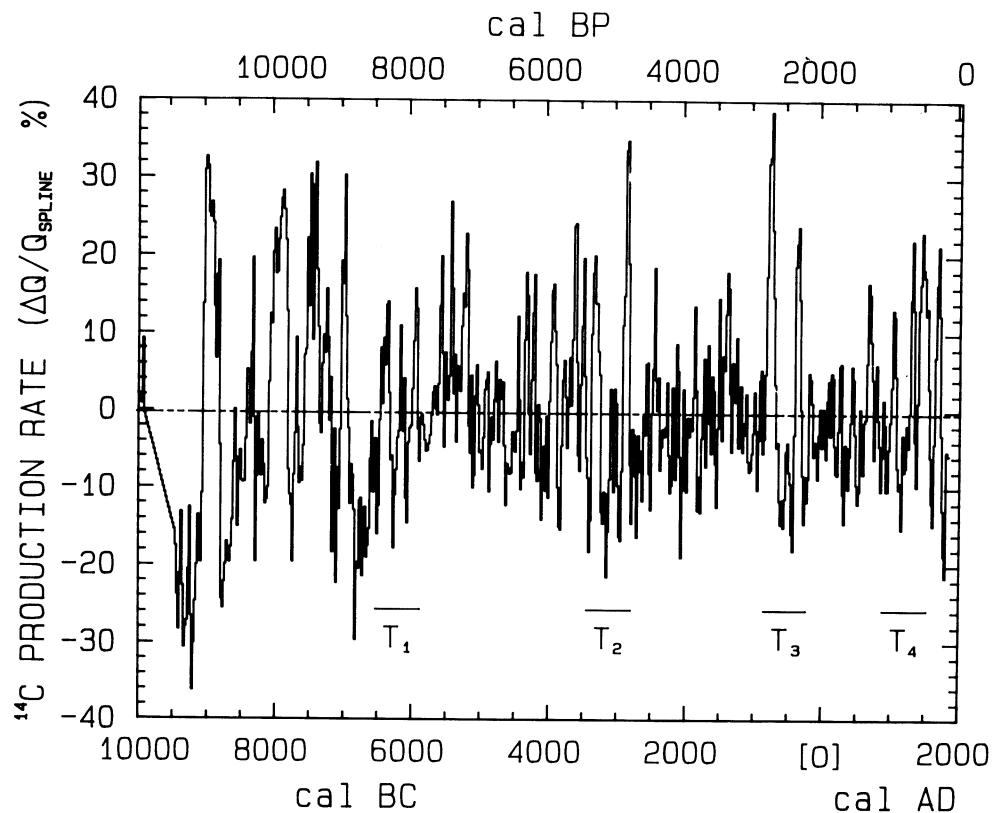
Fig. 8. Relative detrended model calculated ^{14}C production rate variations (for $\Delta Q/Q_{spline}$ definition, see text) for the last 12,000 yr. Triplet episodes are identified as T1–T4. The input for the first 500 yr was based on the Fig. 1 coral spline, that of the remaining interval on the tree-ring record (see Fig. 1).

$-7\permil$, and of the ocean at $0.92\permil$, with $\delta^{13}C$ of the terrestrial biosphere set at $-25\permil$. Relative to the simpler modeling approach without explicit fractionation, absolute rates of ^{14}C production and decay are elevated $\approx 5\%$, and ocean $\Delta^{14}C$ levels are affected by $1\permil$, because absolute oceanic ^{14}C activities are enhanced. The surface-ocean reservoir age of 402 yr also reflects the non-zero atmospheric $\Delta^{14}C$ value of $1.2\permil$ in AD 1830.

MODEL CALCULATIONS

Figure 2 shows the post-10,000 BC atmospheric (tree-ring) $\Delta^{14}C$ bidecadal record and the model-derived global marine response for surface (0–75 m depth), thermocline (75–1000 m), and deep (1000–3800 m) waters. The corresponding ^{14}C age *vs.* cal age plots are depicted in Figure 3. The 10,000–9440 BC portion of the atmospheric curve derived from the pre- and early Holocene spline representing the coral-based $\Delta^{14}C$ trend (Figure 1). As discussed above, our simulation produces marine $\Delta^{14}C$ and ^{14}C-age time series in response to changes in ^{14}C production rate, rather than climatic variations, because changes in climate during the last deglaciation are not considered in the model. Uncertainties in our model-based ocean reservoir ages that are related to the measurement standard deviations, σ, *i.e.*, $\pm$ 1–8$\permil$ for tree-ring data and $\pm$ 10–25$\permil$ for coral data, were estimated by adding $\pm$ 1 σ to the Figure 1 data. The later Holocene portions of the oceanic curves generated by the model differ between these extremes ($\pm$ 1 σ) by generally <20 ^{14}C yr.
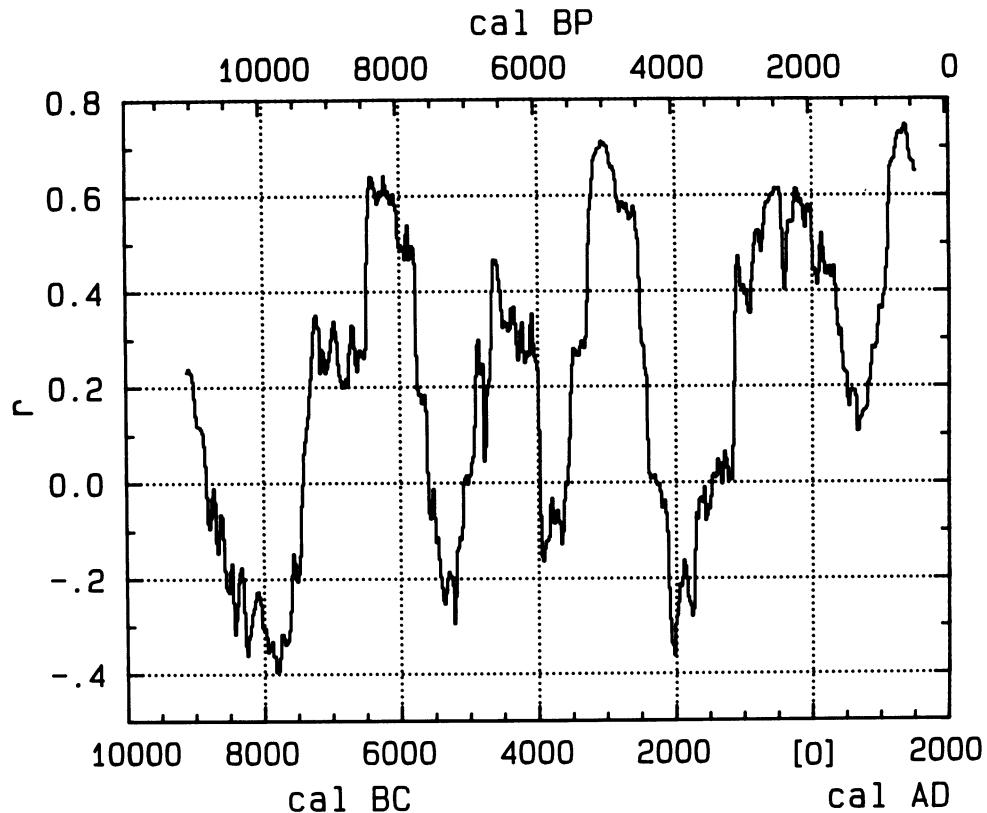
Fig. 9. Correlation coefficient, r, of a 700-yr sliding portion of the ^{14}C production rate with the curve generated from Eq. (1) of Stuiver and Braziunas (1989), as discussed in the text. The 700-yr sliding window results in a loss of 350 yr at either end of the curve.

AMS ^{14}C age measurements on contemporaneous benthic and planktonic foraminifera (Andrée *et al.* 1986; Shackleton *et al.* 1988) suggest that major changes in the rate of deep-ocean ventilation occurred prior to (but not after) 12,500 ^{14}C yr BP. The δ^{13}C record from a sediment core in the deep Southern Ocean is also consistent with a sharp transition in the influx of ^{13}C-enriched North Atlantic Deep Water at *ca.* 12,500 ^{14}C yr BP, followed by essentially modern conditions for deep-water ventilation (Charles & Fairbanks 1992). In Figure 4, the modeled ^{14}C age differences (ventilation ages) between deep ocean and surface ocean are compared to foraminifera ^{14}C data for the post-12,000 BC era. The foraminifera ^{14}C data were calibrated using the marine calibration curve (part of which is shown in Figure 17, explained below) with $\Delta R = 0$. Such an approximate calibration is needed; otherwise, calendar foraminifera dates may be too young by up to 2000 cal yr. The agreement shown in Figure 4 supports the validity of our modeling approach.

Model reservoir ages are plotted *vs.* cal age in Figure 5A; Figure 5B gives more detail of surface-ocean reservoir ages *vs.* conventional ^{14}C ages. The century-type variations in deep-ocean reservoir ages (Fig. 5A) reflect the atmospheric Δ^{14}C change relative to a "constant" deep-ocean Δ^{14}C level; the corresponding surface-ocean reservoir age changes are smaller, because the surface ocean can react on this time scale to the atmospheric Δ^{14}C change.

For the past 7000 cal yr, the new surface-ocean-model reservoir ages differ by only two decades from those calculated in Stuiver, Braziunas and Pearson (1986). A difference in input for the older
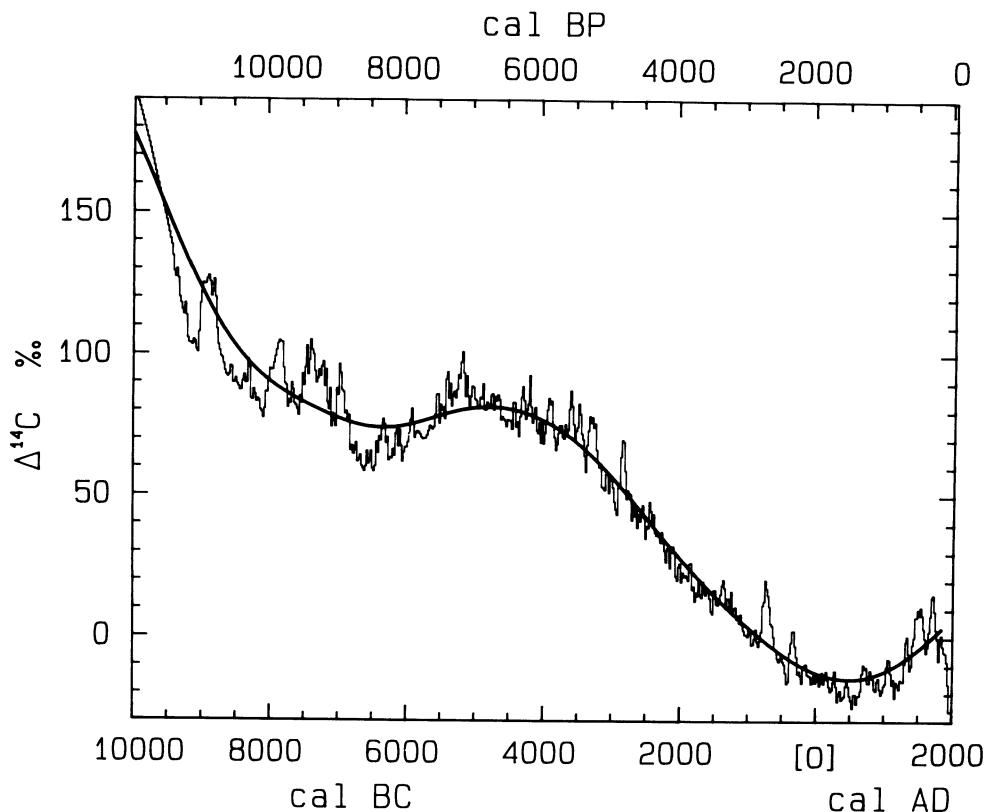
Fig. 10. Atmospheric $\Delta^{14}C$ (coral-derived for the first 500 yr, see Fig. 1) for the past 12,000 yr. The long-term $\Delta^{14}C$ spline was calculated from the Fig. 7 Q spline, but resembles a 2000-yr $\Delta^{14}C$ moving average as well.

part of the record (steady-state in 1986 paper *vs.* coral-based on long-term atmospheric $\Delta^{14}C$ decline now) results in surface-ocean reservoir age discrepancies of generally less than 50 but up to 140 yr for the 7000–9000 cal yr BP interval.

Surface-ocean $\Delta^{14}C$ and reservoir age from AD 1600–1950 are depicted in Figure 6. Alternative pre-Holocene conditions do not change this recent portion of model ocean history. The AD 1950 "bidecade," in effect, does not consider post-AD 1954 nuclear bomb ^{14}C activity changes. It should be noted that the new atmospheric ^{14}C data base and the treatment of the terrestrial biosphere, as well as mixed reservoirs, modifies the results of our calculations compared to earlier studies (*e.g.*, Stuiver *et al.* 1991; Oeschger *et al.* 1975). A change to a model with increased carbon storage in the terrestrial biosphere and ocean (*e.g.*, Damon 1988), balanced by increased (from 1.6 to 2.15 ^{14}C atoms cm^{-2}sec^{-1} averaged over the Holocene) equilibrium Q values more reflective of present neutron flux measurements (*e.g.*, Lingenfelter & Ramaty 1970), yields only slightly different (<15 ^{14}C yr) calibration curves. The calculated Q history does not change in fine structure, and displays only a nearly uniform shift throughout the last 12,000 cal yr.

SPECTRAL PROPERTIES AND MODEL-DERIVED ^{14}C PRODUCTION RATE *VS.* OCEANIC VARIATIONS

Model calculations yield information on atmospheric $\Delta^{14}C$ values, production rates, Q, and alternative changes in oceanic mixing rates K_z, and demonstrate the validity of the production modulation approach to calibration.
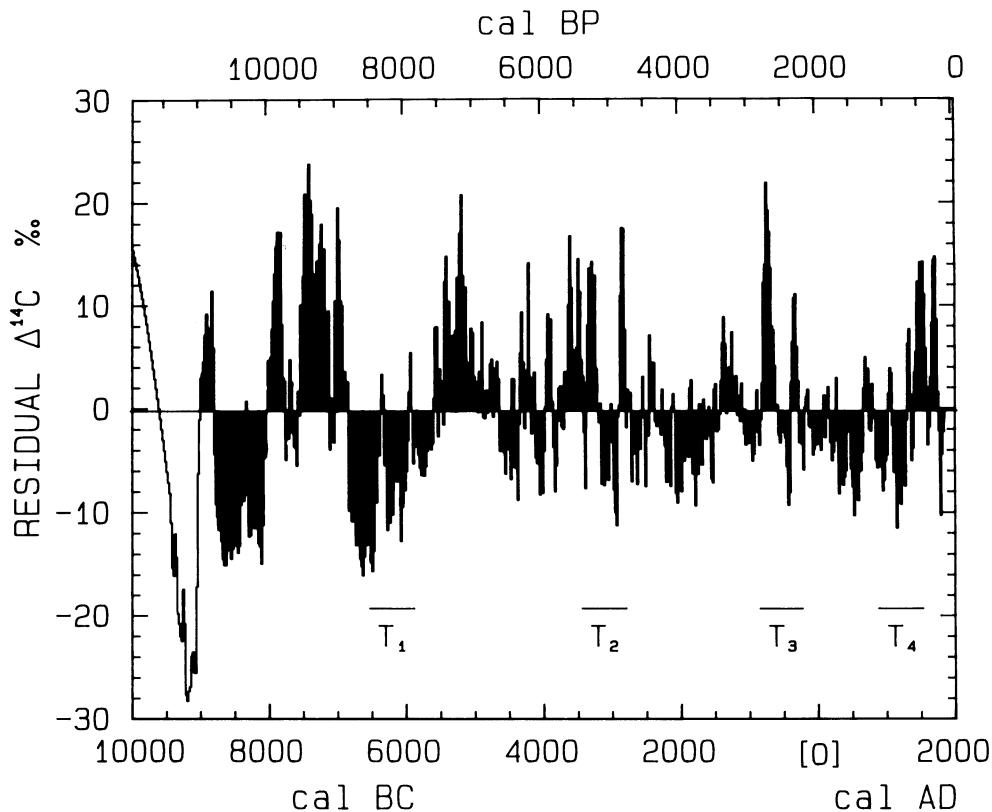
Fig. 11. Residual $\Delta^{14}C$ obtained by deducting the Fig. 10 long-term trend. The $\Delta^{14}C$ trend of the first 500 yr was estimated from coral determinations, the remaining $\Delta^{14}C$ values were derived from tree-ring measurements (see Fig. 1). Lowest residual $\Delta^{14}C$ value following the YD (Younger Dryas) climate oscillation is at 9190 BC (11,140 cal BP); the rapid change (duration *ca.* 150 yr) to Holocene $\Delta^{14}C$ conditions starts at 9060 BC (11,010 cal BP).

In Figures 7 and 8, we present for the AD 1950–10,000 BC interval, respectively, the calculated absolute production rate, Q, and the detrended $\Delta Q/Q_{spline}$ record. Here ΔQ is the difference between Q and the Figure 7 Q_{spline} (the latter approximates, but is not equal to, a 2000-yr moving average).

One interpretation of this record is that solar modulation of the cosmic-ray flux causes a substantial part of the detrended ΔQ variance. Triplets (three successive cycle episodes), T_1 to T_4, are especially notable solar features, and are identified in the figures. These episodes were identified previously, and a best-fit equation was obtained describing these triplet segments (Eq. 1, Stuiver & Braziunas 1989). Figure 9 represents the correlation coefficient, r, between sliding 700-yr portions of the Eq. 1 curve and the detrended ^{14}C production rate record. Although substantial correlation coefficients (0.6–0.7) are found for the T_1–T_4 triplets (Stuiver & Braziunas 1989), the newly added pre-7800 BC part evidently does not contain triplets of the same character, because its correlation coefficients are appreciably lower. Whereas century-type variations of the later part of the ^{14}C record presumably relate mainly to solar forcing (and are dominated by the periodicities of Eq. 1), climate (oceanic) forcing may well have prevailed during the earlier (pre-7000 BC) part of the record.

The oceanic influence has not been accounted for in our marine calibration curves, because the entire atmospheric $\Delta^{14}C$ variablilty was attributed to ^{14}C production rate, Q, change. Whereas Q-
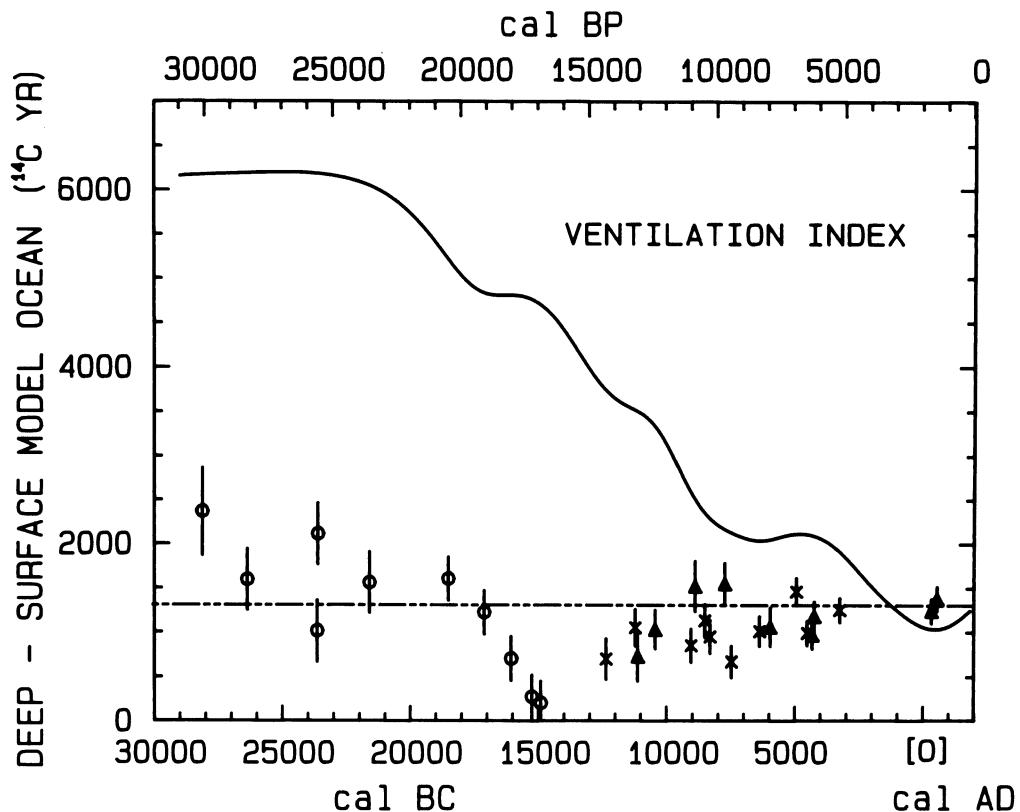
Fig. 12A. Observed ^{14}C age difference of benthic-planktonic species (ventilation index, Andrée *et al.* (1986) ▲ and ×; Shackleton *et al.* (1988) ○) compared to model-calculated age difference (top curve). For deriving the age differences, we assumed that ocean-circulation change was solely responsible for the Fig. 10 long-term Δ^{14}C trend. As in Fig. 4, the South China Sea data have been shifted 295 ^{14}C yr; the East Pacific measurements of Shackleton *et al.* have similarly been shifted by 230 ^{14}C yr to normalize on current conditions. Shackleton *et al.* [14]C ages were calibrated using the Stuiver and Reimer (1993) program with ΔR = 180 yr.

related atmospheric Δ^{14}C perturbations are attenuated in the oceans, oceanic Δ^{14}C changes must be at least as large as atmospheric changes when oceanic circulation is the cause. The difference in mixed-layer response for century-type variations approaches a factor of two for these scenarios (*ca.* 60 ^{14}C yr, see Stuiver *et al.* 1991). These differences will be less for perturbations of longer durationas the system approaches equilibrium. The postulated oceanic influence is confined to relatively low periodicities (500–3000 yr, see below). Therefore, the impact of our Q-forcing assumption on calibration calculations will be restricted to a few decades.

Figures 10 and 11 depict, respectively, absolute atmospheric Δ^{14}C and residual Δ^{14}C. The long-term trend in the Δ^{14}C record can be determined in various ways (sine equations, moving averages, splines, *etc.*). In this instance, we took the Figure 7 production rate spline and calculated the corresponding Figure 10 atmospheric Δ^{14}C trend; the calculated trend also strongly resembles the 2000-yr Δ^{14}C moving average. Residual Δ^{14}C values were obtained by subtracting the Figure 10 long-term trend.

[14]C production rate variation induced by change in the geomagnetic dipole intensity appears to cause most of the long-term Δ^{14}C trend (Bard *et al.* 1990; Stuiver *et al.* 1991; Mazaud *et al.* 1991).
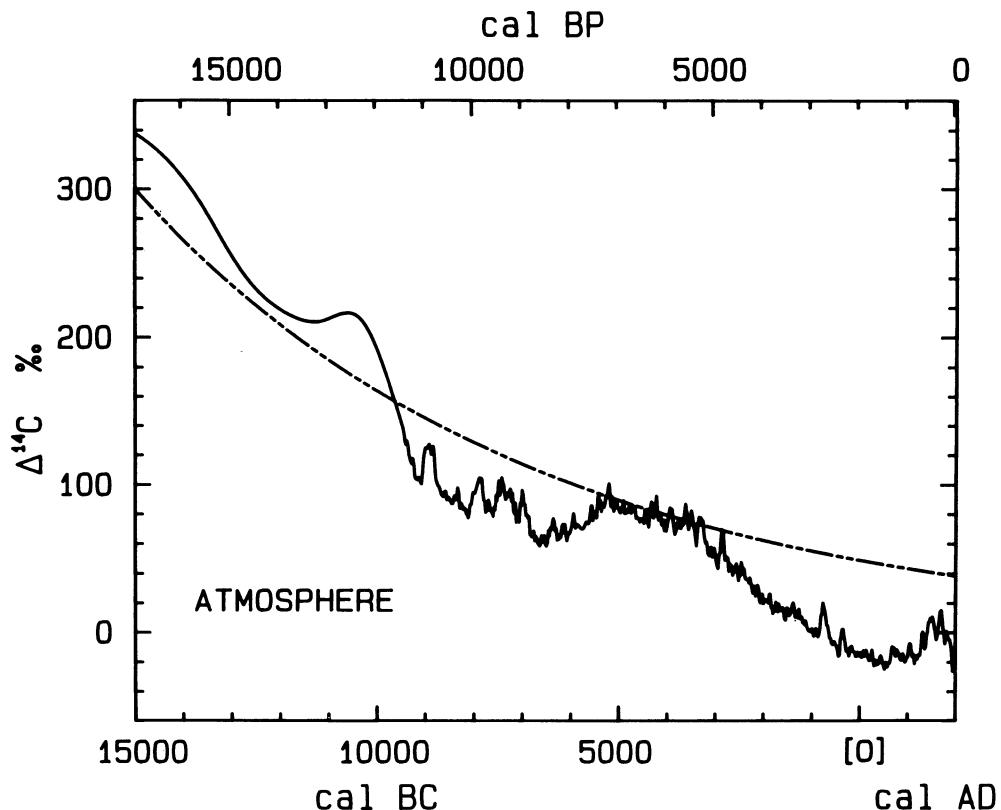
Fig. 12B. Atmospheric $\Delta^{14}C$ compared to decay of excess ^{14}C (– – —, see text).

The incompatibility of the long-term $\Delta^{14}C$ trend with oceanic forcing as an alternative can also be seen in Figure 12A. Here we compare "ventilation indices", representing observed ^{14}C age differences between the deep and surface ocean, to a ventilation history resulting from the ocean circulation changes required to explain the observed long-term atmospheric $\Delta^{14}C$ trend. This ventilation history was calculated using the carbon reservoir model by fixing the ^{14}C production rate at the post-AD 1000 average of the Figure 7 curve. The long-term $\Delta^{14}C$ trend can be explained only by drastic reduction of deep-water formation during the glacial period (K_z about 1/7th of Holocene values), which resulted in a ventilation index value exceeding 6000 ^{14}C yr.

Lower geomagnetic dipole intensity before *ca*. 15,000 yr BP (Mazaud *et al.* 1991) evidently was responsible for elevating $\Delta^{14}C$ up to 50%. The $\Delta^{14}C$ decrease after 15,000 yr BP may be largely the decay of "excess" ^{14}C. The decay curve (dashed line) given in Figure 12B is compatible with a sudden change in steady-state ^{14}C production rate (a reduction by 1.3) at 15,000 BC.

The steep decline in $\Delta^{14}C$ (Fig. 11) between 10,000 and 9190 BC (11,950–11,140 cal BP) is associated with the 10,000 ^{14}C-yr plateau in ^{14}C age *vs*. cal age plots. The termination of the Younger Dryas (YD) interval is not necessarily near the end of this plateau. Although Becker, Kromer and Trimborn (1991) suggest it to be near 11,140 cal BP, annual counting of the Greenland GISP core indicates an age of 11,650 ± 250 cal BP (Alley 1993). Laminated sediments from a Polish lake (Rozanski *et al.* 1992) yield a comparable 11,000–11,700 cal BP range, with a preferred value of 11,200 cal BP. Lehman and Keigwin (1992) place the YD termination near 10,500 ^{14}C BP
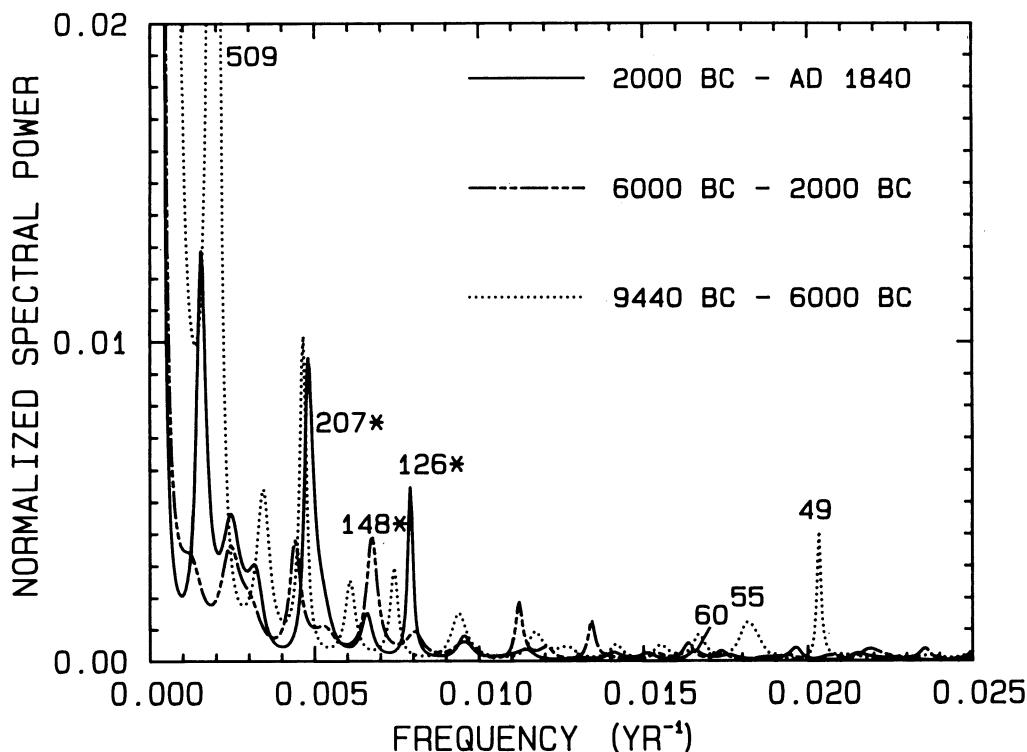
Fig. 13A. MEM power spectrum (AR order *ca.* 50) of Fig. 10 Δ^{14}C values for the intervals given above. Starred periodicities have spectral power exceeding the 2 σ significance level, the others fall in the 1.5–2.0 σ range. Periodicities for the intervals 2000 BC–AD 1840, 6000–2000 BC, and 9440–6000 BC are, respectively, 60, 126 and 207 yr, 148 yr, and 49, 55 and 509 yr.

(*ca.* 12,420 cal BP, Stuiver & Reimer 1993). We consider the oldest Fig. 11 residual Δ^{14}C changes, starting with the 12,000–11,140 cal BP decline, to be caused by fluctuations in North Atlantic Deep Water (NADW) formation and transport. The initial Δ^{14}C decline would be due to an increased rate of upwelling of water relatively low in ^{14}C. Specific details will be published elsewhere.

Adding freshwaters to the surface ocean lowers densities, which, in turn, reduces the potential for sinking of higher-density waters to abyssal depths. A reduced deep-water formation rate agrees with our vertical diffusivity coefficient (K_z) calculations, whereby, according to the carbon reservoir model, K_z values must be reduced by nearly 40% to generate the Δ^{14}C maximum near 10,900 cal BP (see Fig. 1 inset). However, the timing of the Δ^{14}C maximum differs from the 11,300 cal BP meltwater pulse discussed by Fairbanks (1990).

In the earliest part of the record, residual Δ^{14}C amplitudes are among the largest, and durations of the Δ^{14}C variations among the longest; these lengthened durations are also observed in the spectral properties of the Δ^{14}C and Q records (both without trend removal). Figures 13A and 13B depict normalized spectral power for three subintervals, each lasting 3.5–4 millennia. We used the maximum entropy method (MEM) or autoregressive (AR) model for AR order n/4, where n = number of data points. The periods where spectral power of atmospheric Δ^{14}C exceeds the 2 σ significance level, or falls in the 1.5–2.0 σ range (Mitchell *et al.* 1966), change from 60, 126 and 207 yr for the 2000 BC–AD 1840 interval to 49, 55 and 509 yr for the 9440 BC–6000 BC interval. High- and intermediate-frequency production rate variations result in substantially attenuated Δ^{14}C variations
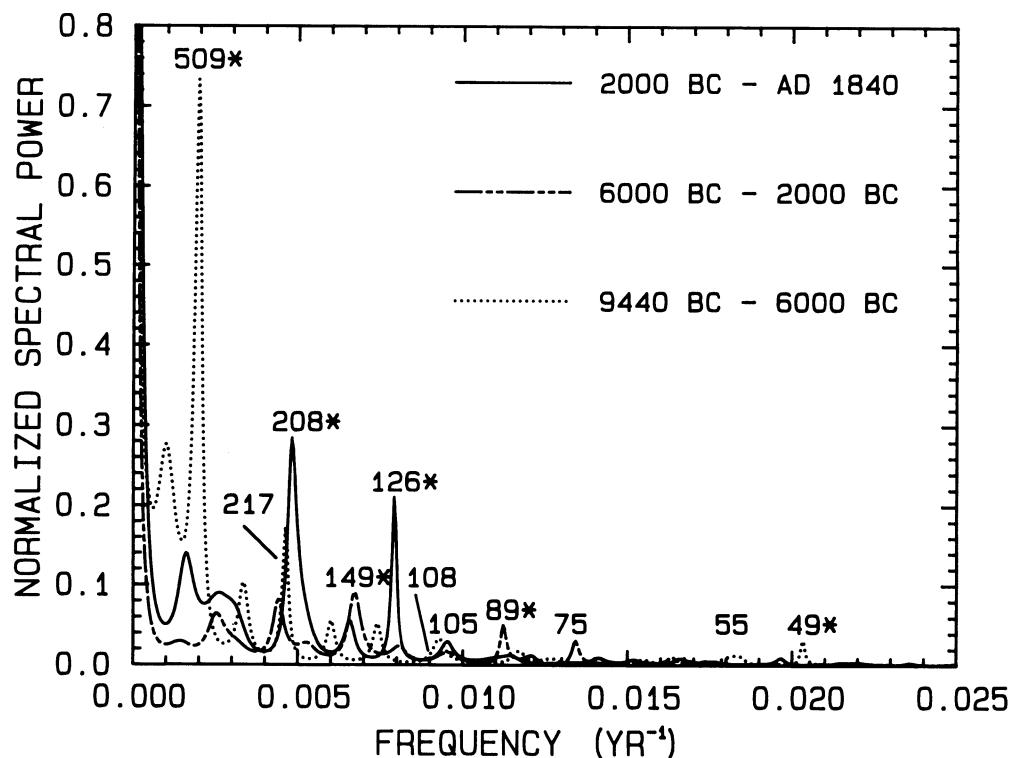
Fig. 13B. MEM power spectrum (AR order *ca.* 50) of the Fig. 7 calculated ^{14}C production rate variations, Q. Starred periodicities have spectral power exceeding the 2 σ significance level, the others fall in the 1.5–2.0 σ range. Periodicities for the intervals listed above are, respectively, 105, 126 and 208 yr, 75, 89 and 149 yr, and 49, 55, 108, 217 and 509 yr.

in the atmosphere, resulting in a loss of frequencies relative to the Q spectrum. Periods where spectral power of Q exceeds or approaches the 2 σ level are 105, 126 and 208 yr for the 2000 BC–AD 1840 interval, and 49, 55, 108, 217 and 509 yr for the 9440–6000 BC interval.

After removal of the long-term trend, the complete detrended Δ^{14}C record reveals periods with spectral power density exceeding the 2 σ level at 46, 49, 87, 148, 206 and 512 yr. A 2860-yr periodicity was found to be significant in the 1.5 to 2.0 σ range. While the 512- and 2860-yr periodicities may well relate to oceanic (and climate) changes, several higher frequencies appear to be solar-induced. These findings will be discussed elsewhere.

RADIOCARBON AGE AND ΔR DETERMINATION

Figure 14 presents model surface-ocean conventional ^{14}C ages *vs.* calendar ages for the post-AD 1500 period. An independent estimate of the calendar age of a sample from a particular location allows the user to determine a model-generated ^{14}C age. This age can be compared to the conventional marine ^{14}C age of the sample from this location. The difference constitutes ΔR, an assumed time-constant offset in ^{14}C ages for that particular region, that should be removed from sample ^{14}C ages before application of the marine calibration curve (see Figs. 16 and 17). The time dependency of reservoir age, R(t), is included in the marine calibration curve.

In some instances, such as with a pair of contemporaneous wood and shell samples from a single location, the reservoir deficiency may be calculated without a direct calibration to the calendar time
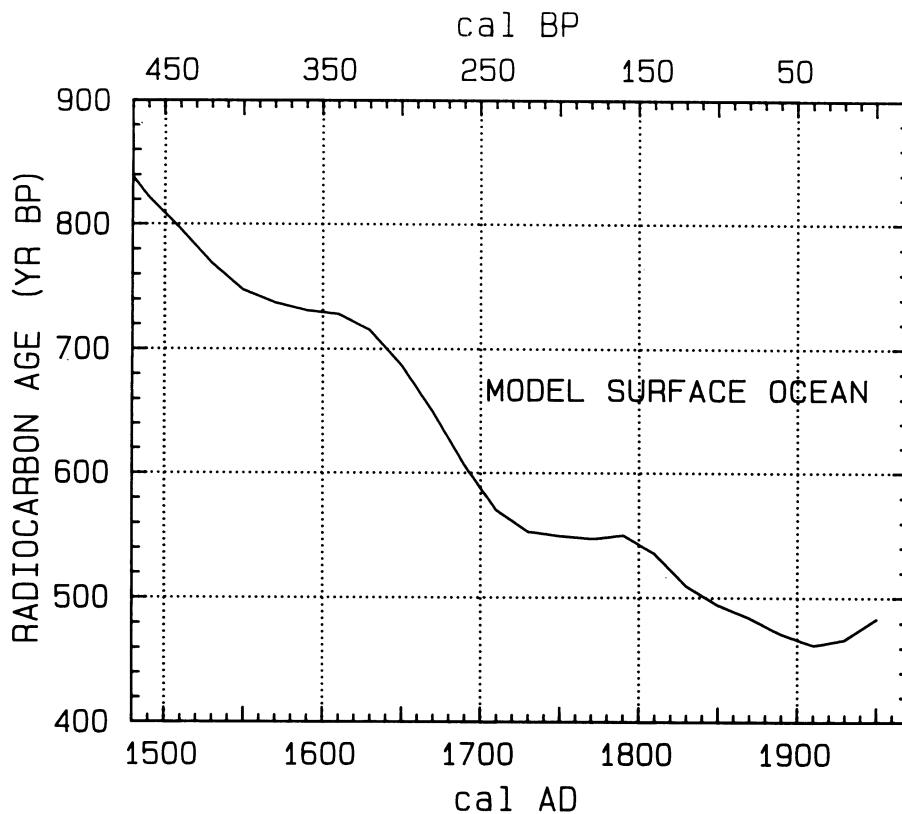
Fig. 14. Post-AD 1500 surface ocean ^{14}C yr *vs.* cal yr

scale. In this case, one can use Figure 15, in which model marine conventional ^{14}C ages are plotted against atmospheric conventional ^{14}C ages. The atmospheric (wood) sample can be initially calibrated using the atmospheric calibration curves (Stuiver & Reimer 1993), and its cal age subsequently applied to the calculation of ΔR by using Figure 14 (or Figure 17); however, one canavoid the middle step in this process by applying Figure 15. The measured wood ^{14}C age is converted through Figure 15 to a model marine ^{14}C age, which, when deducted from the measured shell ^{14}C age, yields ΔR. A 40-yr correction must be applied to the ^{14}C ages of southern hemisphere atmospheric samples before using this figure.

Figure 15 illustrates obvious multiple marine ^{14}C age intercepts for a specific atmospheric ^{14}C age. Similar multiple marine ages (and thus multiple ΔR choices) would also result from using Figure 14 or 17, and by using the cal age derivation of the wood ^{14}C age from the Stuiver and Reimer (1993) atmospheric calibration curves; again, deduct 40 ^{14}C yr for southern hemispheric samples.

A survey of independently calibrated shell ^{14}C samples approximates the geographic distribution of ΔR values for oceanic regions in both hemispheres. A summary of ΔR values, given in the 1986 paper, is augmented in Figure 16 with ΔR data from New Zealand (McFadgen & Manning 1990), South Africa (Talma 1990), Portugal (Soares 1989) and the North American east coast (E. Little, personal communication, 1992). It should be noted that ΔR values for the coast of California, given as 225 ^{14}C yr in Figure 16, are controversial, because recent work indicates values of about 300 ± 35 ^{14}C yr (Terry Jones, personal communication, 1992) and 500 ± 100 ^{14}C yr (Bouey & Basgall 1991).
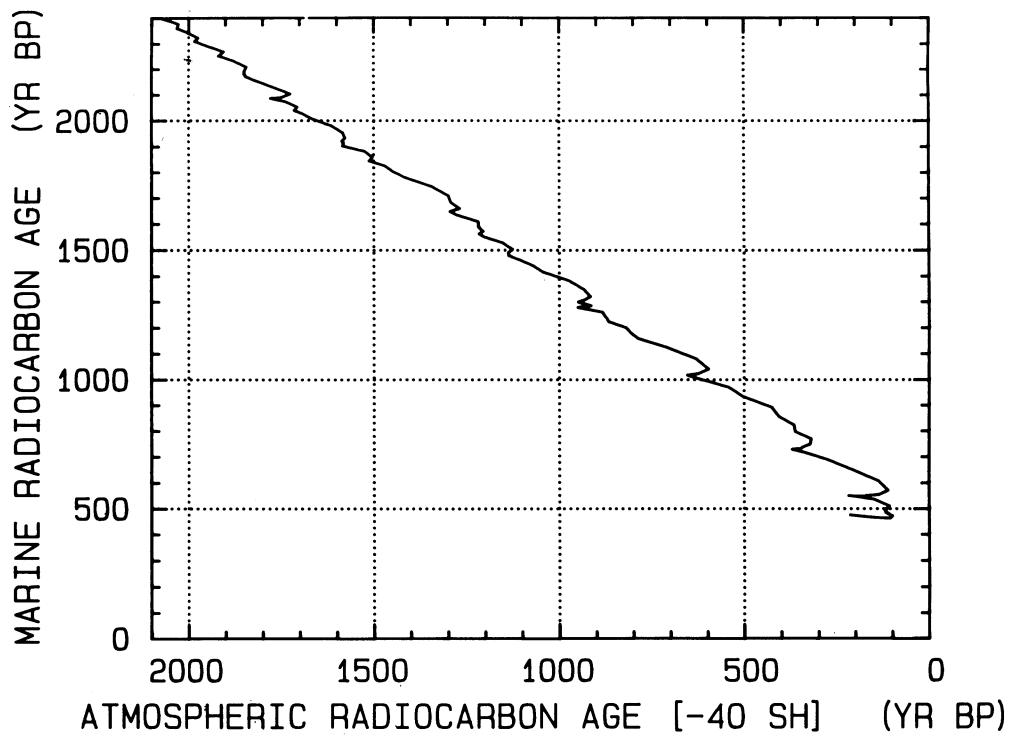
Fig. 15A–C. Holocene surface-ocean ^{14}C ages *vs.* atmospheric ^{14}C ages of the northern hemisphere. Southern hemispheric atmospheric ^{14}C ages should be reduced by 40 yr prior to using the graphs.
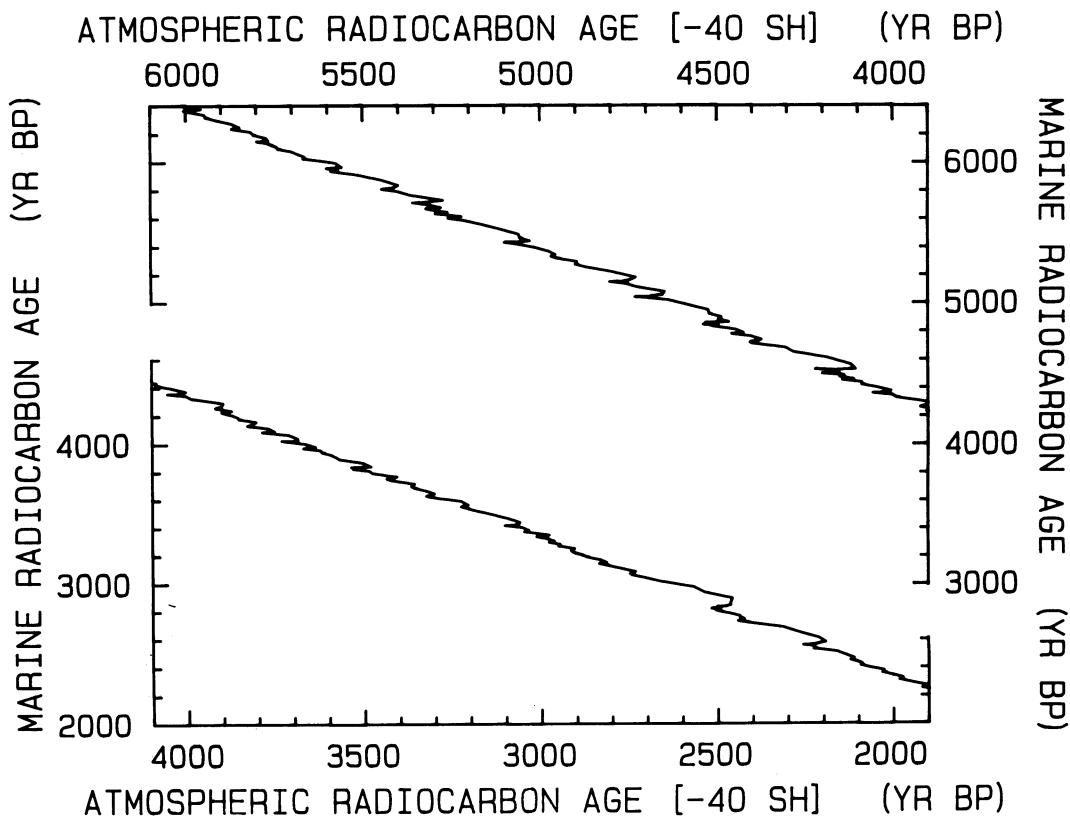
Fig. 15B
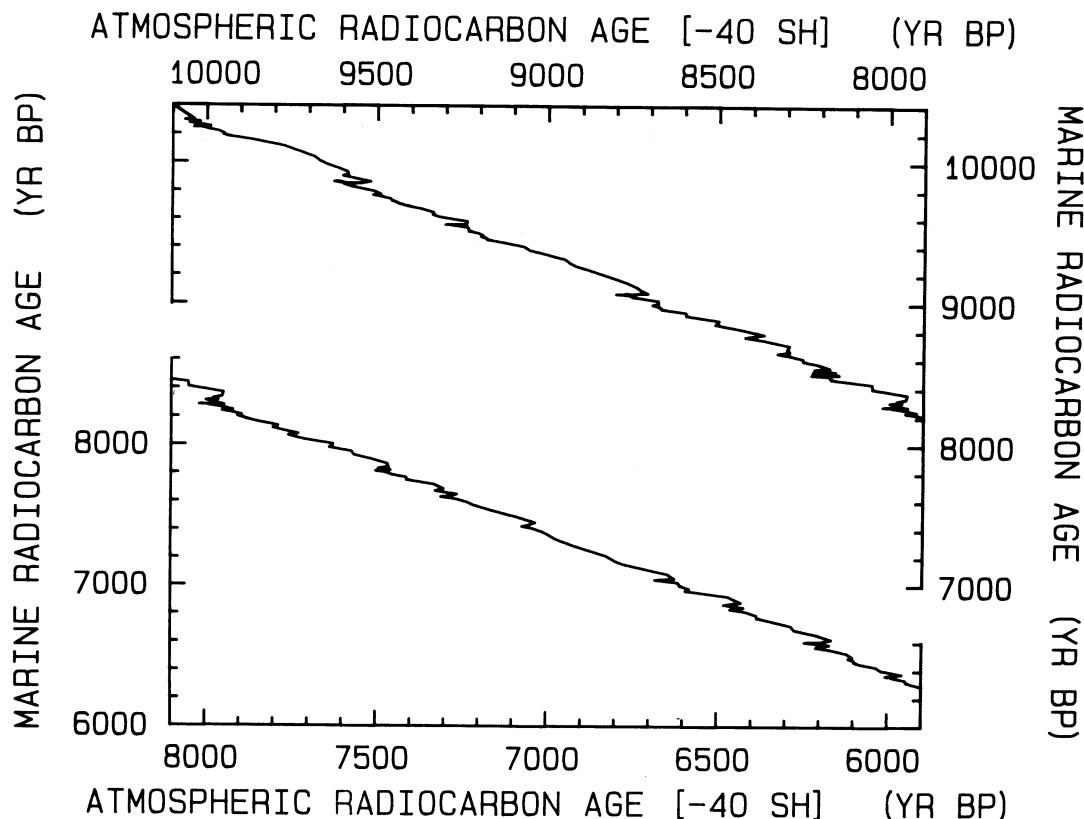
Fig. 15C

Complications may arise (*e.g.*, increase in ΔR) in estuaries, where a mixture of marine and riverine materials are incorporated in the shell. For example, estimated local ΔR values within Long Island Sound (E. Little, personal communication, 1992) vary greatly from the average Sound value of about 120 ± 55 ^{14}C yr; this average value also is distinctly different from the value of -85 ± 75 ^{14}Cyr listed for a single sample in our 1986 paper. Open ocean values from the Massachusetts coast yield ΔR = –95 ± 45 ^{14}C yr (E. Little, personal communication, 1992).

Complications also occur when rates of regional upwelling vary. For example, Soares (1989) determined ΔR of 280 ± 35 ^{14}C yr (38°N – 41°N) and 235 ± 35 ^{14}C yr (37°N) for the coast of Portugal, for samples with conventional ^{14}C ages less than 2000 ^{14}C yr BP. A *ca.* 250-^{14}C-yr reduction in ΔR value is encountered for the earlier part of the Holocene. Such an increase may be related to reduced upwelling of deeper (older) water. Southon, Nelson and Vogel (1990), on the other hand, find, except for one outlier, only minor changes in ΔR for five Holocene determinations from the west coast of British Columbia. Talma (1990) reports, for 15 charcoal-shell sample pairs from the west coast of South Africa (1000 BC–AD 1500 cal age range), that "the spread of ΔR values with age seems fairly random and is probably only the result of measurement imprecision and some natural variability". Figure 16 ΔR values are based on the 1986 calibration curves, with global R(1830) = 409 yr, whereas current calculations yield global R(1830) = 402 yr. No attempt was made to update the regional ΔR determinations, because minor changes in calibration results for the last few centuries would result in corrections about equal to the rounding error (up to 5 yr) of the original data set.
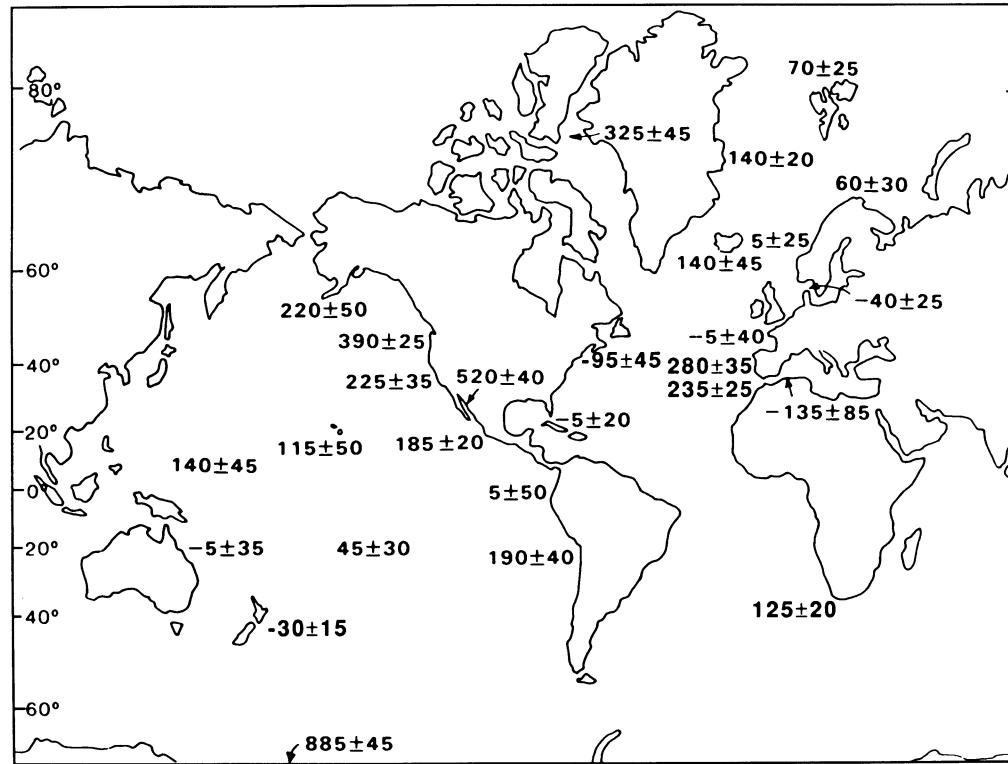
Fig. 16. Geographic distribution of coastal region ΔR values (in ^{14}C yr). The ± values are minimum standard deviations based on the scatter of the data, or the measurement precison, whichever is larger (Stuiver, Pearson & Braziunas 1986). For Long Island Sound ΔR, see text.

A corresponding tabulation of reservoir ages for the AD 1830 bidecade can be derived from the Figure 16 ΔR values by adding 402 and 362 ^{14}C yr for the northern and southern hemispheres, respectively. Such a tabulation gives oceanic ^{14}C levels at one single point in time, and applies to both hemispheres (the southern hemispheric atmosphere was assumed to be 40 yr older than the "global" tree-ring record).

Figure 17 should be used to calibrate surface ocean samples. For such calibration, ΔR must be selected (or, to a first approximation, assume ΔR = 0). The CALIB 3.0 program (Stuiver & Reimer 1993), which incorporates Figure 17 data, also can be used. For marine samples older than 10,500 ^{14}C yr, the Bard *et al.* (1993) calibration curve is applicable. These data are also part of the CALIB 3.0 program, where a smoothing spline is used to approximate the Bard *et al.* information.

To reduce an offset (from 120 to 35 yr at 11,700 cal yr) between the two marine segments (smoothing spline through coral measurements *vs.* our model-calculated part), we changed the pre-tree-derived (Fig. 1) atmospheric Δ^{14}C model input slightly. This second-order correction allows our model ocean to operate more realistically, in that coral-assigned model reservoir deficiencies prior to 11,700 cal yr BP were allowed to deviate (by 120 yr maximally) from the constant 400-yr reservoir deficiency initially imposed as a simplifying assumption. Specifically, the two marine segments (pre-11,750 cal yr BP smoothing spline through coral measurements *vs.* post-11,650 cal yr BP model-calculated part) are connected by a short (100-yr) linear interpolation to smooth their 35-yr offset.

ACKNOWLEDGMENTS

REFERENCES

Adams, J. M., Faure, H., Faure-Denard, L., McGlade, J. M. and Woodward, F. I. 1990 Increases in terrestrial carbon storage from the Last Glacial Maximum to the present. *Nature* 348: 711–714.

Alley, R. B., Meese, Shuman, C. A., Gow, A. J., Taylor, K., Ram, M., Waddington, E. D. and Mayewski, P. A. 1993 An old, long, abrupt Younger Dryas event in the GISP2 ice core. *Nature*, in press.

Andrée, M., Beer, J., Loetscher, H. P., Moor, E., Oeschger, H., Bonani, G., Hofmann, H. J., Suter, M., Wölfli, W. and Peng, T. H. 1986 Limits on the ventilation rate for the deep ocean over the last 12000 years. *Climate Dynamics* 1: 53–62.

Bard, E. 1988 Correction of accelerator mass spectrometry ^{14}C ages measured in planktonic foraminifera: Paleoceanographic implications. *Paleoceanography* 3: 635–645.

Bard, E., Arnold, M., Fairbanks, R.G. and Hamelin, B. 1993 $^{230}Th/^{234}U$ and ^{14}C ages obtained by mass spectrometry on corals. *Radiocarbon*, this issue.

Bard, E., Hamelin, B., Fairbanks, R. G. and Zindler, A. 1990 Calibration of the ^{14}C timescale over the past 30,000 years using mass spectrometric U-Th ages from Barbados corals. *Nature* 345: 405–410.

Becker, B., Kromer, B. and Trimborn, P. 1991 A stable isotope tree-ring timescale of the Late Glacial/Holocene boundary. *Nature* 353: 647–649.

Bouey, P. D. and Basgall, M. E. 1991 Archaeological patterns along the South-central coast, Point Piedras Blancas, San Luis Obispo County, California. *California Department of Transportation* 05-SLO-1: 39–48.

Braziunas, T. F. 1990 Nature and origin of variations in late-glacial and Holocene atmospheric ^{14}C as revealed by global carbon cycle modeling. Ph.D. dissertation, University of Washington, Seattle.

Broecker, W. S. and Denton, G. H. 1989. The role of ocean-atmosphere reorganizations in glacial cycles. *Geochimica et Cosmochimica Acta* 53: 2465–2501.

Broecker, W. S., Takahashi, T., Simpson, H. J. and Peng, T.-H. 1979 Fate of fossil fuel carbon dioxide and the global carbon budget. *Science* 206: 409–418.

Charles, C. D. and Fairbanks, R. G. 1992 Evidence from Southern Ocean sediments for the effect of North Atlantic deep-water flux on climate. *Nature* 355: 416–419.

Damon, P. E. 1988 Production and decay of radiocarbon and its modulation by geomagnetic field-solar activity changes with possible implications for global environment. *In* Stephenson, F. R. and Wolfendale, A. W., eds., *Secular Solar and Geomagnetic Variations in the Last 10,000 Years*. Dordrecht, The Netherlands, Kluwer Academic Publishers: 267–285.

Fairbanks, R. G. 1990 The age and origin of the "Younger Dryas climate event" in Greenland ice cores. *Paleoceanography* 5: 937–948.

Keeling, C. D. 1973 The carbon dioxide cycle: Reservoir models to depict the exchange of atmospheric carbon dioxide with the oceans and land plants. *In* Rasool, S. I., ed., *Chemistry of the Lower Atmosphere*. New York, Plenum Press: 251–329.

Kromer, B. and Becker, B. 1993 German oak and pine ^{14}C calibration, 7200 BC–9400 BC. *Radiocarbon*, this issue.

Lassey, K. R., Manning, M. R. and O'Brien, B. J. 1990 An overview of oceanic radiocarbon: Its inventory and dynamics. *Reviews in Aquatic Sciences* 3: 117–146.

Lehman, S. L. and Keigwin, L. D. 1992 Sudden changes in North Atlantic circulation during the last deglaciation. *Nature* 356: 757–762.

Lingenfelter, R. E. and Ramaty, R. 1970 Astrophysical and geophysical variations in ^{14}C production. *In* Olsson, I. U., ed., *Radiocarbon Variations and Absolute Chronology*. Proceedings of the 12th Nobel Symposium. New York, John Wiley & Sons: 513–537.

Mazaud, A., Laj, C., Bard, E., Arnold, M. and Tric, E. 1991 Geomagnetic field control of ^{14}C production over the last 80 ky: Implications for the radiocarbon timescale. *Geophysical Research Letters* 18: 1885–1888.

McFadgen, B. and Manning, M. R. 1990 Calibrating New Zealand radiocarbon dates of marine shells. *Radiocarbon* 32(2): 229–232.

Oeschger, H., Siegenthaler, U., Schotterer, U. and Gugelmann, A. 1975 A box diffusion model to study the carbon dioxide exchange in nature. *Tellus* 27: 168–192.

Pearson, G. W., Becker, B. and Qua, F. 1993 High-precision ^{14}C measurement of German oaks to show the natural ^{14}C variations from 7890 to 5000 BC.

Radiocarbon, this issue.

Pearson, G. W. and Stuiver, M. 1993 High-precision bidecadal calibration of the radiocarbon time scale 500–2500 BC. *Radiocarbon*, this issue.

Rozanski, K., Goslar, T., Dulinski, M., Kuc, T., Pazdur, M. F. and Walanus, A. 1992 The Late Glacial-Holocene transition in central Europe derived from isotope studies of laminated sediments from Lake Gosciaz (Poland), *In* Bard, E. and Broecker, W. S., eds., *The Last Deglaciation: Absolute and Radiocarbon Chronologies*. NATO ASI Series I-2. Heidelberg, Springer Verlag: 69–80.

Shackleton, N. J., Duplessy, J.-C., Arnold, M., Maurice, P., Hall, M. A. and Cartlidge, J. 1988 Radiocarbon age of last glacial Pacific deep water. *Nature* 335: 708–711.

Siegenthaler, U. and Münnich, K. O. 1981 $^{13}C/^{12}C$ fractionation during CO_2 transfer from air to sea. *In* Bolin, B., ed., *Carbon Cycle Modeling: SCOPE 16*. New York, John Wiley & Sons: 249-257.

Soares, A. M. M. 1989 O efeito de reservatório oceânico nas águas costeiras de Portugal continental. ICEN-LNETI, Dept. de Quimica: 135 pp.

Southon, J. R., Nelson, D. E. and Vogel, J. S. 1990 A record of past ocean-atmosphere radiocarbon differences from the Northeast Pacific. *Paleoceanography* 5: 197–206.

Stuiver, M. and Braziunas, T. F. 1989 Atmospheric ^{14}C and century-scale solar oscillations. *Nature* 338: 405–408.

Stuiver, M., Braziunas, T. F., Becker, B. and Kromer,

B. 1991 Climatic, solar, oceanic, and geomagnetic influences on late-glacial and Holocene atmospheric $^{14}C/^{12}C$ change. *Quaternary Research* 35: 1–24.

Stuiver, M. and Pearson, G. W. 1993 High-precision calibration of the radiocarbon time scale, AD 1950–500 BC and 2500–6000 BC. *Radiocarbon*, this issue.

Stuiver, M., Pearson, G. W. and Braziunas, T.F. 1986 Radiocarbon age calibration of marine samples back to 9000 cal yr BP. *In* Stuiver, M. and Kra, R. S., eds., Proceedings of the 12th International ^{14}C Conference. *Radiocarbon* 28(2B): 980–1021.

Stuiver, M. and Polach, H. A. 1977 Discussion: Reporting of ^{14}C data. *Radiocarbon* 19(3): 355–363.

Stuiver, M. and Reimer, P. J. 1993 Extended ^{14}C data base and revised CALIB 3.0 radiocarbon age calibration program. *Radiocarbon*, this issue.

Talma, A. S. 1990 Radiocarbon age calibration of marine shells. Quarterly Report, Quaternary Dating Research Unit. Pretoria, CSIR: 10 pp.

Toggweiler, J. R. and Sarmiento, J. L. 1985 Glacial to interglacial changes in atmospheric carbon dioxide: The critical role of ocean surface water in high latitudes. *In* Sundquist, E. T. and Broecker, W. S., eds., *The Carbon Cycle and Atmospheric CO_2: –Natural Variations Archean to Present*. Washington D.C., American Geophysical Union. *Geophysical Monograph* 32: 163–184.

Vogel, J. C., Fuls, A., Visser, E. and Becker, B. 1993 Pretoria calibration curve for short-lived samples, 1930–3350 BC. *Radiocarbon*, this issue.
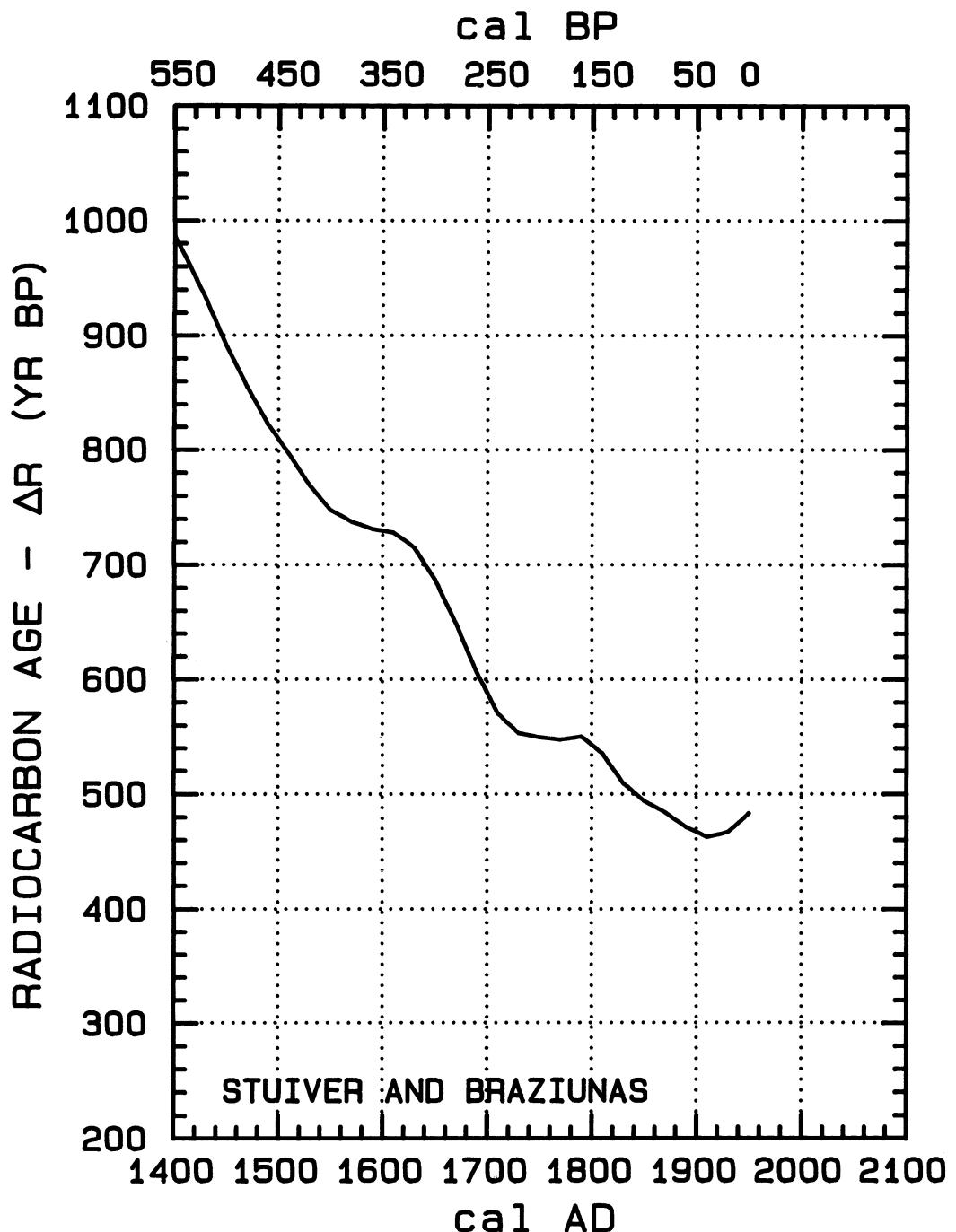
Fig. 17A–X. Calibration curves to be applied for marine (surface ocean) samples. Applicable ΔR values are discussed in the text, and depicted in Fig. 16.
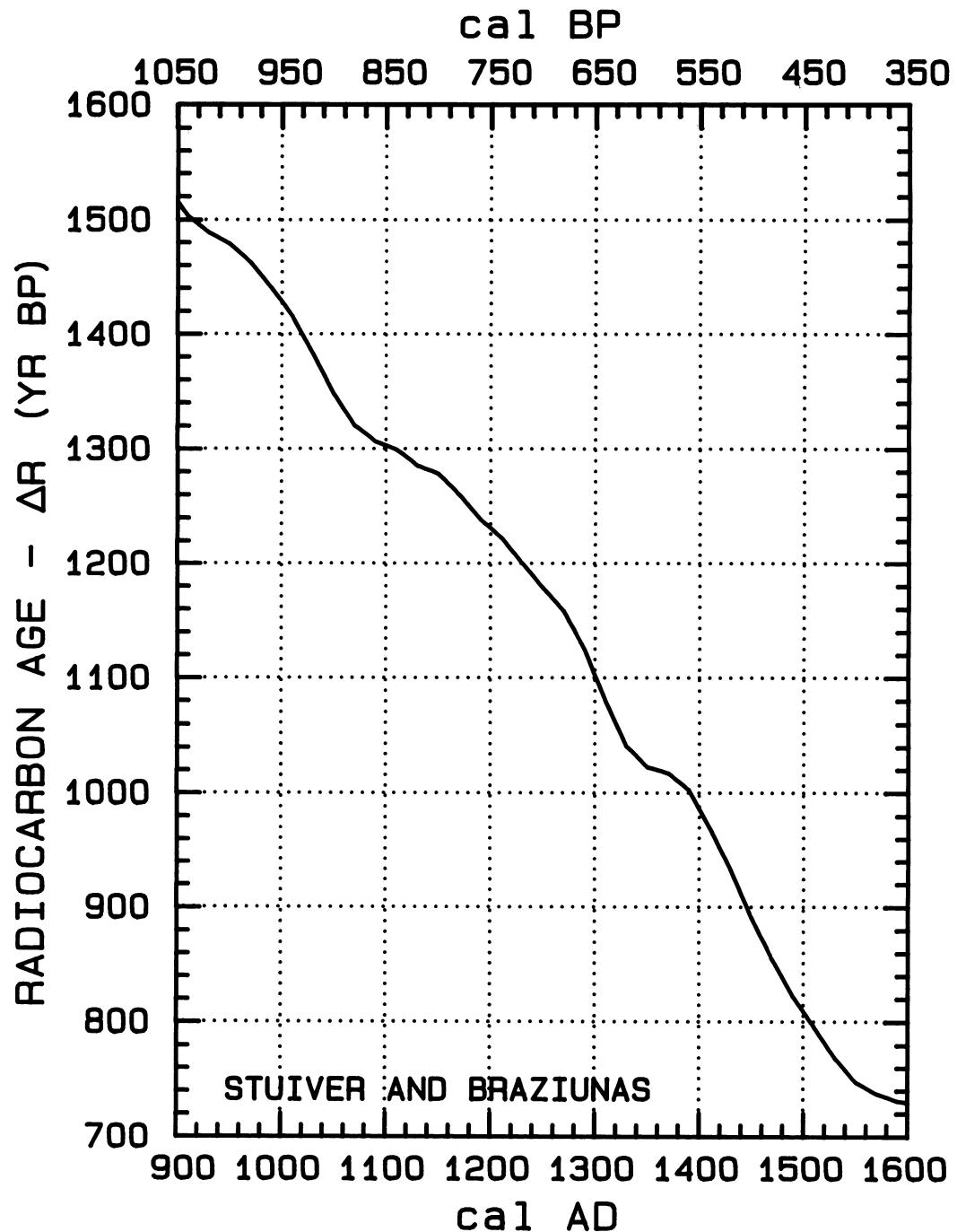
Fig. 17B
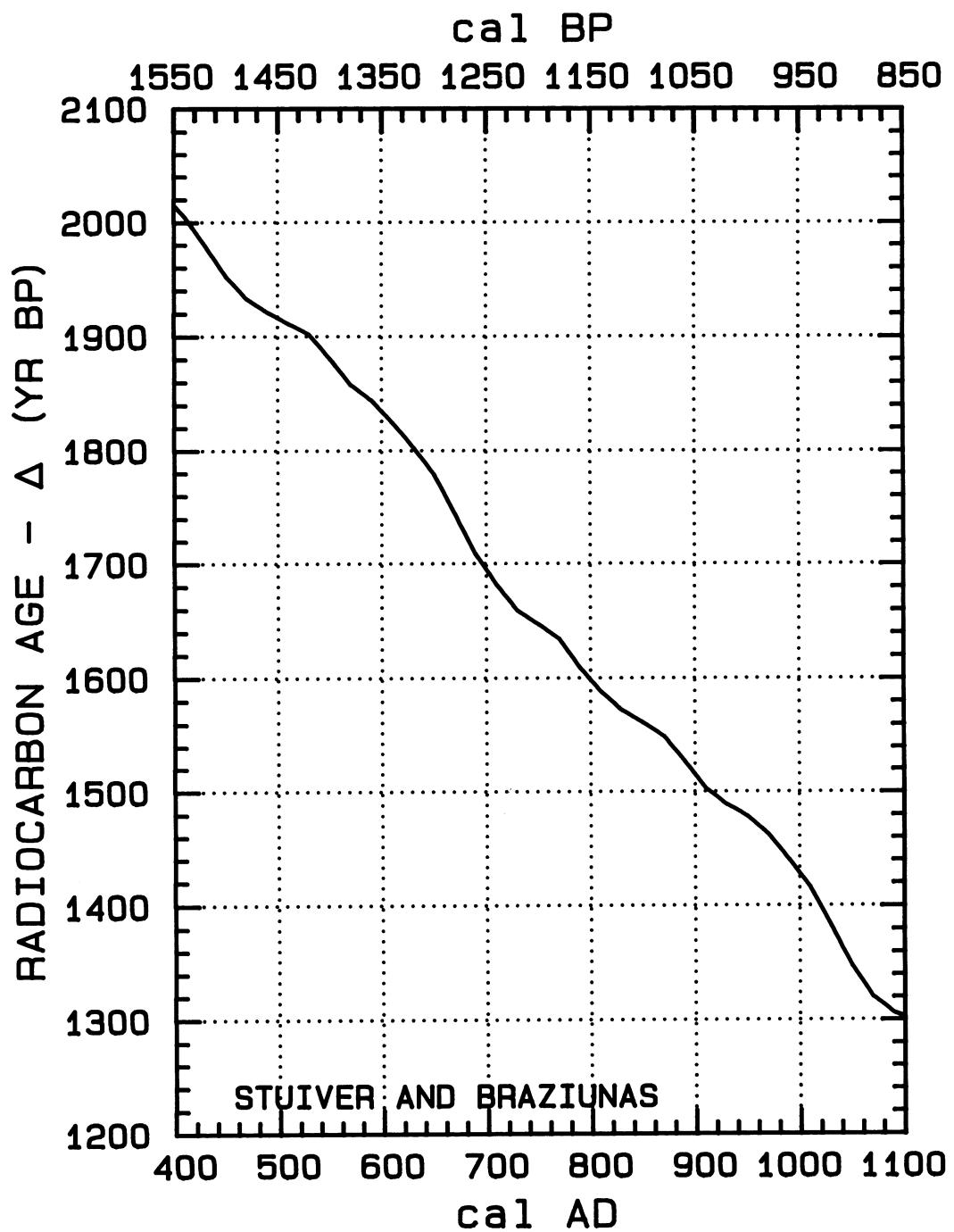
Fig. 17C
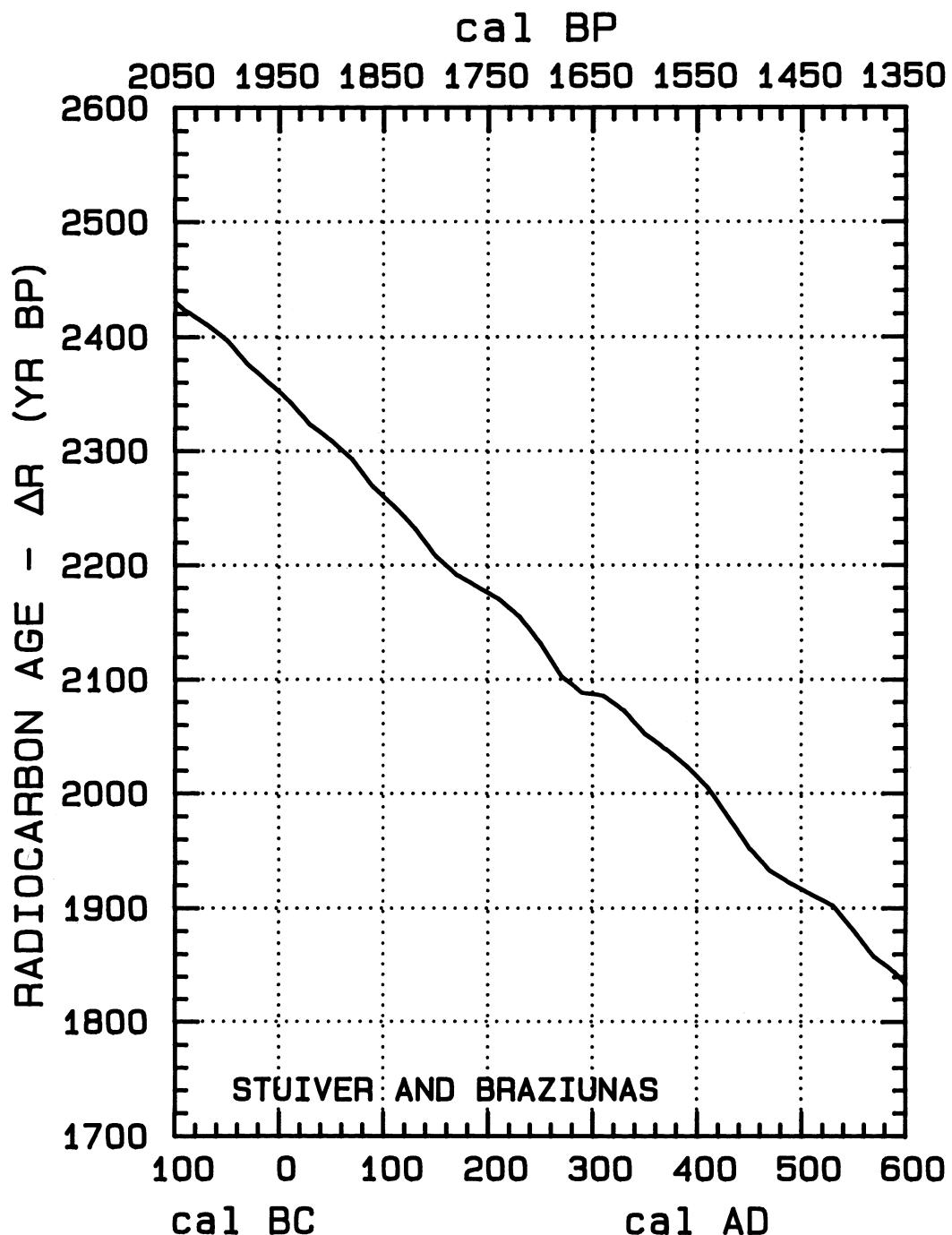
Fig. 17D
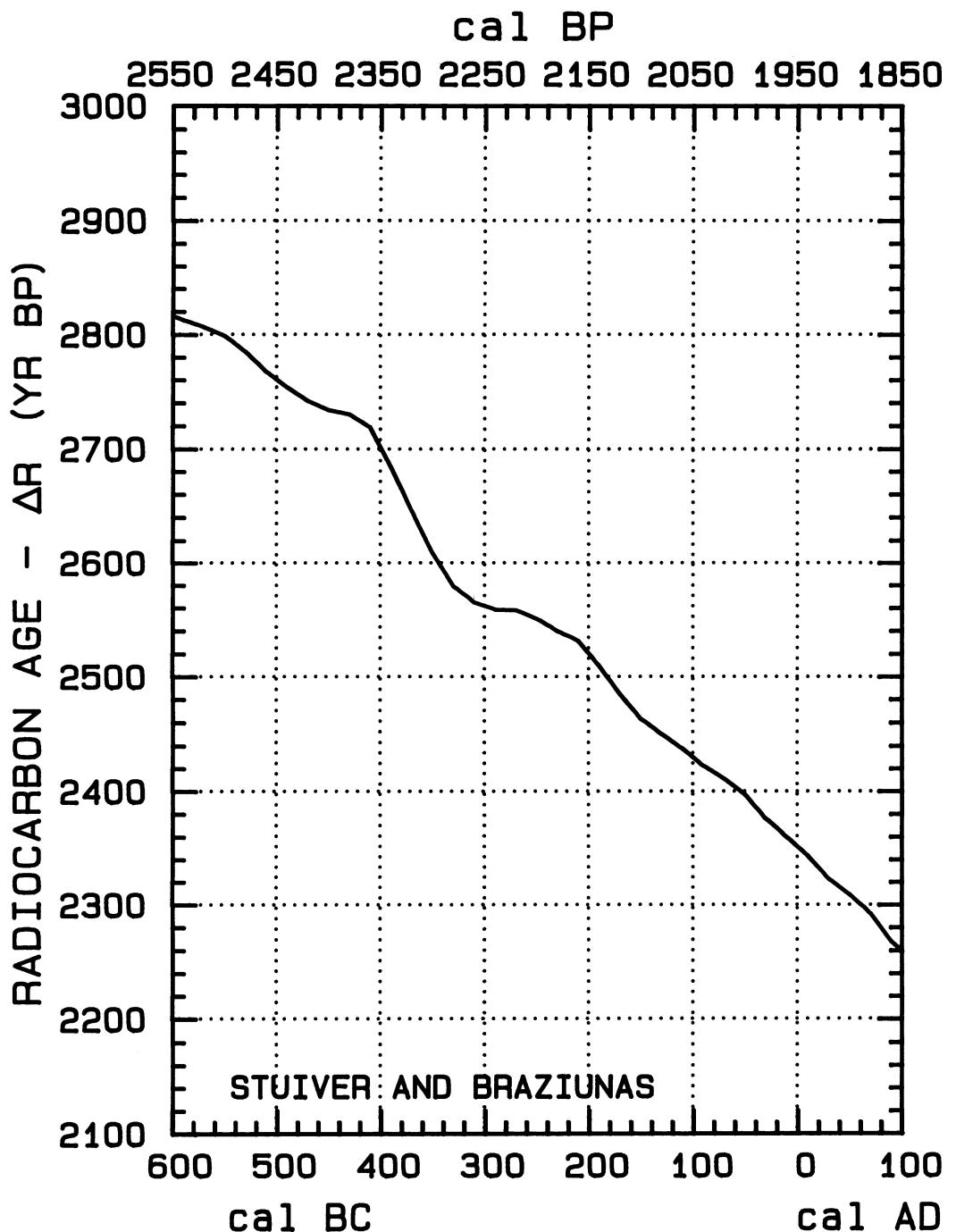
Fig. 17E
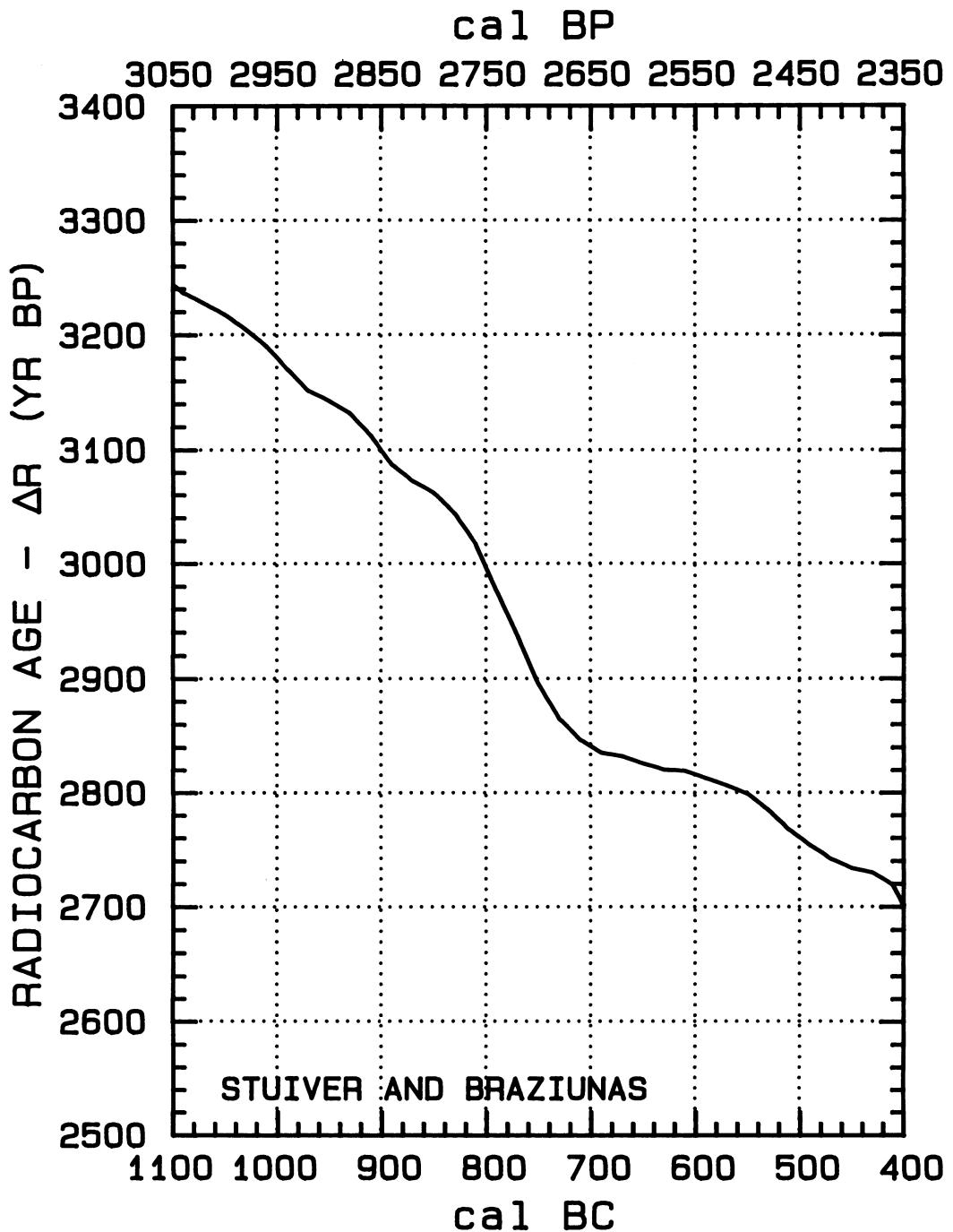
Fig. 17F
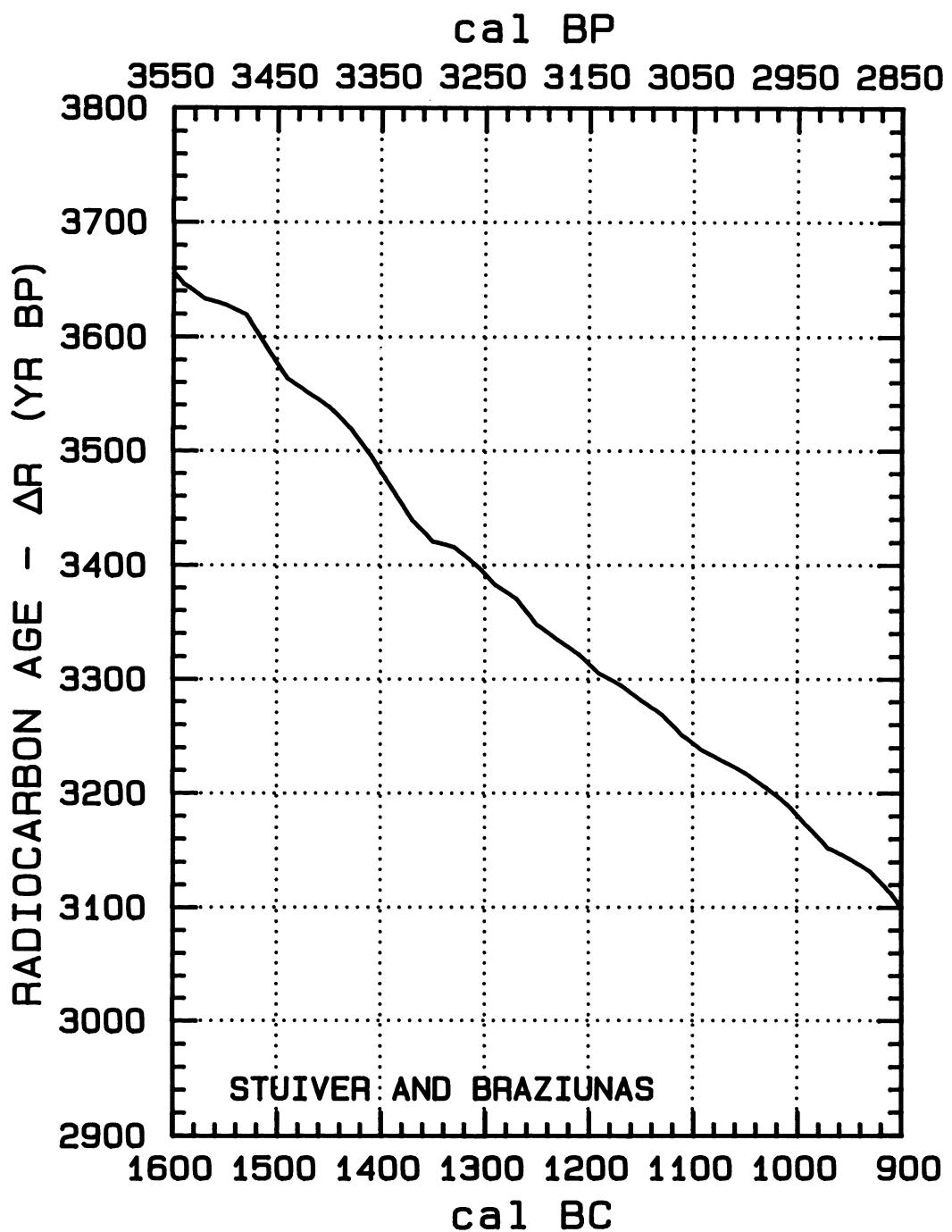
Fig. 17G
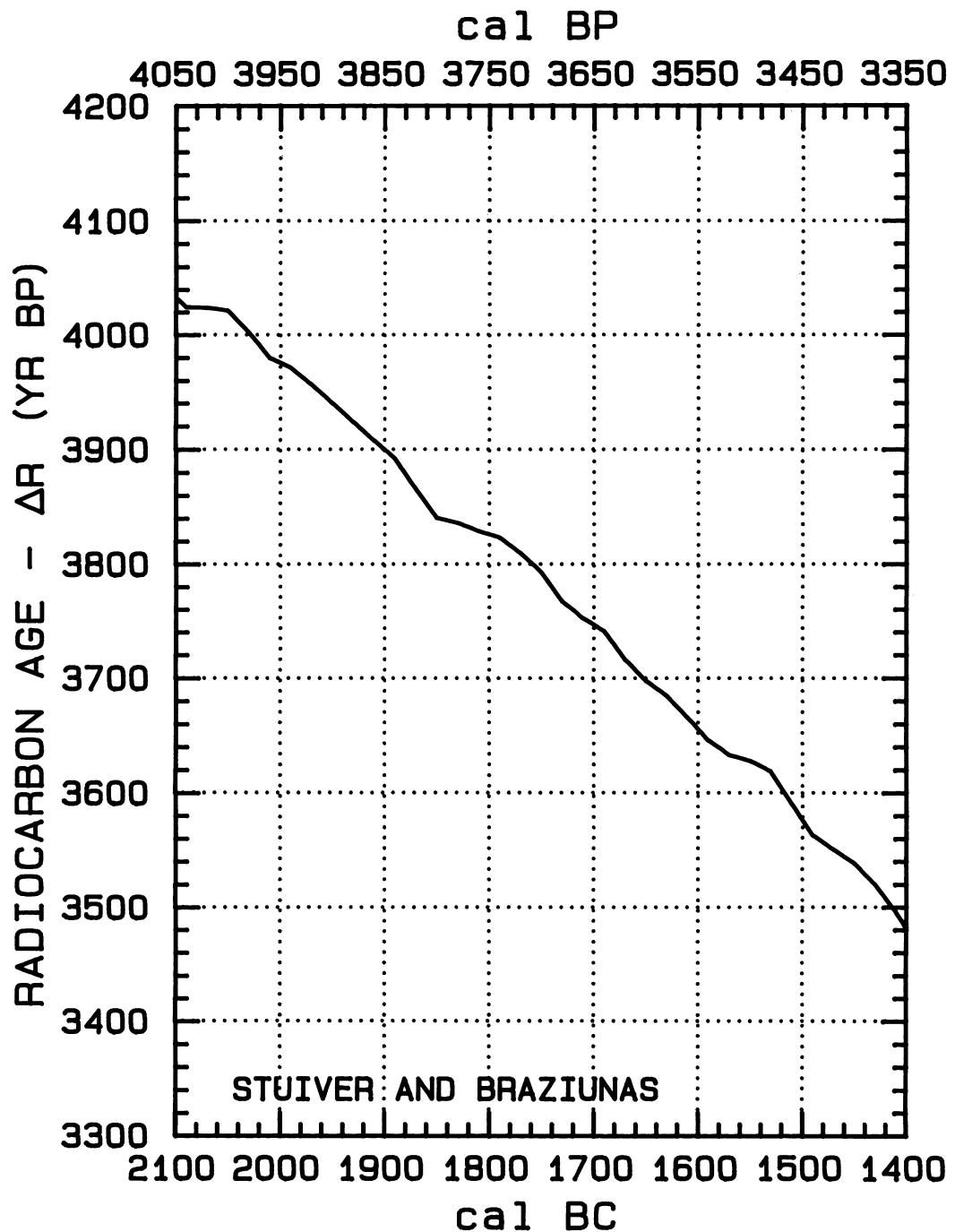
Fig. 17H
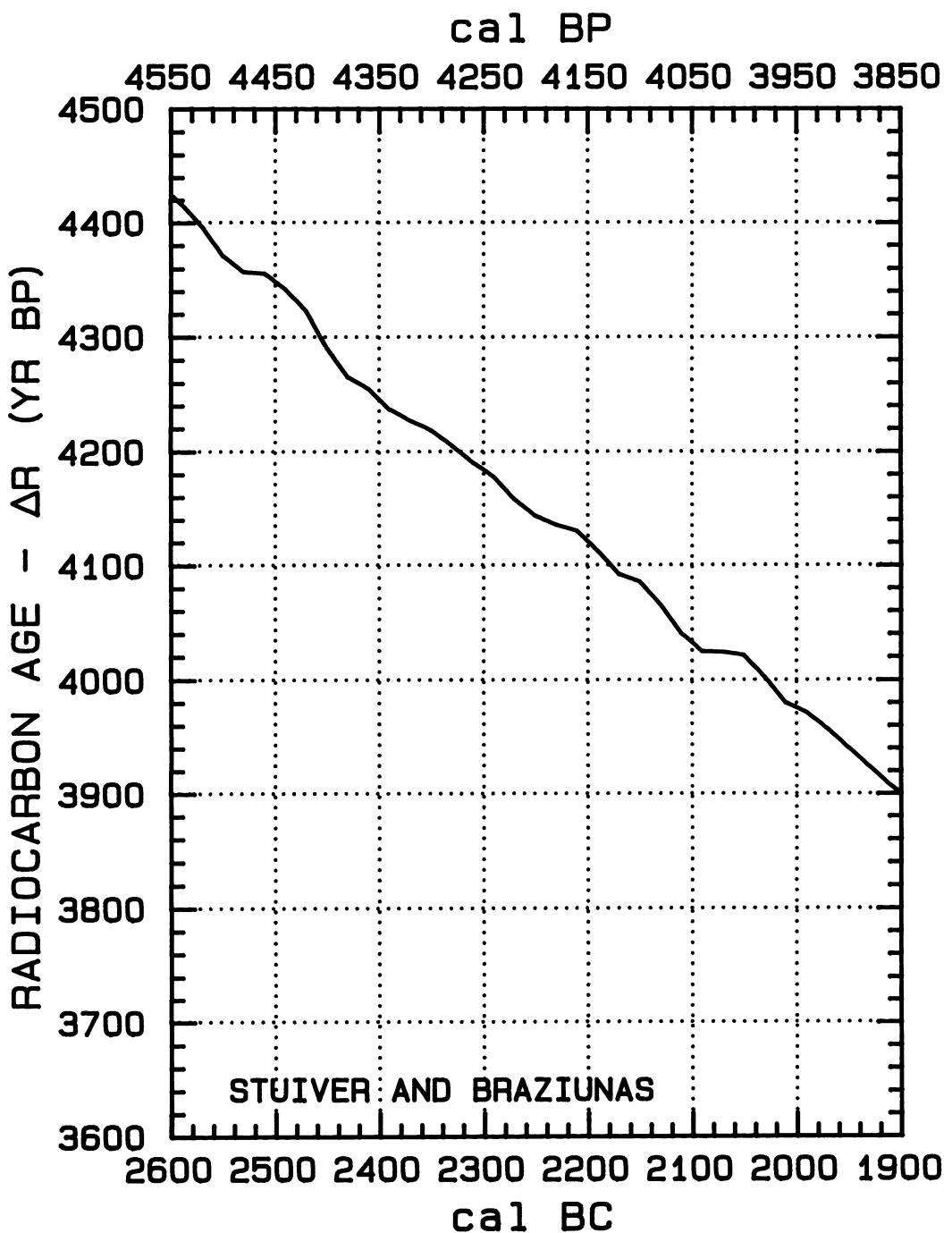
Fig. 17I
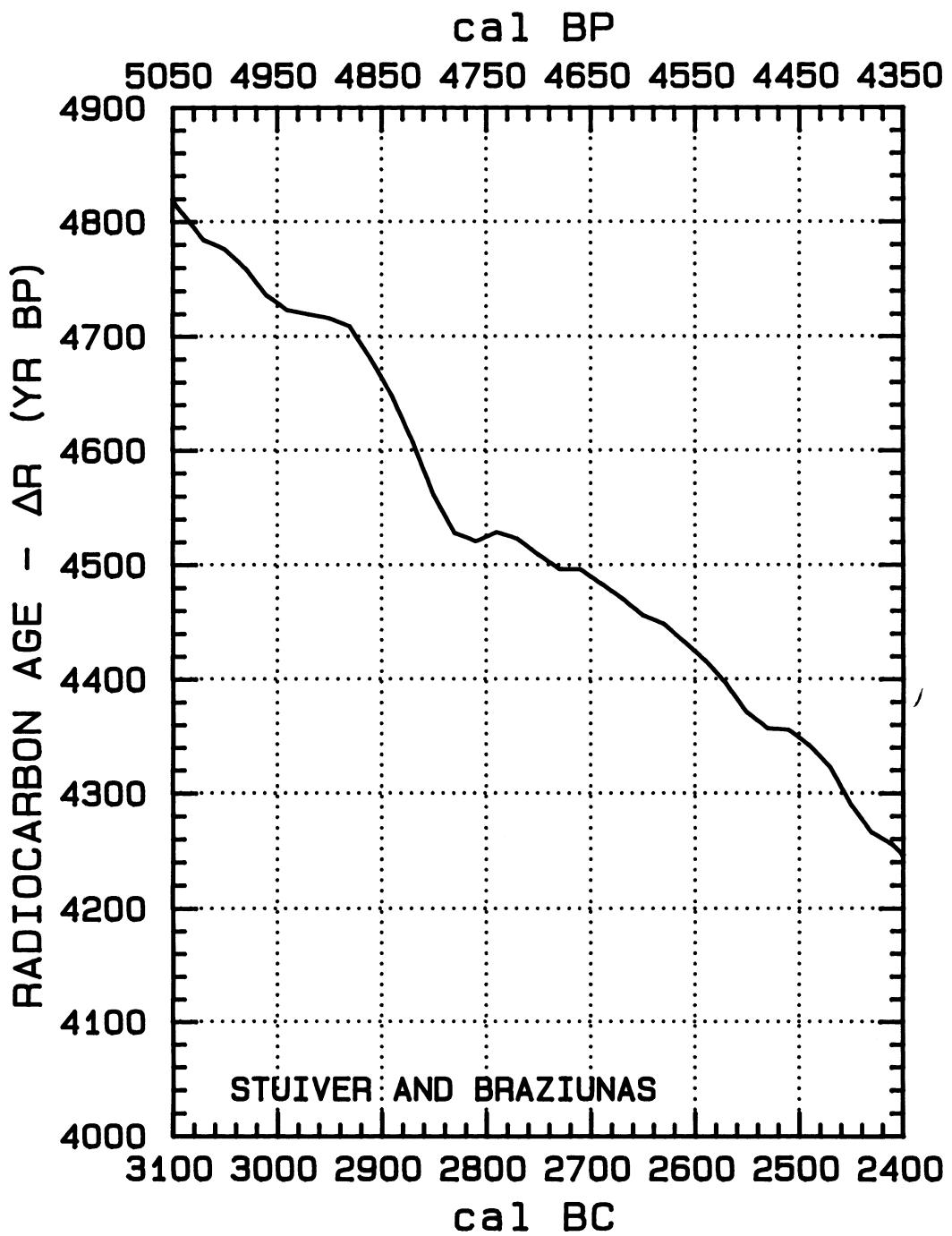
Fig. 17J
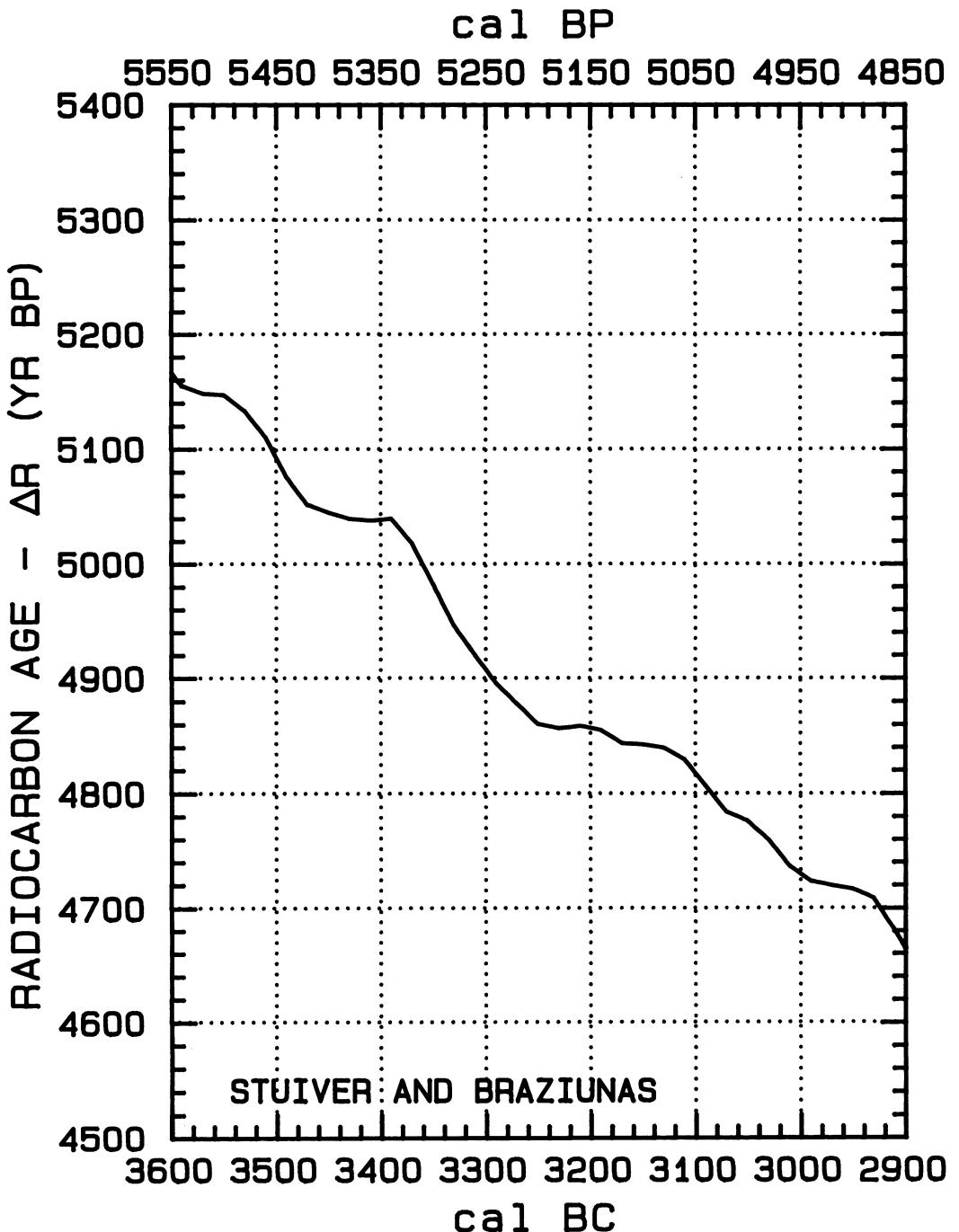
Fig. 17K
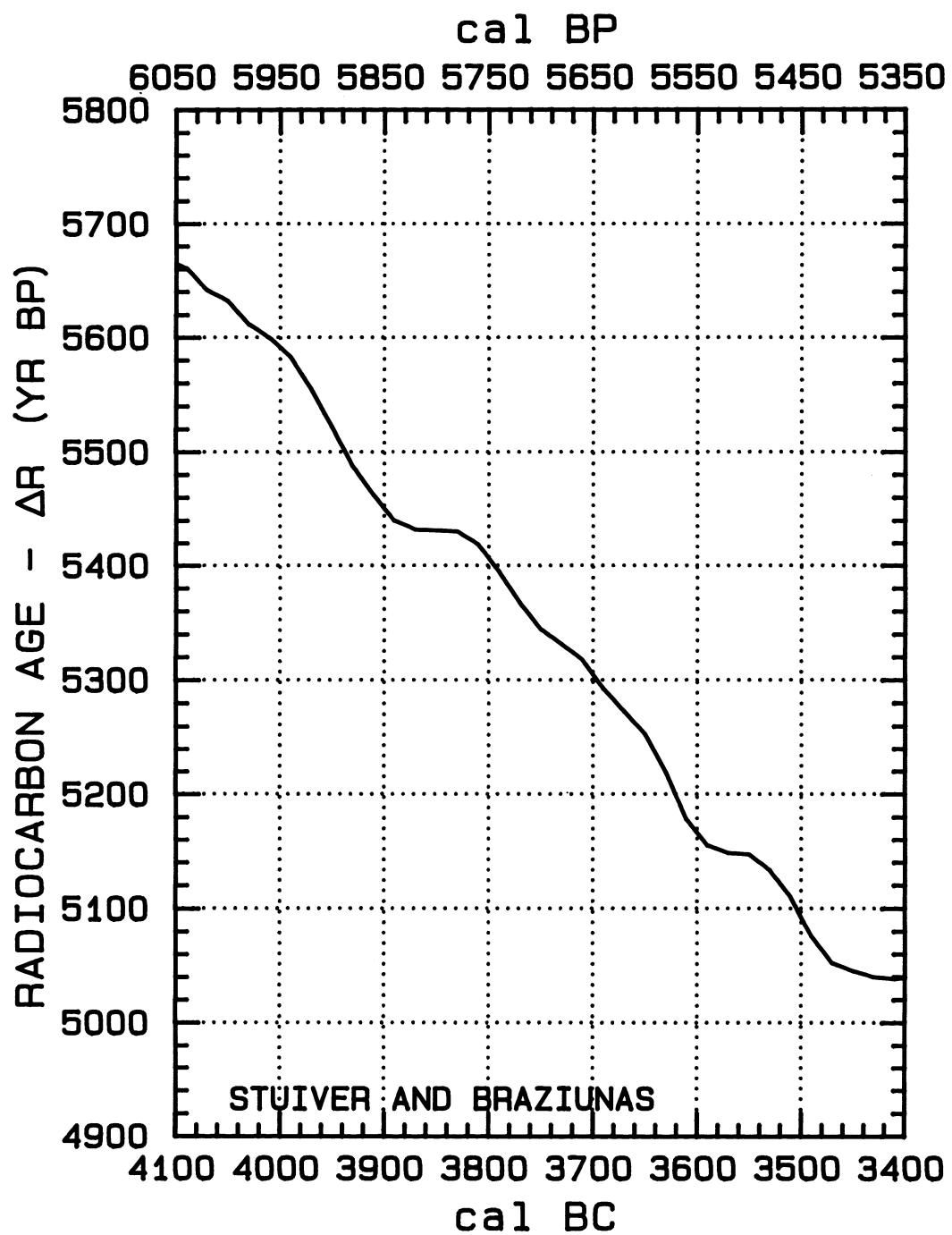
Fig. 17L
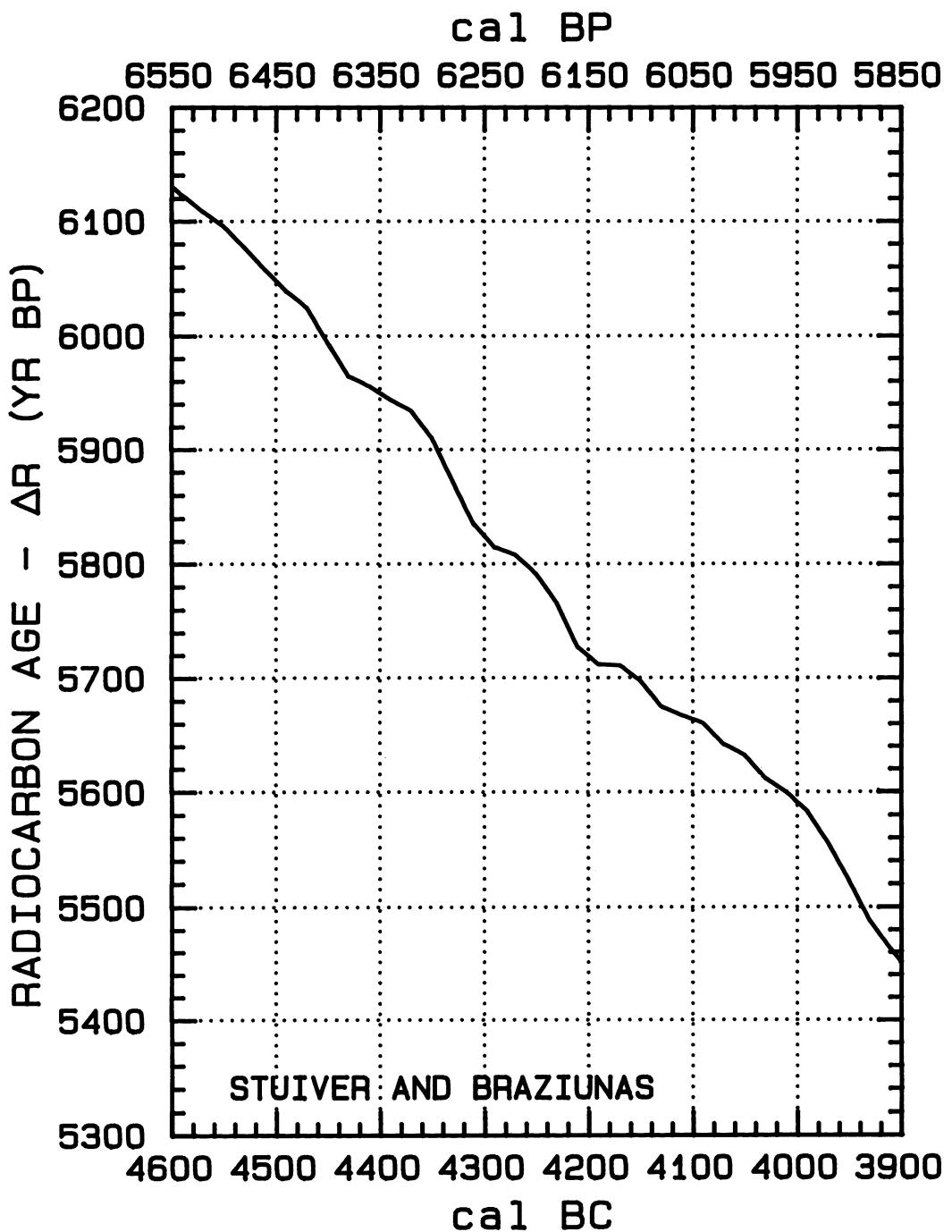
Fig. 17M
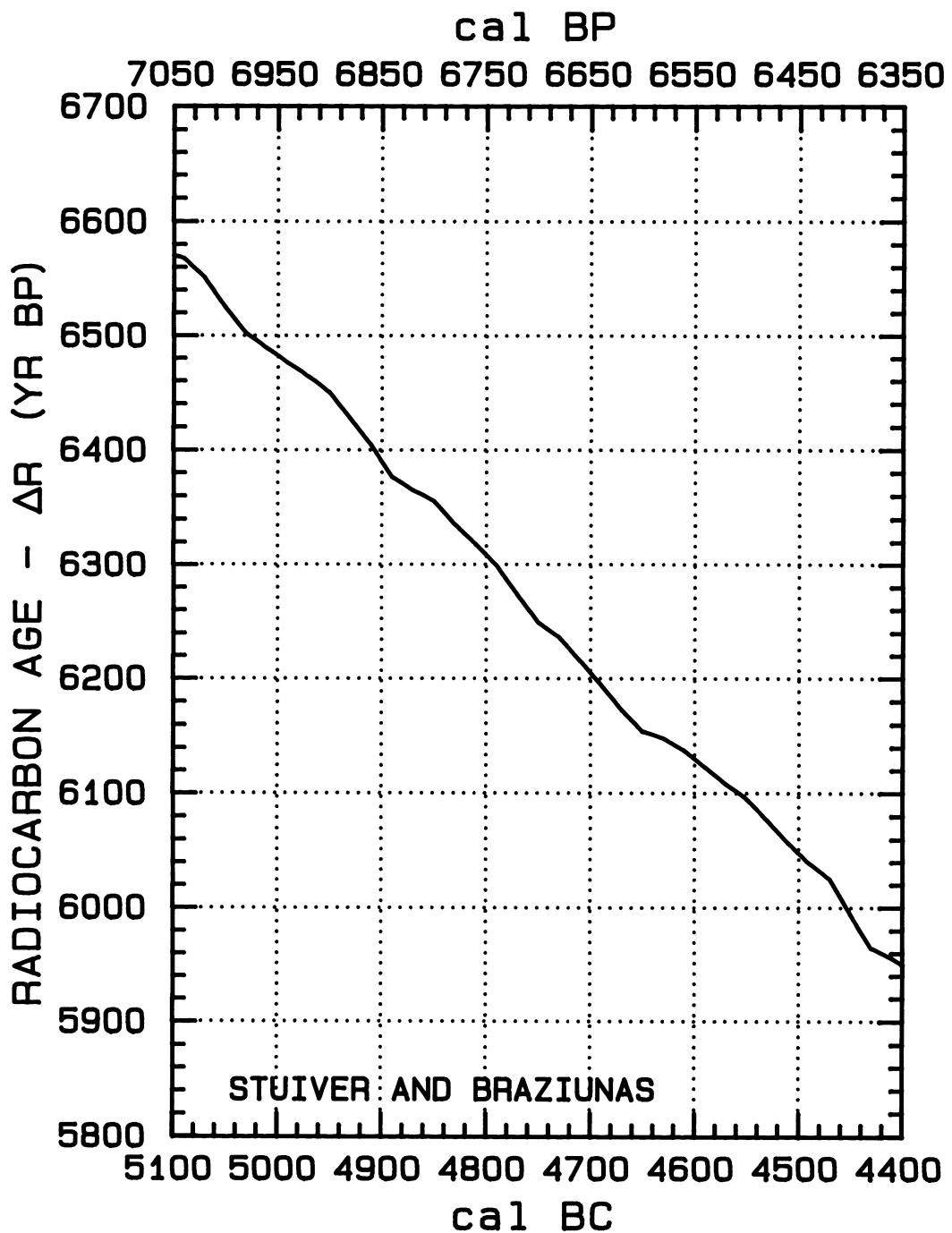
Fig. 17N
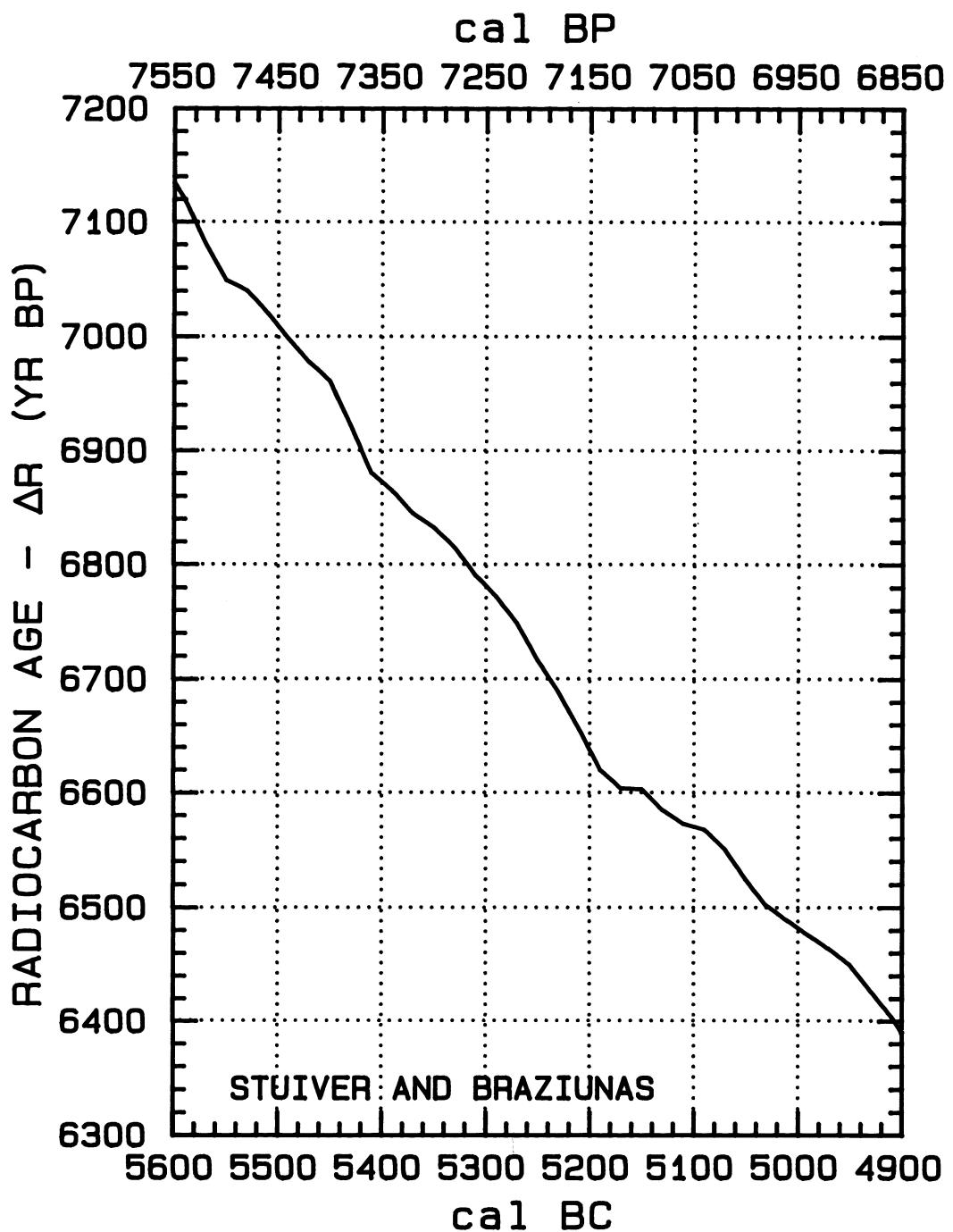
Fig. 17O
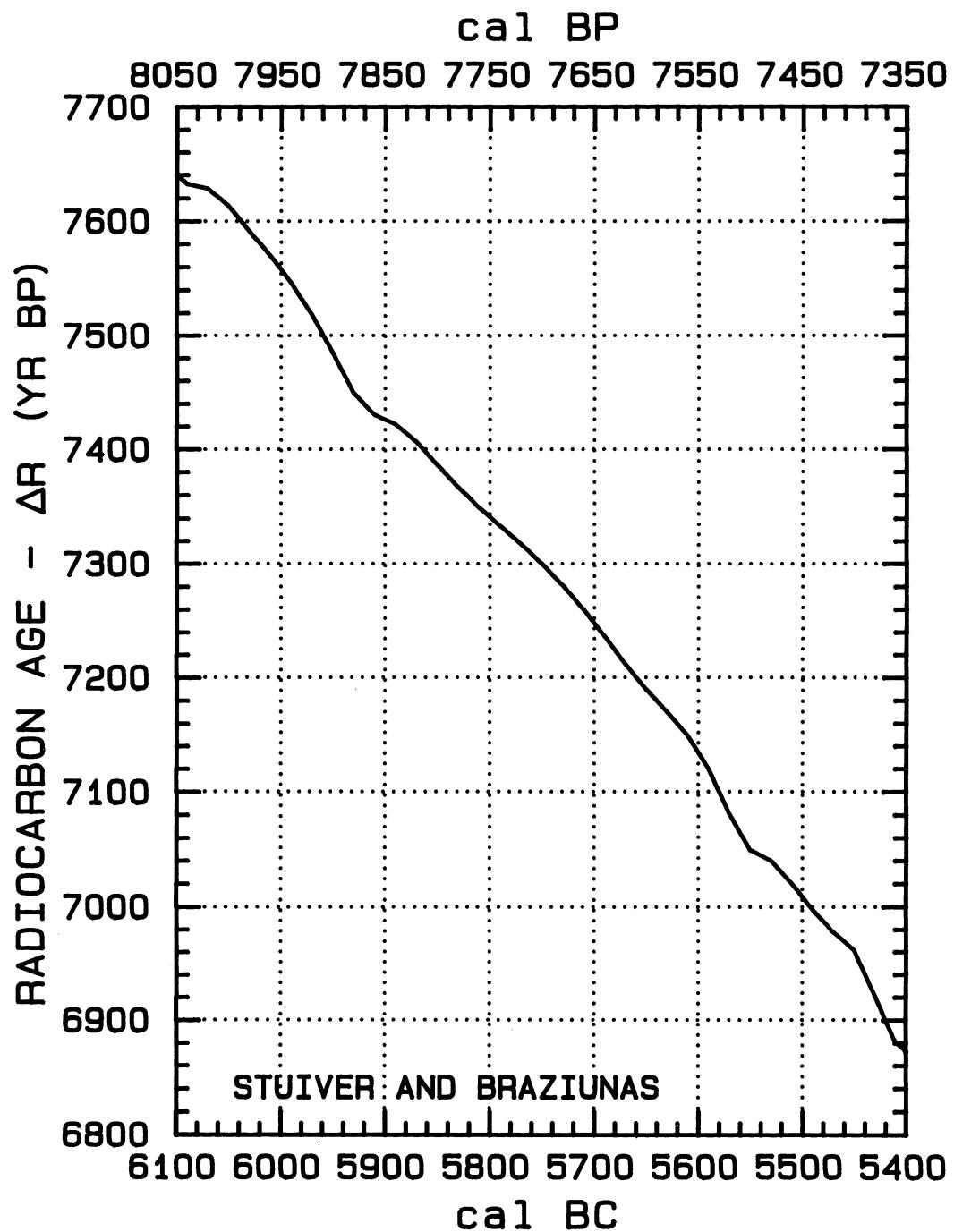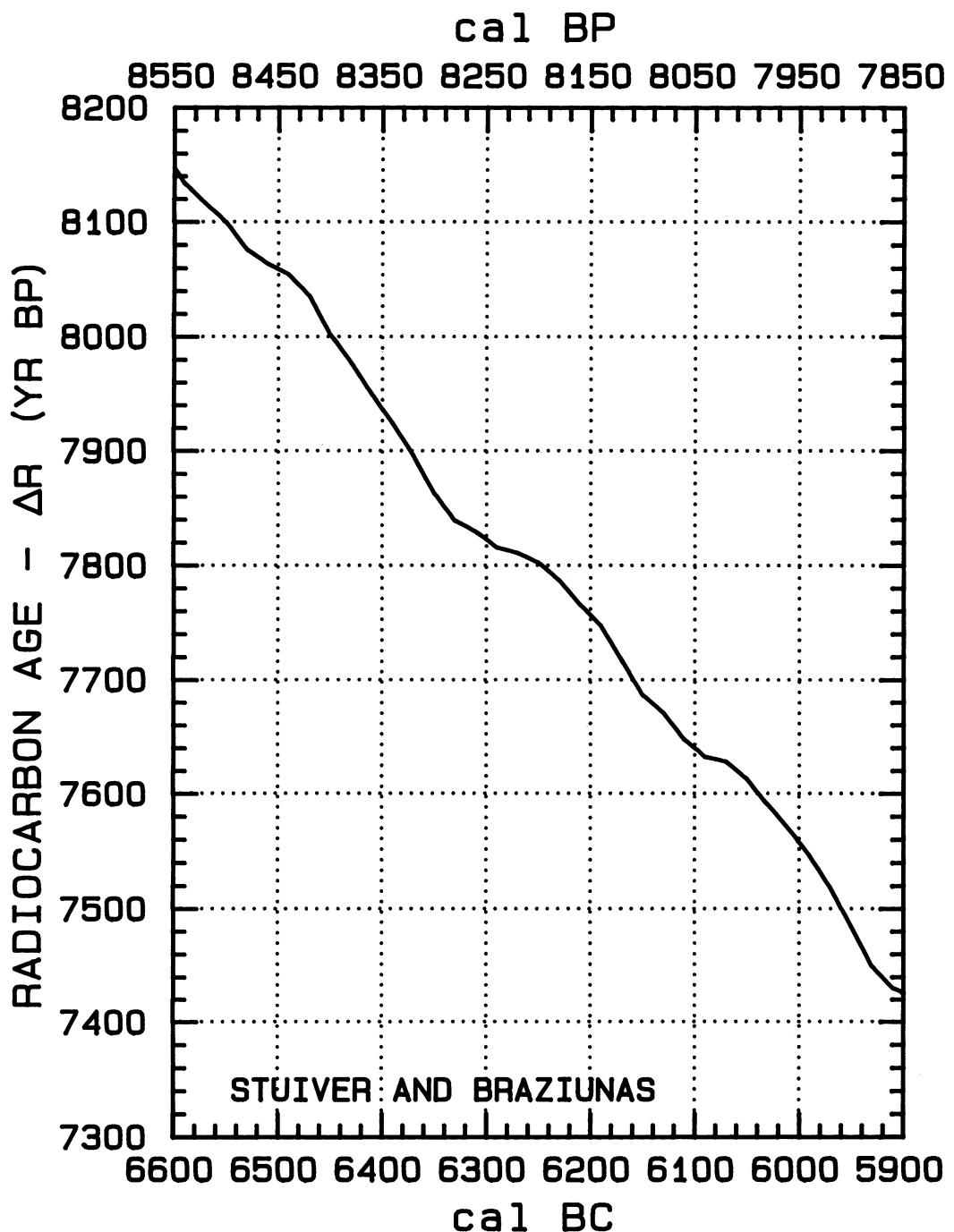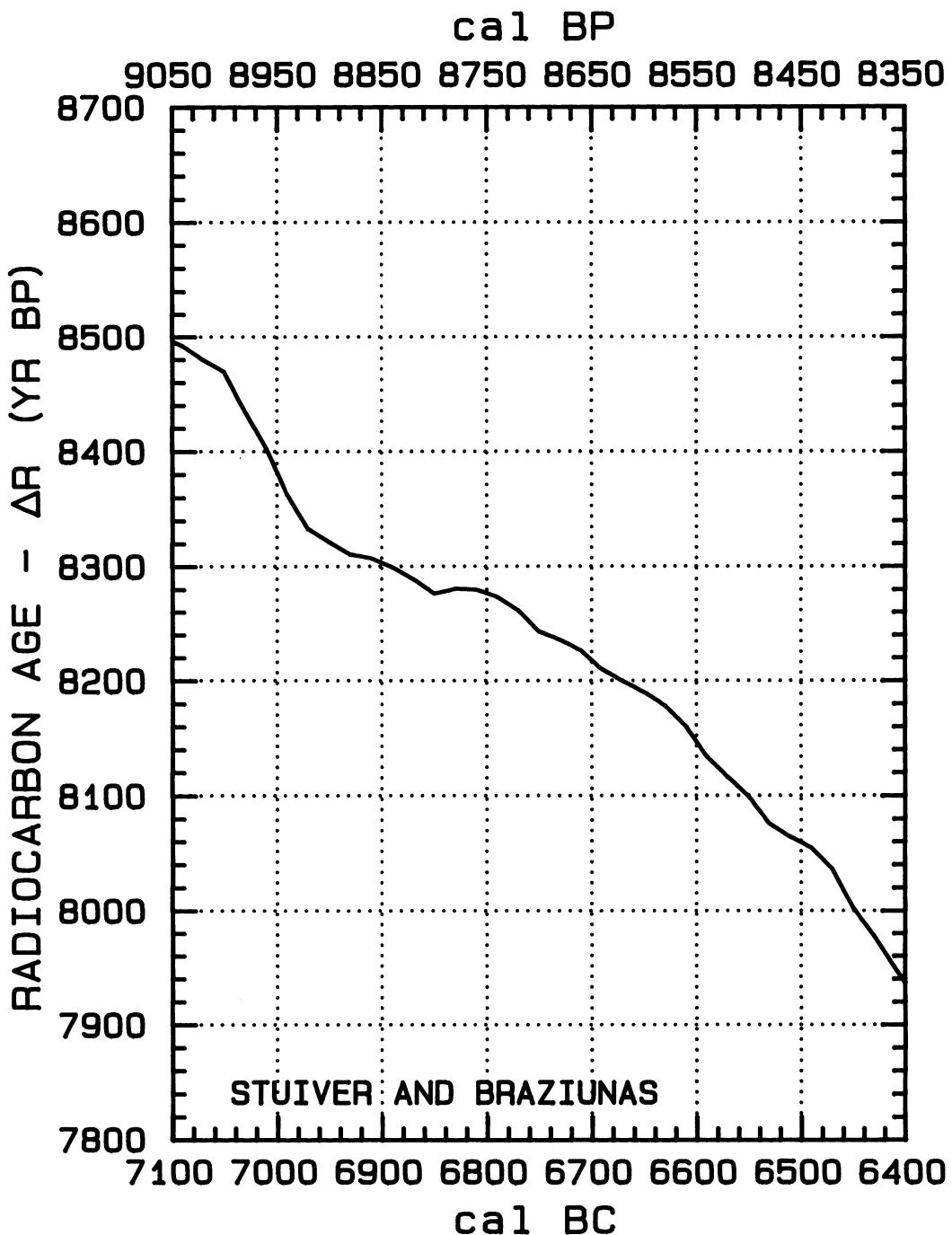
Fig. 17P

Fig. 17Q

Fig. 17R
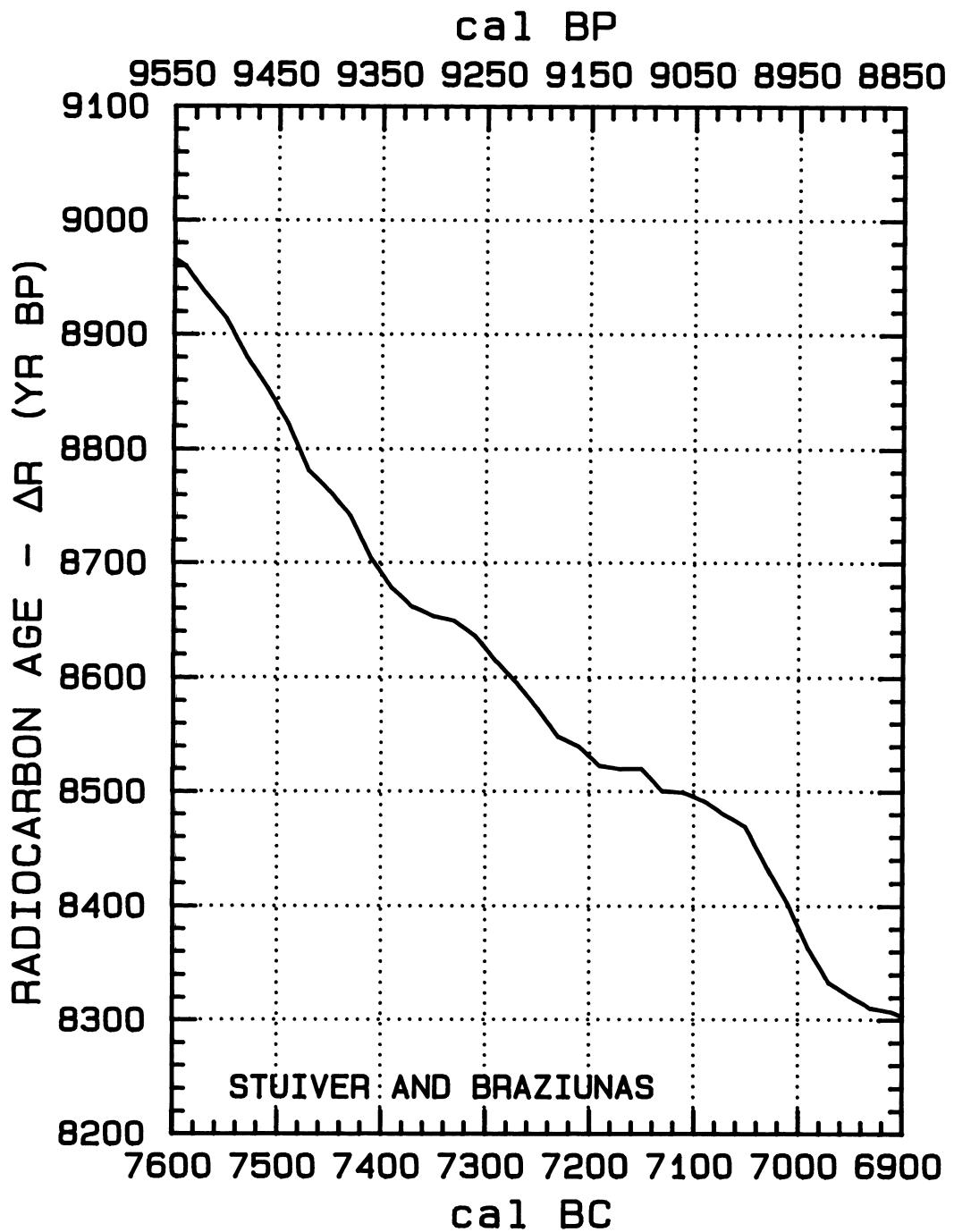
Fig. 17S
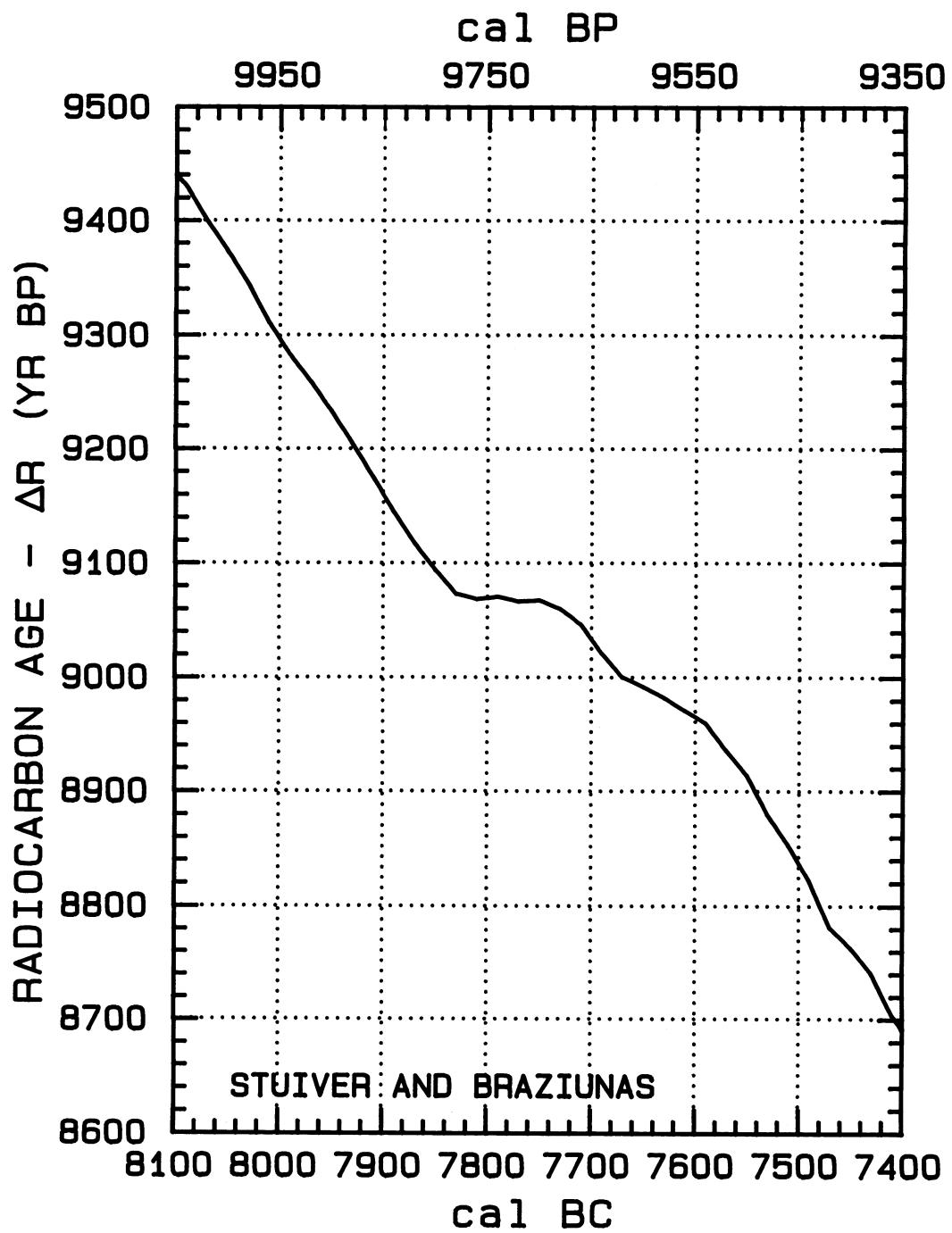
Fig. 17T
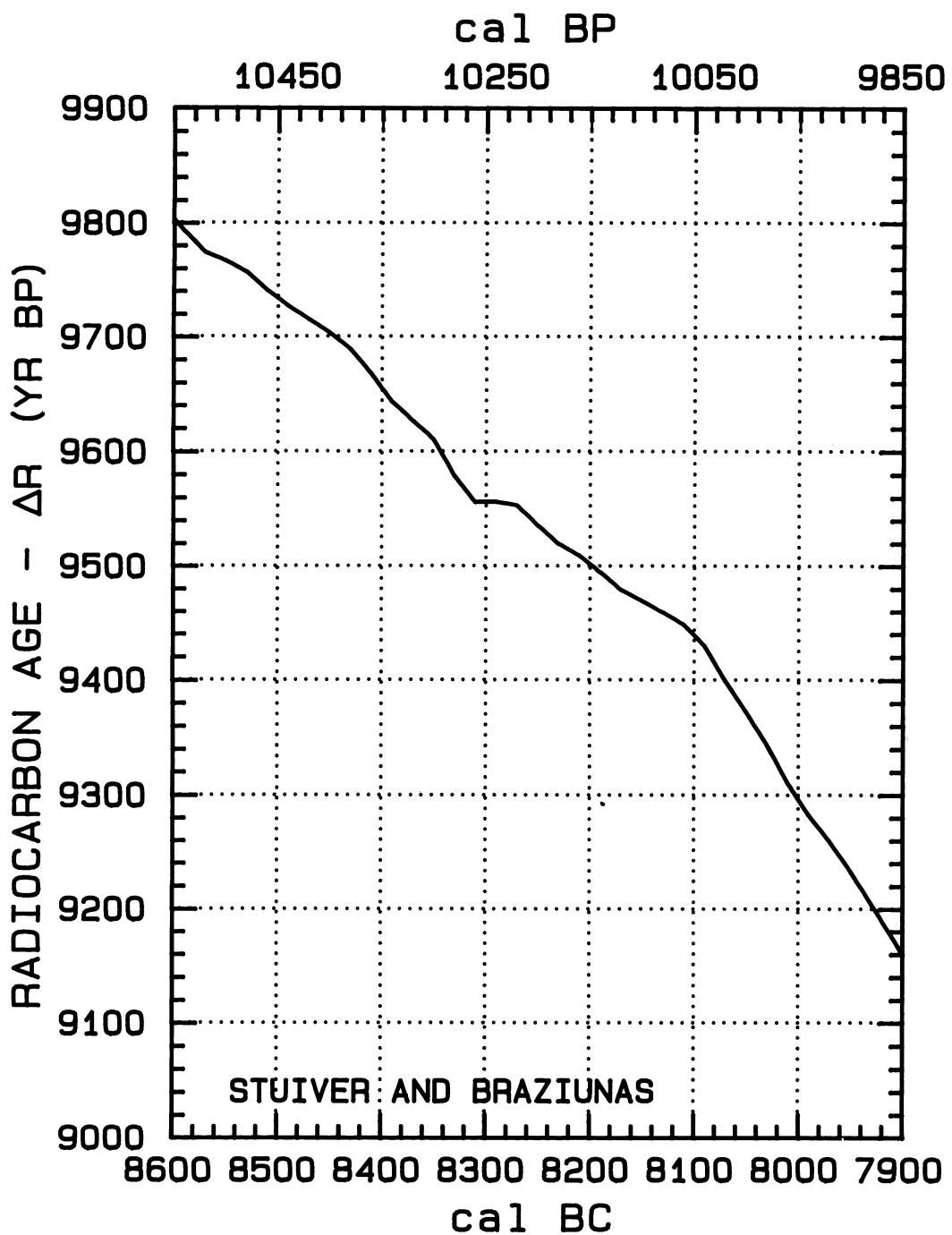
Fig. 17U
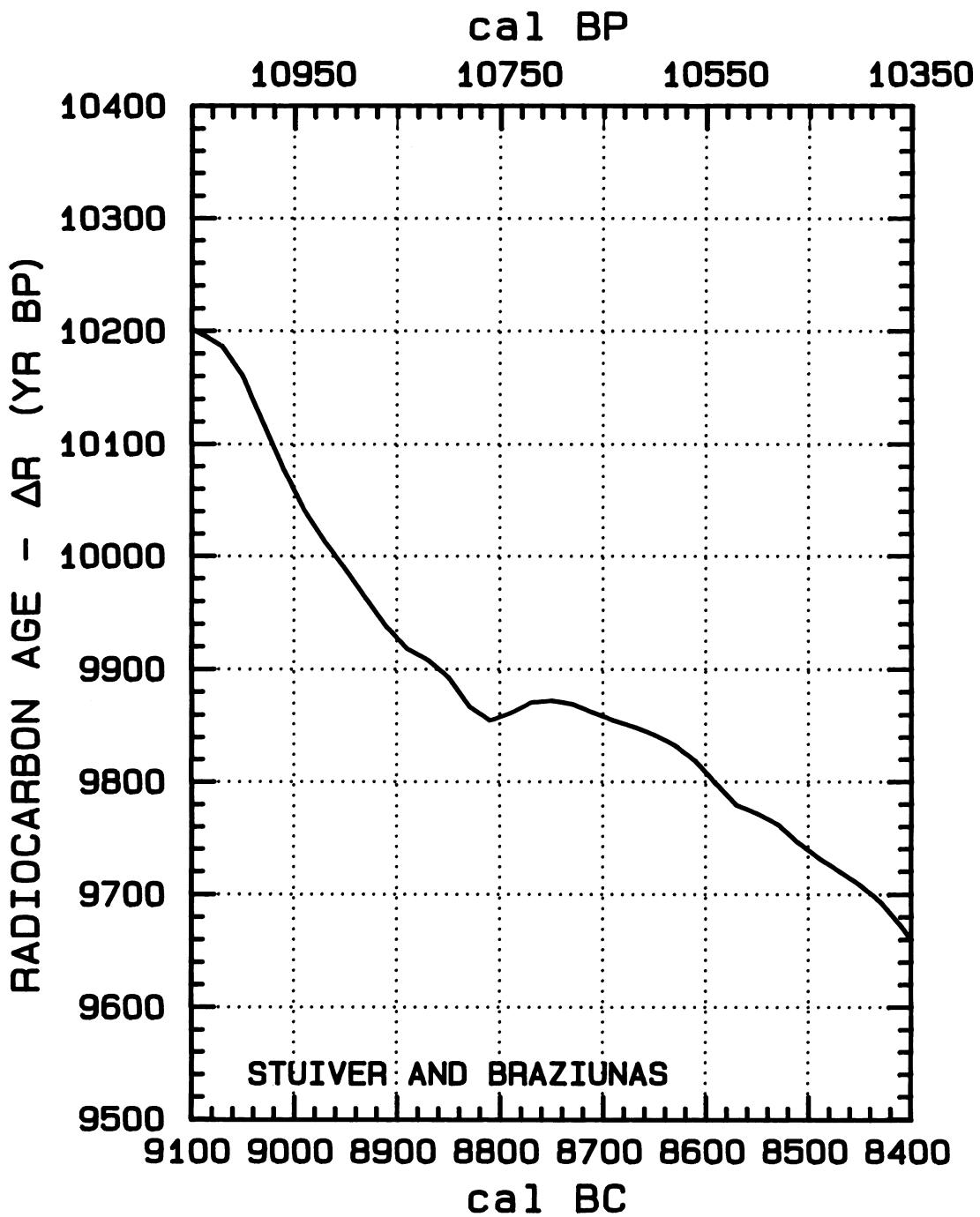
Fig. 17V
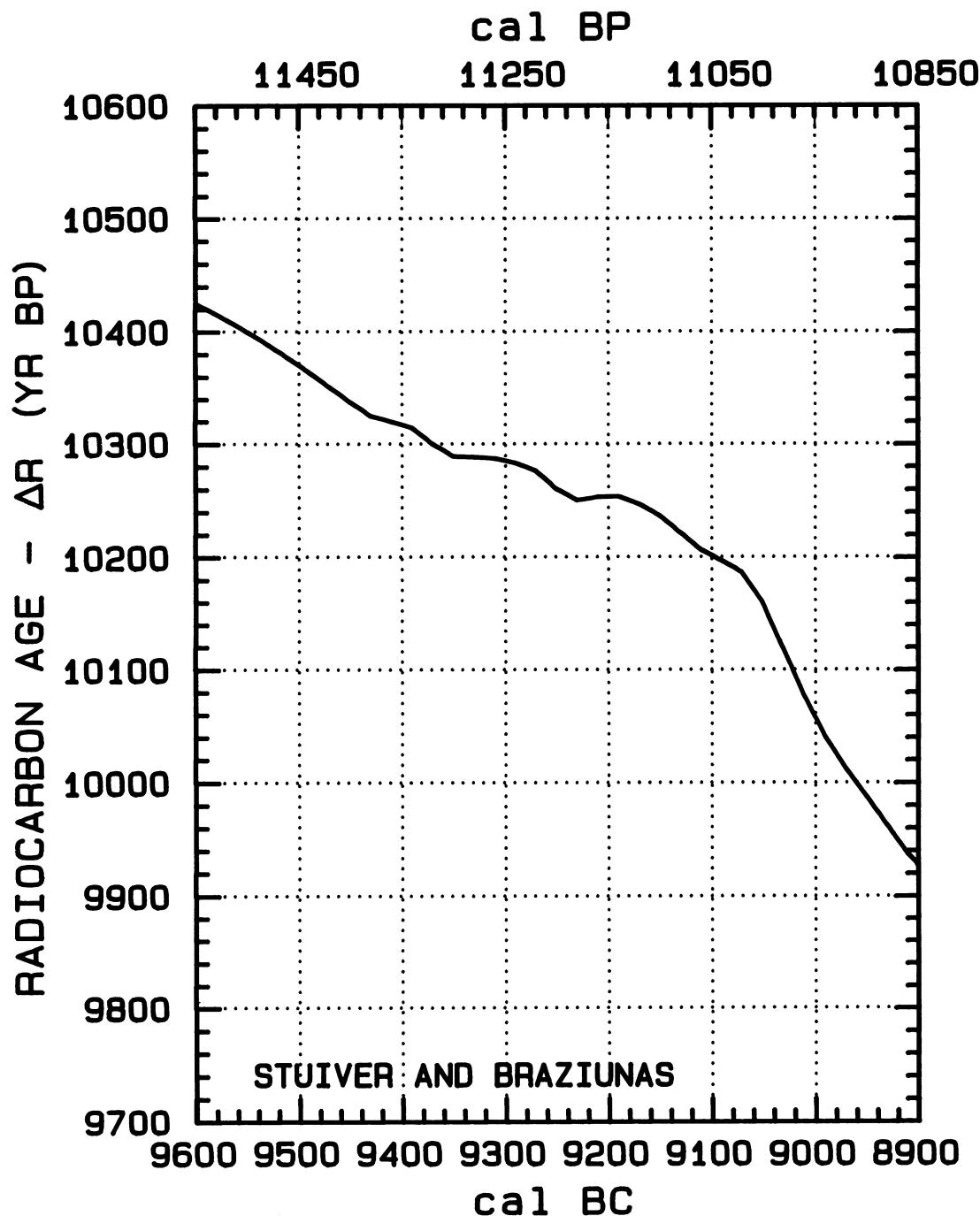
Fig. 17W
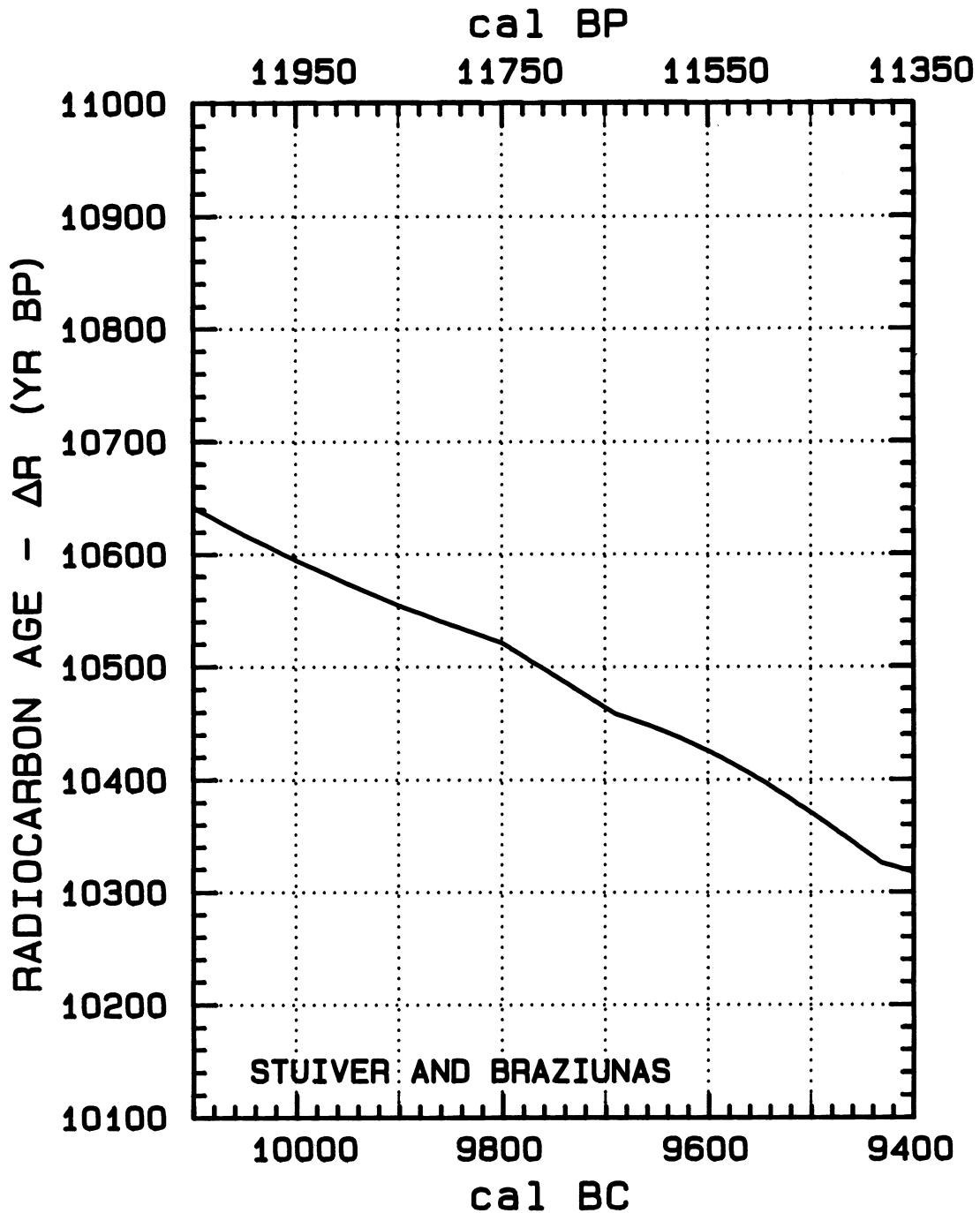
Fig. 17X

TABLE 1. Marine model ^{14}C ages ($\approx$460–10,600 ^{14}C yr BP) calculated from the bidecadal atmospheric tree-ring data from AD 1950–9440 BC and a smoothing spline through coral data to 20,000 BC (Bard *et al.*, 1993; Stuiver & Reimer 1993). The pre-10,000 BC part of the spline was only used as a model start-up. The standard deviations in the ages and Δ^{14}C values reflect the standard deviations in the tree-ring and coral data.

Cal AD/BC	Δ^{14}C ‰	^{14}C age (BP)	Cal BP	Cal AD/BC	Δ^{14}C ‰	^{14}C age (BP)	Cal BP
AD 1950	−58.4 ± 1.6	483 ± 13	BP 0	AD 1090	−56.9 ± .9	1306 ± 8	BP 860
AD 1930	−54.2 ± .5	467 ± 4	BP 20	AD 1070	−56.2 ± .9	1320 ± 7	BP 880
AD 1910	−51.3 ± .6	462 ± 5	BP 40	AD 1050	−57.2 ± 1.0	1347 ± 9	BP 900
AD 1890	−50.1 ± .6	471 ± 5	BP 60	AD 1030	−59.0 ± 1.2	1383 ± 10	BP 920
AD 1870	−49.3 ± .5	484 ± 4	BP 80	AD 1010	−60.6 ± 1.2	1416 ± 11	BP 940
AD 1850	−48.2 ± .5	494 ± 4	BP 100	AD 990	−61.1 ± 1.1	1440 ± 9	BP 960
AD 1830	−47.7 ± .6	509 ± 5	BP 120	AD 970	−61.5 ± 1.2	1462 ± 10	BP 980
AD 1810	−48.5 ± .5	535 ± 4	BP 140	AD 950	−61.1 ± 1.5	1479 ± 12	BP 1000
AD 1790	−47.9 ± .5	550 ± 5	BP 160	AD 930	−60.1 ± 1.4	1489 ± 12	BP 1020
AD 1770	−45.3 ± .5	547 ± 4	BP 180	AD 910	−59.4 ± 1.2	1503 ± 10	BP 1040
AD 1750	−43.2 ± .4	549 ± 4	BP 200	AD 890	−60.0 ± 1.2	1527 ± 11	BP 1060
AD 1730	−41.3 ± .5	553 ± 4	BP 220	AD 870	−60.3 ± 1.3	1549 ± 11	BP 1080
AD 1710	−41.1 ± .3	570 ± 3	BP 240	AD 850	−59.4 ± 1.2	1561 ± 10	BP 1100
AD 1690	−43.0 ± .4	606 ± 3	BP 260	AD 830	−58.4 ± 1.3	1572 ± 11	BP 1120
AD 1670	−45.9 ± .5	649 ± 4	BP 280	AD 810	−58.0 ± 1.3	1588 ± 11	BP 1140
AD 1650	−48.0 ± .5	687 ± 4	BP 300	AD 790	−58.2 ± 1.0	1609 ± 9	BP 1160
AD 1630	−49.1 ± .5	715 ± 4	BP 320	AD 770	−58.9 ± 1.1	1634 ± 10	BP 1180
AD 1610	−48.3 ± .5	728 ± 4	BP 340	AD 750	−58.1 ± 1.0	1647 ± 8	BP 1200
AD 1590	−46.3 ± .5	731 ± 5	BP 360	AD 730	−57.2 ± 1.0	1659 ± 8	BP 1220
AD 1570	−44.8 ± .5	737 ± 5	BP 380	AD 710	−57.6 ± 1.1	1681 ± 9	BP 1240
AD 1550	−43.7 ± .5	747 ± 4	BP 400	AD 690	−58.4 ± 1.7	1708 ± 15	BP 1260
AD 1530	−43.9 ± .5	769 ± 4	BP 420	AD 670	−60.4 ± 1.7	1744 ± 14	BP 1280
AD 1510	−44.8 ± .6	796 ± 5	BP 440	AD 650	−62.2 ± 1.3	1779 ± 12	BP 1300
AD 1490	−45.6 ± 1.3	822 ± 11	BP 460	AD 630	−62.7 ± 1.5	1803 ± 13	BP 1320
AD 1470	−47.2 ± 1.6	855 ± 13	BP 480	AD 610	−63.0 ± 1.8	1825 ± 15	BP 1340
AD 1450	−49.2 ± 1.2	891 ± 11	BP 500	AD 590	−63.0 ± 1.6	1844 ± 14	BP 1360
AD 1430	−51.8 ± 1.5	933 ± 13	BP 520	AD 570	−62.3 ± 1.7	1858 ± 14	BP 1380
AD 1410	−53.8 ± 1.4	969 ± 12	BP 540	AD 550	−62.7 ± 1.5	1881 ± 13	BP 1400
AD 1390	−55.5 ± 1.2	1003 ± 10	BP 560	AD 530	−62.9 ± 1.3	1902 ± 12	BP 1420
AD 1370	−54.9 ± 1.2	1017 ± 10	BP 580	AD 510	−61.7 ± 1.5	1911 ± 13	BP 1440
AD 1350	−53.2 ± 1.3	1022 ± 11	BP 600	AD 490	−60.6 ± 1.5	1921 ± 13	BP 1460
AD 1330	−53.1 ± 1.1	1041 ± 10	BP 620	AD 470	−59.7 ± 1.6	1933 ± 14	BP 1480
AD 1310	−55.4 ± 1.1	1080 ± 9	BP 640	AD 450	−59.7 ± 1.6	1952 ± 14	BP 1500
AD 1290	−58.4 ± 1.3	1125 ± 11	BP 660	AD 430	−60.6 ± 1.5	1979 ± 13	BP 1520
AD 1270	−60.0 ± 2.3	1158 ± 20	BP 680	AD 410	−61.4 ± 1.6	2005 ± 14	BP 1540
AD 1250	−60.1 ± 2.3	1178 ± 19	BP 700	AD 390	−61.3 ± 1.3	2024 ± 11	BP 1560
AD 1230	−60.4 ± 1.0	1200 ± 9	BP 720	AD 370	−60.8 ± 1.3	2039 ± 11	BP 1580
AD 1210	−60.8 ± 1.5	1223 ± 13	BP 740	AD 350	−60.0 ± 1.6	2052 ± 14	BP 1600
AD 1190	−60.3 ± 1.4	1239 ± 12	BP 760	AD 330	−60.1 ± 1.7	2072 ± 14	BP 1620
AD 1170	−60.5 ± 1.0	1260 ± 9	BP 780	AD 310	−59.4 ± 1.6	2085 ± 14	BP 1640
AD 1150	−60.4 ± 1.0	1278 ± 9	BP 800	AD 290	−57.4 ± 1.6	2088 ± 13	BP 1660
AD 1130	−59.0 ± 1.2	1285 ± 10	BP 820	AD 270	−56.8 ± 1.4	2103 ± 12	BP 1680
AD 1110	−58.3 ± 1.1	1299 ± 9	BP 840	AD 250	−58.0 ± 1.0	2132 ± 9	BP 1700

TABLE 1. (Continued)

Cal AD/BC	Δ14C ‰	14C age (BP)	Cal BP	Cal AD/BC	Δ14C ‰	14C age (BP)	Cal BP
AD 230	−58.4 ± 1.5	2155 ± 13	BP 1720	710 BC	−32.2 ± 1.9	2846 ± 16	BP 2660
AD 210	−57.9 ± 1.5	2170 ± 13	BP 1740	730 BC	−32.0 ± 1.5	2865 ± 12	BP 2680
AD 190	−56.8 ± 1.6	2180 ± 14	BP 1760	750 BC	−33.3 ± 1.6	2895 ± 14	BP 2700
AD 170	−55.8 ± 1.7	2191 ± 15	BP 1780	770 BC	−36.0 ± 1.9	2937 ± 16	BP 2720
AD 150	−55.5 ± 1.6	2207 ± 14	BP 1800	790 BC	−38.4 ± 1.2	2976 ± 10	BP 2740
AD 130	−56.0 ± 1.2	2232 ± 10	BP 1820	810 BC	−41.0 ± 1.6	3017 ± 13	BP 2760
AD 110	−56.0 ± 1.7	2251 ± 15	BP 1840	830 BC	−41.8 ± 1.4	3044 ± 12	BP 2780
AD 90	−55.7 ± 1.4	2268 ± 12	BP 1860	850 BC	−41.7 ± 1.5	3062 ± 13	BP 2800
AD 70	−56.3 ± 1.3	2293 ± 11	BP 1880	870 BC	−40.6 ± 1.5	3072 ± 13	BP 2820
AD 50	−56.0 ± 1.1	2309 ± 9	BP 1900	890 BC	−40.1 ± 1.5	3087 ± 13	BP 2840
AD 30	−55.3 ± 1.3	2323 ± 11	BP 1920	910 BC	−40.7 ± 1.4	3112 ± 12	BP 2860
AD 10	−55.4 ± 1.0	2343 ± 9	BP 1940	930 BC	−40.7 ± 1.6	3132 ± 13	BP 2880
10 BC	−55.2 ± 1.1	2360 ± 9	BP 1960	950 BC	−39.7 ± 1.4	3143 ± 12	BP 2900
30 BC	−54.8 ± .9	2376 ± 8	BP 1980	970 BC	−38.5 ± 1.2	3152 ± 10	BP 2920
50 BC	−55.0 ± 1.0	2397 ± 8	BP 2000	990 BC	−38.4 ± 1.4	3171 ± 11	BP 2940
70 BC	−54.4 ± 1.2	2411 ± 10	BP 2020	1010 BC	−38.4 ± 1.0	3190 ± 9	BP 2960
90 BC	−53.4 ± 1.2	2422 ± 10	BP 2040	1030 BC	−37.9 ± 1.4	3205 ± 12	BP 2980
110 BC	−52.9 ± 1.1	2437 ± 9	BP 2060	1050 BC	−37.1 ± 1.2	3218 ± 10	BP 3000
130 BC	−52.1 ± 1.2	2450 ± 10	BP 2080	1070 BC	−35.9 ± 1.3	3228 ± 11	BP 3020
150 BC	−51.4 ± 1.3	2463 ± 11	BP 2100	1090 BC	−34.7 ± 1.3	3237 ± 11	BP 3040
170 BC	−51.6 ± 1.2	2485 ± 10	BP 2120	1110 BC	−34.0 ± 1.3	3250 ± 11	BP 3060
190 BC	−52.2 ± 1.2	2510 ± 11	BP 2140	1130 BC	−33.8 ± 1.5	3269 ± 13	BP 3080
210 BC	−52.5 ± 1.2	2531 ± 10	BP 2160	1150 BC	−33.0 ± 1.6	3281 ± 14	BP 3100
230 BC	−51.2 ± 1.2	2540 ± 10	BP 2180	1170 BC	−32.3 ± 1.6	3295 ± 13	BP 3120
250 BC	−50.2 ± 1.4	2551 ± 12	BP 2200	1190 BC	−31.2 ± 1.6	3305 ± 14	BP 3140
270 BC	−48.8 ± 1.4	2558 ± 12	BP 2220	1210 BC	−30.9 ± 1.3	3322 ± 11	BP 3160
290 BC	−46.6 ± 1.4	2559 ± 12	BP 2240	1230 BC	−30.1 ± 1.6	3334 ± 13	BP 3180
310 BC	−45.0 ± 1.4	2565 ± 12	BP 2260	1250 BC	−29.3 ± 1.5	3347 ± 12	BP 3200
330 BC	−44.4 ± 1.4	2579 ± 12	BP 2280	1270 BC	−29.7 ± 1.7	3370 ± 14	BP 3220
350 BC	−45.6 ± 1.3	2609 ± 11	BP 2300	1290 BC	−28.8 ± 1.7	3382 ± 14	BP 3240
370 BC	−47.6 ± 1.2	2645 ± 10	BP 2320	1310 BC	−28.8 ± 1.8	3401 ± 15	BP 3260
390 BC	−50.0 ± 1.4	2685 ± 12	BP 2340	1330 BC	−28.2 ± 1.6	3416 ± 13	BP 3280
410 BC	−51.7 ± 1.3	2719 ± 11	BP 2360	1350 BC	−26.4 ± 1.7	3420 ± 14	BP 3300
430 BC	−50.7 ± 1.3	2730 ± 11	BP 2380	1370 BC	−26.2 ± 1.7	3439 ± 14	BP 3320
450 BC	−48.9 ± 1.5	2734 ± 13	BP 2400	1390 BC	−27.3 ± 1.4	3467 ± 12	BP 3340
470 BC	−47.5 ± 1.2	2742 ± 10	BP 2420	1410 BC	−28.5 ± 1.5	3496 ± 13	BP 3360
490 BC	−46.6 ± 1.3	2754 ± 11	BP 2440	1430 BC	−29.0 ± 1.5	3520 ± 12	BP 3380
510 BC	−45.9 ± 1.2	2767 ± 10	BP 2460	1450 BC	−28.9 ± 1.1	3538 ± 9	BP 3400
530 BC	−45.7 ± 1.0	2785 ± 9	BP 2480	1470 BC	−28.0 ± 1.3	3550 ± 11	BP 3420
550 BC	−45.1 ± 1.0	2799 ± 8	BP 2500	1490 BC	−27.2 ± 1.5	3563 ± 13	BP 3440
570 BC	−43.7 ± 1.3	2806 ± 11	BP 2520	1510 BC	−28.2 ± 1.6	3591 ± 14	BP 3460
590 BC	−42.1 ± 1.3	2813 ± 11	BP 2540	1530 BC	−29.3 ± 1.6	3619 ± 13	BP 3480
610 BC	−40.6 ± 1.2	2819 ± 10	BP 2560	1550 BC	−28.0 ± 1.8	3628 ± 15	BP 3500
630 BC	−38.4 ± 1.1	2820 ± 9	BP 2580	1570 BC	−26.2 ± 2.0	3633 ± 17	BP 3520
650 BC	−36.7 ± 1.2	2826 ± 10	BP 2600	1590 BC	−25.4 ± 1.5	3646 ± 12	BP 3540
670 BC	−35.1 ± 1.5	2832 ± 13	BP 2620	1610 BC	−25.5 ± 1.4	3666 ± 12	BP 3560
690 BC	−33.2 ± 1.7	2835 ± 14	BP 2640	1630 BC	−25.4 ± 1.5	3684 ± 12	BP 3580

TABLE 1. (Continued)

Cal AD/BC	Δ¹⁴C ‰	¹⁴C age (BP)	Cal BP	Cal AD/BC	Δ¹⁴C ‰	¹⁴C age (BP)	Cal BP
1650 BC	−24.6 ± 1.2	3698 ± 10	BP 3600	2590 BC	−.7 ± 1.2	4417 ± 10	BP 4540
1670 BC	−24.5 ± 1.7	3716 ± 14	BP 3620	2610 BC	−.3 ± 1.7	4433 ± 14	BP 4560
1690 BC	−25.2 ± 1.5	3741 ± 12	BP 3640	2630 BC	.1 ± 1.1	4449 ± 9	BP 4580
1710 BC	−24.2 ± 1.8	3752 ± 15	BP 3660	2650 BC	1.6 ± 1.7	4456 ± 14	BP 4600
1730 BC	−23.6 ± 1.5	3767 ± 12	BP 3680	2670 BC	2.1 ± 1.3	4471 ± 11	BP 4620
1750 BC	−24.4 ± 1.5	3793 ± 12	BP 3700	2690 BC	3.0 ± 1.4	4484 ± 11	BP 4640
1770 BC	−24.1 ± 1.4	3810 ± 11	BP 3720	2710 BC	3.9 ± 1.3	4496 ± 11	BP 4660
1790 BC	−23.3 ± 1.4	3823 ± 11	BP 3740	2730 BC	6.3 ± 1.2	4496 ± 10	BP 4680
1810 BC	−21.7 ± 1.4	3829 ± 12	BP 3760	2750 BC	7.1 ± 1.5	4509 ± 12	BP 4700
1830 BC	−20.2 ± 1.8	3836 ± 15	BP 3780	2770 BC	7.8 ± 1.8	4523 ± 14	BP 4720
1850 BC	−18.3 ± 1.6	3840 ± 13	BP 3800	2790 BC	9.5 ± 1.4	4529 ± 11	BP 4740
1870 BC	−19.1 ± 1.4	3866 ± 12	BP 3820	2810 BC	13.0 ± 1.5	4521 ± 12	BP 4760
1890 BC	−20.0 ± 1.5	3892 ± 12	BP 3840	2830 BC	14.6 ± 1.1	4528 ± 9	BP 4780
1910 BC	−19.4 ± 1.8	3908 ± 15	BP 3860	2850 BC	12.8 ± 1.4	4561 ± 11	BP 4800
1930 BC	−19.0 ± 1.4	3924 ± 12	BP 3880	2870 BC	9.4 ± 1.4	4608 ± 12	BP 4820
1950 BC	−18.7 ± 1.5	3940 ± 13	BP 3900	2890 BC	6.6 ± 1.6	4649 ± 13	BP 4840
1970 BC	−18.3 ± 1.7	3957 ± 14	BP 3920	2910 BC	5.2 ± 1.5	4680 ± 12	BP 4860
1990 BC	−17.7 ± 1.4	3971 ± 11	BP 3940	2930 BC	4.0 ± 1.6	4709 ± 13	BP 4880
2010 BC	−16.4 ± 1.6	3980 ± 13	BP 3960	2950 BC	5.5 ± 1.5	4716 ± 12	BP 4900
2030 BC	−16.7 ± 1.4	4002 ± 12	BP 3980	2970 BC	7.5 ± 1.9	4720 ± 15	BP 4920
2050 BC	−16.7 ± 1.4	4021 ± 11	BP 4000	2990 BC	9.5 ± 1.5	4723 ± 12	BP 4940
2070 BC	−14.6 ± 1.6	4024 ± 13	BP 4020	3010 BC	10.4 ± 1.7	4736 ± 13	BP 4960
2090 BC	−12.3 ± 1.6	4024 ± 13	BP 4040	3030 BC	9.9 ± 1.6	4759 ± 13	BP 4980
2110 BC	−11.9 ± 1.6	4040 ± 13	BP 4060	3050 BC	10.2 ± 1.3	4776 ± 11	BP 5000
2130 BC	−12.6 ± 1.8	4065 ± 15	BP 4080	3070 BC	11.7 ± 1.4	4784 ± 11	BP 5020
2150 BC	−12.7 ± 1.2	4086 ± 10	BP 4100	3090 BC	11.3 ± 1.8	4807 ± 15	BP 5040
2170 BC	−11.1 ± 1.6	4092 ± 13	BP 4120	3110 BC	10.9 ± 1.8	4829 ± 15	BP 5060
2190 BC	−11.2 ± 1.1	4112 ± 9	BP 4140	3130 BC	12.0 ± 1.8	4839 ± 14	BP 5080
2210 BC	−11.0 ± 1.4	4130 ± 11	BP 4160	3150 BC	14.1 ± 1.7	4842 ± 13	BP 5100
2230 BC	−9.2 ± 1.4	4135 ± 12	BP 4180	3170 BC	16.4 ± 1.7	4844 ± 14	BP 5120
2250 BC	−7.8 ± 1.3	4143 ± 11	BP 4200	3190 BC	17.4 ± 1.5	4855 ± 12	BP 5140
2270 BC	−7.2 ± 1.8	4158 ± 15	BP 4220	3210 BC	19.4 ± 1.6	4859 ± 12	BP 5160
2290 BC	−7.3 ± 1.5	4178 ± 12	BP 4240	3230 BC	22.1 ± 1.6	4857 ± 12	BP 5180
2310 BC	−6.4 ± 1.8	4190 ± 14	BP 4260	3250 BC	24.2 ± 1.6	4860 ± 13	BP 5200
2330 BC	−5.8 ± 1.4	4205 ± 11	BP 4280	3270 BC	24.4 ± 1.9	4878 ± 15	BP 5220
2350 BC	−5.1 ± 1.6	4219 ± 13	BP 4300	3290 BC	24.6 ± 1.7	4896 ± 14	BP 5240
2370 BC	−3.7 ± 1.4	4227 ± 11	BP 4320	3310 BC	24.0 ± 1.6	4920 ± 12	BP 5260
2390 BC	−2.6 ± 1.6	4237 ± 13	BP 4340	3330 BC	23.1 ± 1.4	4946 ± 11	BP 5280
2410 BC	−2.4 ± 1.3	4255 ± 11	BP 4360	3350 BC	20.9 ± 1.5	4983 ± 12	BP 5300
2430 BC	−1.3 ± .9	4265 ± 7	BP 4380	3370 BC	18.9 ± 2.0	5018 ± 16	BP 5320
2450 BC	−1.9 ± 1.5	4290 ± 12	BP 4400	3390 BC	18.6 ± 1.7	5040 ± 14	BP 5340
2470 BC	−3.6 ± 1.4	4323 ± 12	BP 4420	3410 BC	21.3 ± 2.0	5038 ± 16	BP 5360
2490 BC	−3.6 ± 1.4	4342 ± 12	BP 4440	3430 BC	23.6 ± 1.7	5040 ± 13	BP 5380
2510 BC	−2.8 ± 1.2	4356 ± 10	BP 4460	3450 BC	25.4 ± 2.0	5045 ± 16	BP 5400
2530 BC	−.6 ± 1.3	4357 ± 10	BP 4480	3470 BC	27.0 ± 1.6	5052 ± 13	BP 5420
2550 BC	.1 ± 1.4	4371 ± 11	BP 4500	3490 BC	26.4 ± 1.7	5076 ± 13	BP 5440
2570 BC	−.7 ± 1.2	4397 ± 10	BP 4520	3510 BC	24.5 ± 1.7	5110 ± 13	BP 5460

TABLE 1. (Continued)

Cal AD/BC	Δ^{14}C ‰	^{14}C age (BP)	Cal BP	Cal AD/BC	Δ^{14}C ‰	^{14}C age (BP)	Cal BP
3530 BC	24.1 ± 1.7	5133 ± 13	BP 5480	4490 BC	27.5 ± 1.9	6039 ± 15	BP 6440
3550 BC	24.7 ± 1.7	5147 ± 13	BP 5500	4510 BC	27.6 ± 2.0	6057 ± 15	BP 6460
3570 BC	27.1 ± 1.7	5148 ± 13	BP 5520	4530 BC	27.6 ± 2.0	6077 ± 16	BP 6480
3590 BC	28.7 ± 1.5	5155 ± 12	BP 5540	4550 BC	27.7 ± 2.0	6096 ± 16	BP 6500
3610 BC	28.2 ± 1.5	5178 ± 11	BP 5560	4570 BC	28.6 ± 1.7	6109 ± 13	BP 6520
3630 BC	25.4 ± 1.9	5220 ± 15	BP 5580	4590 BC	29.2 ± 1.8	6123 ± 14	BP 6540
3650 BC	23.6 ± 1.7	5254 ± 13	BP 5600	4610 BC	29.8 ± 1.9	6138 ± 15	BP 6560
3670 BC	23.5 ± 1.5	5273 ± 12	BP 5620	4630 BC	30.9 ± 1.6	6148 ± 13	BP 6580
3690 BC	23.5 ± 1.6	5293 ± 13	BP 5640	4650 BC	32.7 ± 1.5	6154 ± 12	BP 6600
3710 BC	22.8 ± 1.6	5318 ± 13	BP 5660	4670 BC	32.8 ± 2.0	6173 ± 16	BP 6620
3730 BC	23.6 ± 1.8	5331 ± 14	BP 5680	4690 BC	32.4 ± 1.5	6195 ± 12	BP 6640
3750 BC	24.4 ± 1.6	5345 ± 12	BP 5700	4710 BC	32.2 ± 1.7	6216 ± 14	BP 6660
3770 BC	23.9 ± 1.6	5368 ± 13	BP 5720	4730 BC	32.1 ± 2.0	6236 ± 16	BP 6680
3790 BC	22.9 ± 1.5	5395 ± 12	BP 5740	4750 BC	32.9 ± 2.0	6249 ± 16	BP 6700
3810 BC	22.3 ± 1.7	5419 ± 13	BP 5760	4770 BC	32.3 ± 2.0	6274 ± 16	BP 6720
3830 BC	23.3 ± 1.8	5430 ± 14	BP 5780	4790 BC	31.5 ± 2.1	6300 ± 16	BP 6740
3850 BC	25.7 ± 1.3	5431 ± 10	BP 5800	4810 BC	31.6 ± 2.1	6318 ± 16	BP 6760
3870 BC	28.1 ± 1.2	5432 ± 9	BP 5820	4830 BC	31.8 ± 1.8	6336 ± 14	BP 6780
3890 BC	29.5 ± 1.4	5440 ± 11	BP 5840	4850 BC	31.8 ± 1.9	6356 ± 14	BP 6800
3910 BC	29.2 ± 1.3	5462 ± 11	BP 5860	4870 BC	33.1 ± 2.1	6365 ± 17	BP 6820
3930 BC	28.4 ± 1.5	5488 ± 12	BP 5880	4890 BC	34.1 ± 1.9	6376 ± 15	BP 6840
3950 BC	26.5 ± 1.4	5523 ± 11	BP 5900	4910 BC	33.0 ± 1.5	6404 ± 12	BP 6860
3970 BC	24.7 ± 1.1	5555 ± 9	BP 5920	4930 BC	32.6 ± 1.3	6427 ± 10	BP 6880
3990 BC	23.7 ± 1.5	5583 ± 12	BP 5940	4950 BC	32.1 ± 1.3	6450 ± 10	BP 6900
4010 BC	24.0 ± 1.6	5600 ± 13	BP 5960	4970 BC	32.8 ± 1.4	6464 ± 11	BP 6920
4030 BC	25.0 ± 1.4	5612 ± 11	BP 5980	4990 BC	33.8 ± 1.5	6476 ± 12	BP 6940
4050 BC	24.9 ± 1.6	5632 ± 13	BP 6000	5010 BC	34.6 ± 1.9	6489 ± 15	BP 6960
4070 BC	26.1 ± 1.6	5642 ± 13	BP 6020	5030 BC	35.4 ± 2.1	6502 ± 16	BP 6980
4090 BC	26.2 ± 1.5	5661 ± 12	BP 6040	5050 BC	35.0 ± 2.0	6525 ± 16	BP 7000
4130 BC	29.3 ± 1.8	5675 ± 14	BP 6080	5070 BC	34.1 ± 1.7	6551 ± 13	BP 7020
4150 BC	28.9 ± 3.3	5697 ± 26	BP 6100	5090 BC	34.4 ± 1.4	6568 ± 11	BP 7040
4170 BC	29.7 ± 1.9	5711 ± 15	BP 6120	5110 BC	36.3 ± 1.5	6573 ± 12	BP 7060
4190 BC	32.1 ± 1.9	5712 ± 14	BP 6140	5130 BC	37.2 ± 1.5	6585 ± 12	BP 7080
4210 BC	32.6 ± 2.0	5727 ± 15	BP 6160	5150 BC	37.4 ± 1.7	6604 ± 14	BP 7100
4230 BC	30.1 ± 1.6	5766 ± 12	BP 6180	5170 BC	39.8 ± 1.5	6605 ± 12	BP 7120
4250 BC	29.3 ± 1.8	5792 ± 14	BP 6200	5190 BC	40.2 ± 1.8	6621 ± 14	BP 7140
4270 BC	29.7 ± 1.8	5808 ± 14	BP 6220	5210 BC	38.1 ± 2.0	6657 ± 15	BP 7160
4290 BC	31.3 ± 1.8	5815 ± 14	BP 6240	5230 BC	36.3 ± 2.0	6689 ± 15	BP 7180
4310 BC	31.2 ± 1.8	5835 ± 14	BP 6260	5250 BC	35.3 ± 1.6	6717 ± 13	BP 7200
4330 BC	28.9 ± 1.7	5873 ± 14	BP 6280	5270 BC	33.6 ± 1.7	6749 ± 13	BP 7220
4350 BC	26.5 ± 1.7	5911 ± 13	BP 6300	5290 BC	33.1 ± 1.7	6773 ± 14	BP 7240
4370 BC	26.0 ± 1.6	5934 ± 13	BP 6320	5310 BC	33.2 ± 1.8	6791 ± 14	BP 7260
4390 BC	27.2 ± 1.9	5944 ± 15	BP 6340	5330 BC	32.6 ± 1.8	6816 ± 14	BP 7280
4410 BC	28.2 ± 1.9	5956 ± 15	BP 6360	5350 BC	32.9 ± 1.7	6833 ± 13	BP 7300
4430 BC	29.6 ± 2.0	5965 ± 15	BP 6380	5370 BC	33.8 ± 2.0	6845 ± 15	BP 7320
4450 BC	28.3 ± 1.9	5994 ± 15	BP 6400	5390 BC	33.7 ± 2.0	6866 ± 16	BP 7340
4470 BC	26.8 ± 1.7	6025 ± 14	BP 6420	5410 BC	34.2 ± 1.8	6881 ± 14	BP 7360

TABLE 1. (Continued)

Cal AD/BC	Δ^{14}C ‰	^{14}C age (BP)	Cal BP	Cal AD/BC	Δ^{14}C ‰	^{14}C age (BP)	Cal BP
5430 BC	31.3 ± 1.8	6923 ± 14	BP 7380	6370 BC	23.6 ± 2.6	7897 ± 20	BP 8320
5450 BC	28.8 ± 1.8	6962 ± 14	BP 7400	6390 BC	22.4 ± 2.3	7925 ± 18	BP 8340
5470 BC	29.2 ± 1.8	6978 ± 14	BP 7420	6410 BC	21.6 ± 2.5	7951 ± 19	BP 8360
5490 BC	29.1 ± 2.0	6998 ± 15	BP 7440	6430 BC	20.5 ± 2.7	7979 ± 21	BP 8380
5510 BC	28.7 ± 2.0	7021 ± 15	BP 7460	6450 BC	19.9 ± 2.6	8004 ± 21	BP 8400
5530 BC	28.7 ± 2.0	7041 ± 15	BP 7480	6470 BC	18.1 ± 2.4	8037 ± 19	BP 8420
5550 BC	30.0 ± 1.8	7050 ± 14	BP 7500	6490 BC	18.2 ± 2.5	8056 ± 20	BP 8440
5570 BC	28.4 ± 1.5	7082 ± 12	BP 7520	6510 BC	19.5 ± 2.0	8065 ± 16	BP 8460
5590 BC	25.9 ± 1.7	7121 ± 13	BP 7540	6530 BC	20.4 ± 3.1	8077 ± 25	BP 8480
5610 BC	24.6 ± 1.5	7150 ± 12	BP 7560	6550 BC	19.9 ± 3.2	8101 ± 25	BP 8500
5630 BC	24.4 ± 1.5	7171 ± 12	BP 7580	6570 BC	20.2 ± 4.1	8117 ± 32	BP 8520
5650 BC	24.4 ± 1.4	7190 ± 11	BP 7600	6590 BC	20.5 ± 4.3	8135 ± 34	BP 8540
5670 BC	24.1 ± 1.5	7212 ± 12	BP 7620	6610 BC	19.5 ± 4.1	8162 ± 32	BP 8560
5690 BC	23.4 ± 1.6	7237 ± 12	BP 7640	6630 BC	19.7 ± 4.1	8179 ± 32	BP 8580
5710 BC	22.9 ± 1.6	7261 ± 13	BP 7660	6650 BC	20.7 ± 3.5	8191 ± 27	BP 8600
5730 BC	22.7 ± 1.6	7282 ± 12	BP 7680	6670 BC	22.0 ± 3.5	8200 ± 27	BP 8620
5750 BC	22.8 ± 1.4	7300 ± 11	BP 7700	6690 BC	23.2 ± 3.5	8211 ± 27	BP 8640
5770 BC	23.0 ± 1.5	7318 ± 11	BP 7720	6710 BC	23.5 ± 3.5	8228 ± 27	BP 8660
5790 BC	23.5 ± 1.5	7334 ± 11	BP 7740	6730 BC	24.8 ± 3.5	8237 ± 27	BP 8680
5810 BC	23.9 ± 1.4	7350 ± 11	BP 7760	6750 BC	26.4 ± 4.1	8244 ± 32	BP 8700
5830 BC	24.2 ± 1.5	7367 ± 12	BP 7780	6770 BC	26.4 ± 4.1	8263 ± 32	BP 8720
5850 BC	24.2 ± 1.8	7387 ± 14	BP 7800	6790 BC	27.4 ± 4.1	8275 ± 32	BP 8740
5870 BC	24.1 ± 2.1	7407 ± 16	BP 7820	6810 BC	29.0 ± 4.1	8281 ± 32	BP 8760
5890 BC	24.6 ± 2.0	7422 ± 16	BP 7840	6830 BC	31.4 ± 4.1	8283 ± 32	BP 8780
5910 BC	26.0 ± 1.9	7431 ± 15	BP 7860	6850 BC	34.5 ± 2.6	8278 ± 20	BP 8800
5930 BC	26.0 ± 2.0	7450 ± 15	BP 7880	6870 BC	35.4 ± 4.4	8291 ± 34	BP 8820
5950 BC	24.0 ± 2.1	7485 ± 17	BP 7900	6890 BC	36.6 ± 4.4	8301 ± 34	BP 8840
5970 BC	22.1 ± 2.0	7519 ± 16	BP 7920	6910 BC	38.1 ± 4.4	8309 ± 34	BP 8860
5990 BC	21.0 ± 1.9	7547 ± 15	BP 7940	6930 BC	40.1 ± 4.4	8312 ± 34	BP 8880
6010 BC	20.6 ± 3.0	7571 ± 24	BP 7960	6950 BC	41.2 ± 4.4	8323 ± 34	BP 8900
6030 BC	20.4 ± 4.1	7592 ± 32	BP 7980	6970 BC	42.3 ± 4.4	8334 ± 34	BP 8920
6050 BC	20.0 ± 4.1	7614 ± 32	BP 8000	6990 BC	40.9 ± 4.4	8365 ± 34	BP 8940
6070 BC	20.5 ± 4.1	7629 ± 32	BP 8020	7010 BC	38.2 ± 4.4	8404 ± 34	BP 8960
6090 BC	22.5 ± 3.3	7633 ± 26	BP 8040	7030 BC	36.7 ± 4.4	8436 ± 34	BP 8980
6110 BC	23.0 ± 2.8	7649 ± 22	BP 8060	7050 BC	34.7 ± 2.6	8471 ± 20	BP 9000
6130 BC	22.5 ± 2.8	7672 ± 22	BP 8080	7070 BC	35.8 ± 3.3	8481 ± 26	BP 9020
6150 BC	23.0 ± 2.9	7687 ± 22	BP 8100	7090 BC	36.8 ± 3.3	8494 ± 26	BP 9040
6170 BC	21.5 ± 2.7	7718 ± 21	BP 8120	7110 BC	38.3 ± 3.3	8501 ± 26	BP 9060
6190 BC	20.2 ± 2.3	7749 ± 18	BP 8140	7130 BC	40.6 ± 4.2	8502 ± 32	BP 9080
6210 BC	20.3 ± 2.6	7767 ± 21	BP 8160	7150 BC	40.6 ± 4.2	8522 ± 32	BP 9100
6230 BC	20.0 ± 2.6	7788 ± 21	BP 8180	7170 BC	43.2 ± 4.2	8522 ± 32	BP 9120
6250 BC	20.6 ± 2.7	7803 ± 21	BP 8200	7190 BC	45.3 ± 4.2	8524 ± 32	BP 9140
6270 BC	22.0 ± 2.3	7812 ± 18	BP 8220	7210 BC	45.7 ± 4.2	8541 ± 32	BP 9160
6290 BC	23.9 ± 2.6	7817 ± 21	BP 8240	7230 BC	47.1 ± 4.2	8550 ± 32	BP 9180
6310 BC	24.6 ± 2.8	7830 ± 22	BP 8260	7250 BC	46.4 ± 4.0	8575 ± 31	BP 9200
6330 BC	25.9 ± 2.8	7840 ± 22	BP 8280	7270 BC	45.9 ± 4.0	8598 ± 31	BP 9220
6350 BC	25.3 ± 2.4	7864 ± 19	BP 8300	7290 BC	46.1 ± 3.8	8616 ± 29	BP 9240

TABLE 1. (Continued)

Cal AD/BC	Δ^{14}C ‰	^{14}C age (BP)	Cal BP	Cal AD/BC	Δ^{14}C ‰	^{14}C age (BP)	Cal BP
7310 BC	45.7 ± 4.0	8638 ± 31	BP 9260	8250 BC	47.2 ± 5.5	9540 ± 43	BP 10200
7330 BC	46.6 ± 4.4	8651 ± 34	BP 9280	8270 BC	47.5 ± 4.7	9558 ± 36	BP 10220
7350 BC	48.5 ± 4.4	8655 ± 34	BP 9300	8290 BC	49.6 ± 3.8	9560 ± 29	BP 10240
7370 BC	50.0 ± 4.0	8663 ± 31	BP 9320	8310 BC	52.2 ± 4.8	9560 ± 37	BP 10260
7390 BC	50.4 ± 4.4	8680 ± 34	BP 9340	8330 BC	51.7 ± 5.1	9584 ± 39	BP 10280
7410 BC	49.5 ± 3.8	8706 ± 29	BP 9360	8350 BC	50.2 ± 5.6	9615 ± 43	BP 10300
7430 BC	47.2 ± 3.8	8744 ± 29	BP 9380	8370 BC	50.6 ± 5.6	9631 ± 43	BP 10320
7450 BC	46.9 ± 3.8	8766 ± 29	BP 9400	8390 BC	50.9 ± 4.8	9648 ± 37	BP 10340
7470 BC	47.0 ± 3.8	8783 ± 29	BP 9420	8410 BC	50.3 ± 5.7	9672 ± 43	BP 10360
7490 BC	44.2 ± 3.8	8825 ± 29	BP 9440	8430 BC	50.0 ± 4.6	9694 ± 35	BP 10380
7510 BC	42.7 ± 4.0	8856 ± 31	BP 9460	8450 BC	50.7 ± 2.9	9708 ± 22	BP 10400
7530 BC	41.8 ± 4.0	8882 ± 31	BP 9480	8470 BC	51.6 ± 5.0	9720 ± 38	BP 10420
7550 BC	39.9 ± 5.5	8916 ± 43	BP 9500	8490 BC	52.6 ± 6.0	9732 ± 46	BP 10440
7570 BC	39.5 ± 4.0	8939 ± 31	BP 9520	8510 BC	53.4 ± 5.0	9746 ± 38	BP 10460
7590 BC	38.9 ± 4.0	8963 ± 31	BP 9540	8530 BC	53.8 ± 6.6	9762 ± 50	BP 10480
7610 BC	40.0 ± 4.0	8974 ± 31	BP 9560	8550 BC	55.1 ± 7.6	9772 ± 58	BP 10500
7630 BC	41.1 ± 4.0	8985 ± 31	BP 9580	8570 BC	56.6 ± 7.6	9779 ± 58	BP 10520
7650 BC	42.4 ± 4.0	8994 ± 31	BP 9600	8590 BC	56.7 ± 6.0	9798 ± 46	BP 10540
7670 BC	43.8 ± 4.0	9003 ± 31	BP 9620	8610 BC	56.6 ± 5.0	9818 ± 38	BP 10560
7690 BC	43.6 ± 4.0	9024 ± 31	BP 9640	8630 BC	57.3 ± 4.4	9832 ± 33	BP 10580
7710 BC	42.8 ± 4.4	9049 ± 34	BP 9660	8650 BC	58.6 ± 3.8	9842 ± 29	BP 10600
7730 BC	43.6 ± 4.4	9063 ± 34	BP 9680	8670 BC	60.2 ± 4.4	9849 ± 33	BP 10620
7750 BC	45.1 ± 4.4	9071 ± 34	BP 9700	8690 BC	62.0 ± 3.6	9855 ± 27	BP 10640
7770 BC	47.8 ± 4.4	9069 ± 34	BP 9720	8710 BC	63.6 ± 2.9	9862 ± 22	BP 10660
7790 BC	49.7 ± 4.4	9074 ± 34	BP 9740	8730 BC	65.3 ± 3.3	9869 ± 25	BP 10680
7810 BC	52.6 ± 4.0	9072 ± 31	BP 9760	8750 BC	67.4 ± 4.0	9873 ± 30	BP 10700
7830 BC	54.5 ± 4.0	9076 ± 31	BP 9780	8770 BC	70.2 ± 4.6	9871 ± 35	BP 10720
7850 BC	54.4 ± 4.0	9097 ± 31	BP 9800	8790 BC	74.0 ± 4.7	9862 ± 35	BP 10740
7870 BC	53.8 ± 4.0	9121 ± 31	BP 9820	8810 BC	77.6 ± 6.2	9855 ± 46	BP 10760
7890 BC	52.7 ± 4.0	9149 ± 31	BP 9840	8830 BC	78.5 ± 6.4	9867 ± 48	BP 10780
7910 BC	51.3 ± 4.2	9179 ± 32	BP 9860	8850 BC	77.7 ± 4.3	9892 ± 32	BP 10800
7930 BC	50.0 ± 4.4	9208 ± 34	BP 9880	8870 BC	78.3 ± 4.4	9908 ± 33	BP 10820
7950 BC	48.8 ± 4.6	9237 ± 35	BP 9900	8890 BC	79.5 ± 5.4	9918 ± 40	BP 10840
7970 BC	47.9 ± 4.8	9263 ± 37	BP 9920	8910 BC	79.6 ± 5.1	9937 ± 38	BP 10860
7990 BC	47.4 ± 5.2	9286 ± 40	BP 9940	8930 BC	78.8 ± 5.9	9962 ± 44	BP 10880
8010 BC	46.3 ± 5.3	9314 ± 41	BP 9960	8950 BC	78.0 ± 6.8	9988 ± 51	BP 10900
8030 BC	44.4 ± 4.6	9348 ± 36	BP 9980	8970 BC	77.3 ± 4.6	10012 ± 34	BP 10920
8050 BC	43.2 ± 3.6	9377 ± 28	BP 10000	8990 BC	76.1 ± 3.2	10041 ± 24	BP 10940
8070 BC	42.2 ± 3.5	9403 ± 27	BP 10020	9010 BC	73.9 ± 3.2	10077 ± 24	BP 10960
8090 BC	40.9 ± 4.5	9434 ± 35	BP 10040	9030 BC	70.9 ± 3.0	10118 ± 23	BP 10980
8110 BC	40.9 ± 4.8	9452 ± 37	BP 10060	9050 BC	67.9 ± 4.9	10160 ± 37	BP 11000
8130 BC	42.1 ± 4.0	9463 ± 31	BP 10080	9070 BC	67.0 ± 5.6	10186 ± 43	BP 11020
8150 BC	43.3 ± 3.7	9473 ± 29	BP 10100	9090 BC	68.2 ± 5.2	10197 ± 39	BP 11040
8170 BC	44.5 ± 4.5	9483 ± 35	BP 10120	9110 BC	69.5 ± 5.9	10207 ± 44	BP 11060
8190 BC	45.0 ± 5.2	9499 ± 40	BP 10140	9130 BC	70.1 ± 5.4	10222 ± 41	BP 11080
8210 BC	45.7 ± 5.5	9513 ± 43	BP 10160	9150 BC	70.7 ± 4.6	10237 ± 35	BP 11100
8230 BC	46.8 ± 5.5	9524 ± 43	BP 10180	9170 BC	71.9 ± 4.4	10247 ± 33	BP 11120

TABLE 1. (Continued)

Cal AD/BC	Δ14C ‰	14C age (BP)	Cal BP	Cal AD/BC	Δ14C ‰	14C age (BP)	Cal BP
9190 BC	73.5 ± 5.0	10254 ± 37	BP 11140	9550 BC	101.2 ± 7.9	10400 ± 58	BP 11500
9210 BC	76.2 ± 4.6	10254 ± 34	BP 11160	9570 BC	102.4 ± 8.0	10410 ± 58	BP 11520
9230 BC	79.2 ± 5.2	10250 ± 39	BP 11180	9590 BC	103.7 ± 8.0	10420 ± 58	BP 11540
9250 BC	80.5 ± 5.5	10260 ± 41	BP 11200	9610 BC	105.1 ± 8.0	10429 ± 58	BP 11560
9270 BC	81.0 ± 4.5	10276 ± 33	BP 11220	9630 BC	106.7 ± 8.1	10438 ± 59	BP 11580
9290 BC	82.7 ± 4.9	10283 ± 36	BP 11240	9650 BC	108.3 ± 8.1	10445 ± 59	BP 11600
9310 BC	84.8 ± 6.1	10287 ± 45	BP 11260	9670 BC	110.1 ± 8.2	10452 ± 59	BP 11620
9330 BC	87.2 ± 7.2	10288 ± 53	BP 11280	9690 BC	111.9 ± 8.2	10458 ± 59	BP 11640
9350 BC	89.8 ± 7.8	10289 ± 57	BP 11300	9710 BC	113.0 ± 8.2	10469 ± 59	BP 11660
9370 BC	90.9 ± 6.5	10300 ± 48	BP 11320	9730 BC	114.1 ± 8.3	10481 ± 60	BP 11680
9390 BC	91.6 ± 5.7	10314 ± 42	BP 11340	9750 BC	115.3 ± 8.3	10492 ± 60	BP 11700
9410 BC	93.5 ± 6.0	10320 ± 44	BP 11360	9770 BC	116.4 ± 8.3	10503 ± 60	BP 11720
9430 BC	95.5 ± 6.5	10325 ± 48	BP 11380	9790 BC	117.5 ± 8.4	10515 ± 60	BP 11740
9450 BC	96.4 ± 7.8	10338 ± 57	BP 11400	9800 BC	118.0 ± 8.4	10521 ± 60	BP 11750
9470 BC	97.2 ± 7.8	10351 ± 57	BP 11420	9850 BC	122.6 ± 8.5	10537 ± 61	BP 11800
9490 BC	98.1 ± 7.8	10364 ± 57	BP 11440	9900 BC	126.9 ± 8.6	10554 ± 61	BP 11850
9510 BC	99.0 ± 7.9	10377 ± 58	BP 11460	9950 BC	131.1 ± 8.7	10573 ± 62	BP 11900
9530 BC	100.0 ± 7.9	10389 ± 58	BP 11480	10000 BC	135.0 ± 8.8	10594 ± 62	BP 11950